Simple glide for a nonlinear elastic Cosserat model: analytical and computational results with induced microstructure.

Patrizio Neff *
TU Darmstadt
and
Ingo Münch
TU Karlsruhe

September 1, 2005

Abstract

We study the static simple glide problem for a geometrically exact, generalized continua of micropolar type. In contrast to linear micropolar elasticity, where the unique solution is available in closed form we exhibit a multitude of solutions to the nonlinear problem, even if the two fields of deformations φ and microrotations $\overline{R}$ can remain homogeneous. This motivates a search for new conditions on the microrotations $\overline{R}$ which single out a unique, physically acceptable, response.

The influence of material parameters, notably the Cosserat couple modulus μ_c and the length scale L_c on the response is also studied. For small Cosserat couple modulus $\mu_c > 0$ we observe a pitchfork bifurcation of the homogeneous response and for vanishing internal length and zero Cosserat couple modulus $\mu_c = 0$ the Cosserat model may show highly oscillating "microstructure" solutions which are energetically better than the homogeneous response. The numerical results show that even for $\mu > 0$ the nonlinear Cosserat model has a quite different qualitative response than the linear model.

Key words: Simple glide, polar-materials, microstructure, structured continua, solid mechanics, variational methods.
AMS 2000 subject classification: 74A35, 74A30, 74C05, 74C10 74C20, 74D10, 74E05, 74E10, 74E15, 74E20, 74G30, 74G65, 74N15

Contents

*Corresponding author: Patrizio Neff, AG6, Fachbereich Mathematik, Darmstadt University of Technology, Schlossgartenstrasse 7, 64289 Darmstadt, Germany, email: neff@mathematik.tu-darmstadt.de, Phone: +49-6151-16-3495

1 Introduction

This note investigates the simple-glide problem for a nonlinear elastic Cosserat solid under various boundary conditions for the microrotations and different constitutive parameters.

General continuum models involving **independent rotations** have been introduced by the Cosserat brothers [6] at the beginning of the last century. Their nonlinear, geometrically exact development has been largely forgotten for decades only to be rediscovered in a linearized setting in the early sixties [41, 19, 1, 16, 14, 46, 47, 20, 32, 45, 48]. At that time theoretical investigations on non-classical extended continuum theories were the main motivation [29]. Since then, the original Cosserat concept has been generalized in various directions, notably by Eringen and his coworkers who extended the Cosserat concept to include also microinertia effects and to rename it subsequently into **micropolar theory**. For an overview of these so called **microcontinuum** theories we refer to [15, 13, 4, 3, 5, 21, 31, 40].

The Cosserat model includes in a natural way **size effects**, i.e. small samples behave comparatively stiffer than large samples. These effects have recently received new attention in conjunction with nano-devices. From a computational point of view, theories with size-effect are increasingly **used to regularize non-wellposed situations**, e.g. shear-banding in elasto-plasticity without hardening [27, 11, 42, 7, 9, 8]. It has been shown by the author that infinitesimal elasto-plasticity augmented with (elastic) Cosserat effects indeed leads to a well-posed problem [38] in contrast to classical elasto-plasticity. The mathematical analysis establishing well-posedness for the infinitesimal strain, linear Cosserat elastic solid is presented in [23, 12, 22, 17, 18] and in [26, 24, 25] for so called linear microstretch models. This analysis is based on the **uniform positivity** of the free energy of the Cosserat solid, which in turn **implies** that the **Cosserat couple modulus μ_c is strictly positive**. The first author has extended the existence results for both the Cosserat model and the more general micromorphic models to the geometrically exact, finite-strain case, see e.g. [39, 34, 35].

Despite the huge effort already spent in investigating the Cosserat model, two major problems are still controversially discussed. These two points are: the problem of physically meaningful boundary or side-conditions for the microrotations and the physically consistent determination of the Cosserat parameters, notably the value of the Cosserat couple modulus μ_c. These open points may be in part responsible for the fact that 1.(linear) Cosserat parameters for continuous solids have never gained general acceptance even in the "Cosserat community" and 2. that the linear elastic Cosserat model has never been really accepted by a majority of applied scientists as a useful model to describe size effects in continuous solids.

We investigate both open problems again, however, in a **nonlinear framework**. A major difference to the linear setting is that we can allow to set the Cosserat couple modulus $\mu_c \equiv 0$, which is impossible in a "true" linear Cosserat model. Even for the simplest non-trivial problem showing Cosserat effects, namely the one-dimensional simple glide problem, we disclose a complicated behaviour including non-uniqueness depending on $\mu_c \geq 0$ and various boundary conditions for the microrotations. For $\mu_c = 0$ and vanishing internal length $L_c = 0$ e.g. it is possible to construct solutions where the Cauchy stresses are symmetric everywhere to first order but the solution is not homogeneous and does therefore not coincide with the classical solution. The non uniqueness for simple glide already in the class of homogeneous solutions necessitates the introduction of additional conditions on the microrotations which remove this ambiguity.

We approach the simple glide problem both analytically and numerically in great detail since we surmise that what cannot be understood in simple glide will remain open anyway. In doing so, it is hoped that a better comprehension of the role played by the parameter μ_c and the interplay with the boundary conditions can be gained. It is our working hypothesis that the geometrically exact Cosserat model with $\mu_c = 0$ can do justice to the Cosserat approach as a viable physical model for a continuous solid which incorporates length scale effects. **A zero Cosserat couple modulus $\mu_c = 0$ implies that the Cauchy-stress tensor is symmetric to first order and length scale effects are of second order.** This is acceptable for continuous solids.

Our contribution is organized as follows: after the introduction we first present the geometrically exact isotropic Cosserat model in variational form and recall the obtained existence results for both $\mu_c > 0$ and $\mu_c = 0$. Second, we focus on the problem of simple glide of an infinite layer of material under Dirichlet boundary conditions for the glide and various alternative boundary or side conditions for the microrotations. The Euler-Lagrange equations are derived and we show that the finite-strain model allows for **three distinct homogeneous solutions** if $0 \leq \mu_c \leq \mu_c^{\text{crit}}$, where μ_c^{crit} is a value depending on the applied shear γ. The corresponding shear stress response τ is given. Next, we partially simplify the finite-strain problem and prove the existence of a family of weak equilibrium solutions with microstructure, i.e. an absolutely continuous, non-differentiable shear profile (for vanishing internal length $L_c = 0$ and zero Cosserat couple modulus $\mu_c = 0$) which is **energetically better** than the (always possible classical aligned) homogeneous response. Then we turn to the linear Cosserat model in simple glide and rederive the analytical solution. The linear indeterminate couple stress-problem is also included. Thereafter, a classical finite-strain Biot model (quadratic energy in the symmetric stretch tensor U) is presented and specialized to simple-glide. It is shown that the shear-stress response coincides with the finite-strain Cosserat model for specific boundary conditions.

This closes the analytical section and we turn to the numerical part where we investigate the previous problems numerically with an eye on the influence of various boundary conditions for the microrotations as well as the influence of the Cosserat couple modulus μ_c on the solution. Further, by choosing a small internal length scale L_c and by disturbing microrotations on the edges of our sample, theoretically predicted and energetically better microstructure solutions for simple glide can be observed. Thereafter we switch to the planar shear problem. First we investigate the influence of boundary conditions on a two-dimensional beam structure under shear and show that in this case the Cosserat model merely describes strong boundary layer effects for Dirichlet boundary conditions on the microrotations. Following is a comparative study of the linear and nonlinear planar shear problem for various parameters and boundary conditions. We end this contribution by discussing boundary conditions on the microrotations in the three-dimensional case and a conclusion. The notation is found in the appendix.

2 The three-dimensional Cosserat model

2.1 Problem statement in variational form

In [37] a finite-strain, fully frame-indifferent, three-dimensional Cosserat micropolar model is introduced. The **two-field** problem has been posed in a variational setting. The task is to find a pair $(\varphi, \overline{R}) : \Omega \subset \mathbb{R}^3 \mapsto \mathbb{R}^3 \times \mathrm{SO}(3,\mathbb{R})$ of deformation φ and **independent microrotation** $\overline{R} \in \mathrm{SO}(3,\mathbb{R})$, minimizing the energy functional I,

$$I(\varphi,\overline{R}) = \int_\Omega W_{\mathrm{mp}}(\overline{R}^T\nabla\varphi) + W_{\mathrm{curv}}(\overline{R}^T \mathrm{D_x}\overline{R}) - \Pi_f(\varphi) - \Pi_M(\overline{R})\,\mathrm{dV}$$

$$- \int_{\Gamma_S} \Pi_N(\varphi)\,\mathrm{dS} - \int_{\Gamma_C} \Pi_{M_c}(\overline{R})\,\mathrm{dS} \mapsto \min.\ \text{w.r.t.}\ (\varphi,\overline{R})\,, \tag{2.1}$$

together with the Dirichlet boundary condition of place for the deformation φ on Γ: $\varphi_{|_\Gamma} = g_{\mathrm{d}}$ and three **alternative** boundary conditions for the microrotations $\overline{R}$ on Γ,

$$\overline{R}_{|_\Gamma} = \begin{cases} \overline{R}_{\mathrm{d}}\,, & \text{the case of } \textbf{rigid} \text{ prescription}\,, \\ \mathrm{polar}(\nabla\varphi)\,, & \text{the case of } \textbf{strong consistent coupling}\,, \\ \text{no condition for } \overline{R} \text{ on } \Gamma, & \textbf{induced Neumann-type} \text{ relations for } \overline{R} \text{ on } \Gamma\,. \end{cases} \tag{2.2}$$

The constitutive assumptions on the densities are

$$\begin{aligned} W_{\mathrm{mp}}(\overline{U}) &= \mu\,\|\mathrm{sym}(\overline{U}-1\!\!1)\|^2 + \mu_c\,\|\mathrm{skew}(\overline{U})\|^2 + \frac{\lambda}{2}\,\mathrm{tr}\left[\mathrm{sym}(\overline{U}-1\!\!1)\right]^2, \qquad (2.3)\\ W_{\mathrm{curv}}(\mathfrak{K}) &= 2\frac{\mu}{q}\,\left(1+L_c^2\,\|\mathfrak{K}\|^2\right)^{\frac{q}{2}}\,, \quad \overline{U} = \overline{R}^T F\,,\ F = \nabla\varphi\,,\\ \mathfrak{K} &= \overline{R}^T \mathrm{D_x}\overline{R} := \left(\overline{R}^T\nabla(\overline{R}.e_1), \overline{R}^T\nabla(\overline{R}.e_2), \overline{R}^T\nabla(\overline{R}.e_3)\right),\ \ \textbf{curvature tensor}\,, \end{aligned}$$

under the minimal requirement $q \geq 1$. The total elastically stored energy $W = W_{\mathrm{mp}} + W_{\mathrm{curv}}$ is quadratic in the stretch $\overline{U}$ and possibly super-quadratic in the curvature $\mathfrak{K}$. The strain energy W_{mp} depends on the deformation gradient $F = \nabla\varphi$ and the microrotations $\overline{R} \in \mathrm{SO}(3,\mathbb{R})$, which do not necessarily coincide with the **continuum rotations** $R = \mathrm{polar}(F)$. The curvature energy W_{curv} depends moreover on the space derivatives $\mathrm{D_x}\overline{R}$ which describe the self-interaction of the microstructure.[1] In general, the **micropolar stretch tensor** $\overline{U}$ is **not symmetric** and does not coincide with the **symmetric continuum stretch** tensor $U = R^T F = \sqrt{F^TF}$. By abuse of notation we set $\|\,\mathrm{sym}\,\mathfrak{K}\|^2 := \sum_{i=1}^3 \|\,\mathrm{sym}\,\mathfrak{K}^i\|^2$ for third order tensors $\mathfrak{K}$.

Here, $\Omega \subset \mathbb{R}^3$ is an open domain with boundary $\partial\Omega$ and $\Gamma \subset \partial\Omega$ is that part of the boundary, where Dirichlet conditions $g_{\mathrm{d}}, \overline{R}_{\mathrm{d}}$ for deformations and microrotations or coupling conditions for microrotations, are prescribed. $\Gamma_S \subset \partial\Omega$ is a part of the boundary, where traction boundary conditions in the form of the potential of applied surface forces Π_N are given with $\Gamma \cap \Gamma_S = \emptyset$. In addition, $\Gamma_C \subset \partial\Omega$ is the part of the boundary where the potential of external surface couples Π_{M_c} are applied with $\Gamma \cap \Gamma_C = \emptyset$. On the free boundary $\partial\Omega \setminus \{\Gamma \cup \Gamma_S \cup \Gamma_C\}$ corresponding natural boundary conditions for $(\varphi,\overline{R})$ apply. The potential of the external applied volume force is Π_f and Π_M takes on the role of the potential of applied external volume couples. For simplicity we assume

$$\Pi_f(\varphi) = \langle f,\varphi\rangle\,,\ \Pi_M(\overline{R}) = \langle M,\overline{R}\rangle\,,\ \Pi_N(\varphi) = \langle N,\varphi\rangle\,,\ \Pi_{M_c}(\overline{R}) = \langle M_c,\overline{R}\rangle\,, \tag{2.4}$$

for the potentials of applied loads with given functions $f \in L^2(\Omega,\mathbb{R}^3)$, $M \in L^2(\Omega,\mathbb{M}^{3\times3})$, $N \in L^2(\Gamma_S,\mathbb{R}^3)$, $M_c \in L^2(\Gamma_C,\mathbb{M}^{3\times3})$.

[1] Observe that $\overline{R}^T\nabla(\overline{R}.e_i) \neq \overline{R}^T\partial_{x_i}\overline{R} \in \mathfrak{so}(3,\mathbb{R})$.

The parameters μ, $\lambda > 0\,[\mathrm{MPa}]$ are the Lamé constants of classical isotropic elasticity, the additional parameter $\mu_c \geq 0\,[\mathrm{MPa}]$ is called the **Cosserat couple modulus**. For $\mu_c > 0$ the elastic strain energy density $W_{\mathrm{mp}}(\overline{U})$ is **uniformly convex** in $\overline{U}$. Moreover, for all $F \in \mathrm{GL}^+(3,\mathbb{R})$:

$$\begin{aligned}
W_{\mathrm{mp}}(\overline{U}) &= W_{\mathrm{mp}}(\overline{R}^T F) \geq \min(\mu,\mu_c)\,\|\overline{R}^T F - 1\!\!1\|^2 = \min(\mu,\mu_c)\,\|F - \overline{R}\|^2 \\
&\geq \min(\mu,\mu_c) \inf_{R \in \mathrm{O}(3,\mathbb{R})} \|F - R\|^2 = \min(\mu,\mu_c)\,\mathrm{dist}^2(F, \mathrm{O}(3,\mathbb{R})) \\
&= \min(\mu,\mu_c)\,\mathrm{dist}^2(F, \mathrm{SO}(3,\mathbb{R})) = \min(\mu,\mu_c)\,\|F - \mathrm{polar}(F)\|^2 \\
&= \min(\mu,\mu_c)\,\|U - 1\!\!1\|^2 .
\end{aligned} \tag{2.5}$$

In contrast, for the here interesting limit case $\mu_c = 0$ the strain energy density is **only convex** w.r.t. $\overline{U}$ and does not satisfy the estimate (2.5).[2] Despite the convexity w.r.t. $\overline{U}$ the problem (2.1) is non convex in the joint argument $(\varphi, \overline{R})$.

The parameter $L_c > 0$ (with dimension length) introduces an **internal length** which is **characteristic** for the material, e.g. related to the grain size in a polycrystal. The internal length $L_c > 0$ is responsible for **size effects** in the sense that smaller samples may be relatively stiffer than larger samples.[3] We note the **coercivity of curvature**

$$\exists\, c^+ > 0 \quad \forall\, \mathfrak{K} \in \mathfrak{T}(3): \quad W_{\mathrm{curv}}(\mathfrak{K}) \geq c^+\,\|\mathfrak{K}\|^q , \tag{2.6}$$

which is a basic ingredient of the mathematical analysis.

The non-standard boundary condition of **strong consistent coupling** ensures that no unwanted non-classical, polar effects may occur at the Dirichlet boundary Γ. Formally, it can be obtained by setting $\mu_c = \infty$ at the Dirichlet-boundary Γ. It implies for the micropolar stretch $\overline{U}_{|\Gamma} \in \mathrm{Sym}$ and for the second Piola-Kirchhoff stress tensor $S_2 := F^{-1} D_F W_{\mathrm{mp}}(\overline{U}) \in \mathrm{Sym}$ on Γ as in the classical, non-polar case. In the following, we refer to the weaker boundary condition $\overline{U}_{|\Gamma} \in \mathrm{Sym}$ as **weak consistent coupling**. The reader should note that both weak and strong consistent coupling boundary conditions require more smoothness than a priori implied in the variational formulation in order to make sense mathematically.

It is of prime importance to realize that a linearization of this Cosserat bulk model with $\mu_c = 0$ for small displacement and small microrotations decouples the two fields of deformation φ and microrotations $\overline{R}$ and leads to the classical linear elasticity problem for the deformation.[4] For more details on the modelling of the three-dimensional Cosserat model we refer the reader to [37].

2.2 The Boltzmann axiom

In the absence of external couples and for vanishing internal length scale $L_c = 0$ taking free variations of $W_{\mathrm{mp}}(\overline{R}^T F)$ w.r.t. $\overline{R} \in \mathrm{SO}(3,\mathbb{R})$ generates an algebraic side condition (the remaining balance of angular momentum equation). It reads

$$\mathrm{skew}\left(D_{\overline{U}} W_{\mathrm{mp}}(\overline{U}) \cdot \overline{U}^T \right) = 0 . \tag{2.7}$$

It is easy to see that this implies that the **second Piola-Kirchhoff stress** $S_2(F, \overline{R}) := F^{-1} S_1(F, \overline{R}) = F^{-1} D_F \left[W_{\mathrm{mp}}(\overline{R}^T F) \right]$ **is symmetric**. This is the **Boltzmann axiom of classical non-polar elasticity postulating that the second Piola-Kirchhoff stresses and therefore the Cauchy stresses are symmetric.**

In a linearized setting, which can be obtained by writing $\overline{R} = 1\!\!1 + \overline{A} + \ldots$, $\overline{A} \in \mathfrak{so}(3,\mathbb{R})$ and $\varphi = x + u(x)$ and neglecting higher order terms in the displacement gradient ∇u and the skewsymmetric infinitesimal microrotations $\overline{A}$, the **Boltzmann axiom implies for the infinitesimal Cauchy stress** $\sigma \in \mathrm{Sym}$, **which in turn implies for** $\mu_c > 0$ **that the**

[2] The condition $F \in \mathrm{GL}^+(3,\mathbb{R})$ is necessary, otherwise $\|F - \mathrm{polar}(F)\|^2 = \mathrm{dist}^2(F, \mathrm{O}(3,\mathbb{R})) < \mathrm{dist}^2(F, \mathrm{SO}(3,\mathbb{R}))$, as can be easily seen for the reflection $F = \mathrm{diag}(1,-1,1)$.

[3] This is a common experimental observation.

[4] Thinking in the context of an infinitesimal-displacement Cosserat theory one might **erroneously believe** that $\mu_c > 0$ is strictly necessary also for a "true" finite-strain Cosserat theory.

infinitesimal microrotations $\overline{A} \in \mathfrak{so}(3,\mathbb{R})$ coincide with the skew-symmetric part of the displacement gradient ∇u. This amounts to symmetry of the linearized strains $\overline{\varepsilon} = \nabla u - \overline{A}$.

However, in the finite-strain case and for $\mu_c \geq 0$, this consequence of the Boltzmann axiom is not necessarily true. Consider e.g. the strain-energy density $W_{\rm mp}(\overline{U}) = \mu \,\|\, \operatorname{sym} \overline{U} - 1\!\!1\|^2$. Then (2.7) amounts to

$$\operatorname{skew}\left((\overline{U} + \overline{U}^T - 2\,1\!\!1)\,\overline{U}^T\right) = 0 \quad \Leftrightarrow \quad \operatorname{skew}\left((\overline{U}^T\,\overline{U}^T - 2\,\overline{U}^T\right) = 0\,. \tag{2.8}$$

It is clear that for $\overline{U} \in \mathrm{Sym}$ (the classical non-polar situation of symmetric stretches), the condition (2.7) is satisfied. However, the simple non-symmetric matrix

$$\overline{U} = \begin{pmatrix} 1 & \gamma & 0 \\ 0 & 1 & 0 \\ 0 & 0 & 1 \end{pmatrix}, \quad \gamma > 0\,, \tag{2.9}$$

corresponding to simple shear in e_1-direction, also satisfies (2.8). Therefore, **symmetry of the Cauchy-stresses in a geometrically exact Cosserat continuum does not imply that microrotations coincide with continuum rotations!** This result might be compared with a contradicting statement in [43, p.29]. As a consequence, when considering $L_c \to 0$ (limit for large samples or homogeneous response) there is quite some freedom for rotations $\overline{R}$ satisfying (2.7): they do not need to coincide with the continuum rotation $\operatorname{polar}(F)$!

2.3 Classical angular momentum and indeterminacy of microrotations

In a classical continuum, microrotations are absent of the formulation and remain therefore a priori indeterminate: they cannot automatically be identified with the continuum rotations, see Figure 3.14. The balance of angular momentum in the classical case is only a condition on the symmetry of the Cauchy stresses. If it is intended that the yet indeterminate microrotations in a classical continuum should nevertheless coincide with the continuum rotations, an additional (coupling) condition must be supplied.

The apparent ambiguity of microrotations compared to continuum rotations in the finite-strain Cosserat model with zero internal length $L_c = 0$ suggests as well to **look for additional conditions on the microrotations (boundary conditions or side conditions), independent of the chosen material parameters, which guarantee a unique homogeneous equilibrium response for both fields of deformation and microrotations simultaneously provided a homogeneous response is possible** at all. Possible candidates are the **consistent coupling condition** or a **first moment symmetry constraint**, see Corollary 2.4. Both additional conditions determine the microrotations to coincide with continuum rotations in a classical continuum model for homogeneous situations. In the Cosserat model they imply more specifically **for $\mu_c = 0$ and homogeneous response that microrotations and continuum rotations coincide**. This will be a fundamental requirement for us. It should also be noted that the additional conditions should be as weak as possible in order not to artificially stabilize the problem.

Henceforth, we postulate therefore the

Definition 2.1 (Fundamental consistency requirement)
In homogeneous response microrotations and continuum rotations should coincide. ■

2.4 Mathematical results for the Cosserat bulk problem

For conciseness we state only the obtained results for the case without external loads. It can be shown [33]:

Theorem 2.2 (Existence for Cosserat bulk model with $\mu_c > 0$)
Let $\Omega \subset \mathbb{R}^3$ be a bounded Lipschitz domain and assume for the boundary data $g_{\rm d} \in H^1(\Omega,\mathbb{R}^3)$ and $\overline{R}_{\rm d} \in W^{1,1+p}(\Omega, \mathrm{SO}(3,\mathbb{R}))$. Then (2.1) with $q \geq 2$ and either free or rigid prescription for

$\overline{R}$ *on* Γ *admits at least one minimizing solution pair* $(\varphi, \overline{R}) \in H^1(\Omega, \mathbb{R}^3) \times W^{1,q}(\Omega, \mathrm{SO}(3,\mathbb{R}))$. ■

Using the extended Korn's inequality, the following has been shown in [37, 35]:

Theorem 2.3 (Existence for Cosserat bulk model with $\mu_c = 0$)
Let $\Omega \subset \mathbb{R}^3$ *be a bounded Lipschitz domain and assume for the boundary data* $g_{\mathrm{d}} \in H^1(\Omega, \mathbb{R}^3)$ *and* $\overline{R}_{\mathrm{d}} \in W^{1,q}(\Omega, \mathrm{SO}(3,\mathbb{R}))$. *Then* (2.1) *with* $q > 3$ *and either free or rigid prescription for* $\overline{R}$ *on* Γ *admits at least one minimizing solution pair* $(\varphi, \overline{R}) \in H^1(\Omega, \mathbb{R}^3) \times W^{1,q}(\Omega, \mathrm{SO}(3,\mathbb{R}))$. ■

Corollary 2.4 (First moment symmetry constraint)
The same existence results obtain for a geometrically exact **first moment symmetry constraint** $\int_\Omega \overline{U}\, \mathrm{dV} \in \mathrm{PSym}$ *instead of extra boundary conditions for microrotations, since the constraint is closed under weak convergence of* $\overline{U}$. *The constraint ensures that the average Cosserat strain* $\frac{1}{|\Omega|}\int_\Omega \overline{U}\, \mathrm{dV}$ *is a classical strain.* ■

3 The Cosserat model in simple glide

In order to elucidate the proposed nonlinear theory, notably the impact of boundary and side conditions on the microrotations, and to be able to validate numerical results we consider now the deformation of an infinite layer of material with unit height, fixed at the bottom and sheared in e_1-direction with amount γ at the upper face. We impose the boundary conditions $g(x_1, x_2, 0) = (x_1, x_2, 0)^T$, $g(x_1, x_2, 1) = (x_1 + \gamma, x_2, x_3)^T$, $x_1, x_2 \in \mathbb{R}$. The parameter $\gamma \geq 0$ is the amount of maximal shear at the upper face per unit length. The most general deformations are of the form $\varphi(x_1, x_2, x_3) = (x_1 + u(x_1, x_3), x_2, x_3 + v(x_1, x_3))^T$. Hence we look for **energy minimizing** deformations of the form

$$\varphi(x_1,x_2,x_3) = \begin{pmatrix} x_1 + u(x_1,x_3) \\ x_2 \\ x_3 + v(x_1,x_3) \end{pmatrix}, \ \nabla\varphi(x_1,x_2,x_3) = \begin{pmatrix} 1 + u_{x_1}(x_1,x_3) & 0 & u_{x_3}(x_1,x_3) \\ 0 & 1 & 0 \\ v_{x_1}(x_1,x_3) & 0 & 1 + v_{x_3}(x_1,x_3) \end{pmatrix}, \tag{3.1}$$

with $u(x_1, 0) = 0$, $u(x_1, 1) = \gamma$. The infinite extension in e_1-direction implies that ∂_{x_1}-derivatives must vanish and from symmetry of the boundary conditions at the upper and lower face, there is no reason for a displacement in e_3-direction either. Hence the reduced kinematics

$$\varphi(x_1,x_2,x_3) = \begin{pmatrix} x_1 + u(x_3) \\ x_2 \\ x_3 \end{pmatrix}, \ \nabla\varphi(x_1,x_2,x_3) = F = \begin{pmatrix} 1 & 0 & u'(x_3) \\ 0 & 1 & 0 \\ 0 & 0 & 1 \end{pmatrix}, \tag{3.2}$$

with $u(0) = 0$, $u(1) = \gamma$ suffices. The considered problem is therefore the exact formulation of the **simple glide** in e_1-direction with amount γ at the upper face of a layer of material with unit height, fixed at the bottom.

Accordingly, we assume **microrotations** $\overline{R} \in \mathrm{SO}(3,\mathbb{R})$ and corresponding **infinitesimal microrotations** $\overline{A} \in \mathfrak{so}(3,\mathbb{R})$ of the type:

$$\overline{R}(x_1,x_2,x_3) = \begin{pmatrix} \cos\overline{\alpha}(x_3) & 0 & \sin\overline{\alpha}(x_3) \\ 0 & 1 & 0 \\ -\sin\overline{\alpha}(x_3) & 0 & \cos\overline{\alpha}(x_3) \end{pmatrix}, \quad \overline{A}(x_1,x_2,x_3) = \begin{pmatrix} 0 & 0 & \overline{\alpha}(x_3) \\ 0 & 0 & 0 \\ -\overline{\alpha}(x_3) & 0 & 0 \end{pmatrix}. \tag{3.3}$$

In the following we denote x_3 by x. Since $\|\mathfrak{K}\|^2 = \|\overline{R}^T \mathrm{D_x}\overline{R}\|^2 = \|\mathrm{D_x}\overline{R}\|^2$ and

$$\mathrm{D_x}\overline{R} = \begin{pmatrix} -\sin\overline{\alpha}(x)\,\overline{\alpha}'(x) & 0 & \cos\overline{\alpha}(x)\,\overline{\alpha}'(x) \\ 0 & 0 & 0 \\ -\cos\overline{\alpha}(x)\,\overline{\alpha}'(x) & 0 & -\sin\overline{\alpha}(x)\,\overline{\alpha}'(x) \end{pmatrix} \Rightarrow$$

$$\|\mathrm{D_x}\overline{R}\|^2 = 2\sin^2\overline{\alpha}(x)(\overline{\alpha}')^2 + 2\cos^2\overline{\alpha}(x)(\overline{\alpha}')^2 = 2|\overline{\alpha}'(x)|^2\,, \tag{3.4}$$

it holds that $\|\mathrm{D_x}\overline{R}\|^2 = \|\mathrm{D_x}\overline{A}\|^2 = 2\,|\overline{\alpha}'(x_3)|^2$.

We generally try only to find solutions for the **microrotation angle** $\overline{\alpha} : [0,1] \mapsto \mathbb{R}$ satisfying **periodic boundary conditions** $\overline{\alpha}^{(n)}(1) = \overline{\alpha}^{(n)}(0)\,, n \in \mathbb{N}$ and satisfying the **symmetry condition**

$$\overline{\alpha}(1/2 + x) = \overline{\alpha}(1/2 - x)\,, \quad x \in [0, \frac{1}{2}]\,, \tag{3.5}$$

implying that $\overline{\alpha}^{(n)}(1) = (-1)^n\,\overline{\alpha}^{(n)}(0)$. Thus $\overline{\alpha}^{(n)}(1) = \overline{\alpha}^{(n)}(0) = 0$ for $n = 2k+1$, $k \in \mathbb{N}$. Similarly, we assume periodicity for the displacement u in the form $u'(1) = u'(0)$ and the symmetry $u'(1/2+x) = u'(1/2-x)$. Explicit calculation results in

$$\begin{aligned}
\overline{R}^T F &= \begin{pmatrix} \cos\overline{\alpha}(x) & 0 & \cos\overline{\alpha}(x)\cdot u'(x) - \sin\overline{\alpha} \\ 0 & 1 & 0 \\ \sin\overline{\alpha}(x) & 0 & \sin\overline{\alpha}(x)\cdot u'(x) + \cos\overline{\alpha}(x) \end{pmatrix}\,, \\
\operatorname{sym}\overline{R}^T F &= \begin{pmatrix} \cos\overline{\alpha}(x) & 0 & \frac{\cos\overline{\alpha}(x)\cdot u'(x)}{2} \\ 0 & 1 & 0 \\ \frac{\cos\overline{\alpha}(x)\cdot u'(x)}{2} & 0 & \sin\overline{\alpha}(x)\cdot u'(x) + \cos\overline{\alpha}(x) \end{pmatrix}\,, \\
\operatorname{skew}\overline{R}^T F &= \begin{pmatrix} 0 & 0 & \frac{\cos\overline{\alpha}(x)\cdot u'(x) - 2\sin\overline{\alpha}(x)}{2} \\ 0 & 0 & 0 \\ -\frac{\cos\overline{\alpha}(x)\cdot u'(x) - 2\sin\overline{\alpha}(x)}{2} & 0 & 0 \end{pmatrix}\,.
\end{aligned} \tag{3.6}$$

Using a quadratic ansatz for the energy it is clear that our Cosserat model is physically meaningful only for small microrotation angles $\overline{\alpha}$. We apply therefore the restriction $|\overline{\alpha}| < \frac{\pi}{2}$ and $|u'| < 2$ in the following.

Next we consider the **first moment symmetry constraint for simple glide**. It reads

$$\int_0^1 \overline{R}(x)^T F(x)\,\mathrm{dx} = \begin{pmatrix} \int_0^1 \cos\overline{\alpha}(x)\,\mathrm{dx} & 0 & \int_0^1 \cos\overline{\alpha}(x)\cdot u'(x) - \sin\overline{\alpha}(x)\,\mathrm{dx} \\ 0 & 1 & 0 \\ \int_0^1 \sin\overline{\alpha}(x)\,\mathrm{dx} & 0 & \int_0^1 \sin\overline{\alpha}(x)\cdot u'(x) + \cos\overline{\alpha}(x)\,\mathrm{dx} \end{pmatrix} \in \mathrm{PSym}\,. \tag{3.7}$$

Symmetry alone amounts to

$$0 = \int_0^1 \cos\overline{\alpha}(x)\cdot u'(x) - 2\sin\overline{\alpha}(x)\,\mathrm{dx} = \int_0^1 \cos\overline{\alpha}(x)\left[u'(x) - 2\tan\overline{\alpha}(x)\right]\,\mathrm{dx}\,. \tag{3.8}$$

Let $\xi \in \mathbb{R}^3$ be an arbitrary constant vector, then positive definiteness of $\int_0^1 \overline{R}^T F\,\mathrm{dx}$ amounts to

$$\begin{aligned}
0 \le \langle \xi, \left(\int_0^1 \overline{R}(x)^T F(x)\,\mathrm{dx}\right).\xi\rangle_{\mathbb{R}^3} &= \int_0^1 \langle \xi, \left(\overline{R}(x)^T F(x)\right).\xi\rangle_{\mathbb{R}^3}\,\mathrm{dx} \\
&= \int_0^1 \langle \xi, \operatorname{sym}\left(\overline{R}(x)^T F(x)\right).\xi\rangle_{\mathbb{R}^3}\,\mathrm{dx}\,.
\end{aligned} \tag{3.9}$$

For (3.9) to hold it suffices that locally $\operatorname{sym}\left(\overline{R}(x)^T F(x)\right) \in \mathrm{PSym}$, which is true if

$$\begin{aligned}
&\begin{pmatrix} \cos\overline{\alpha}(x) & \frac{\cos\overline{\alpha}(x)\cdot u'(x)}{2} \\ \frac{\cos\overline{\alpha}(x)\cdot u'(x)}{2} & \sin\overline{\alpha}(x)\cdot u'(x) + \cos\overline{\alpha}(x) \end{pmatrix} \in \mathrm{PSym} \quad \Leftrightarrow \\
&\cos\overline{\alpha}(x) > 0\,, \quad \cos\overline{\alpha}(x)\sin\overline{\alpha}(x)u'(x) + \cos^2\overline{\alpha}(x) - \cos^2\overline{\alpha}(x)\frac{u'(x)^2}{4} > 0\,.
\end{aligned} \tag{3.10}$$

The last inequality is equivalent to $\tan\overline{\alpha}(x)\,u'(x) + 1 - \frac{u'(x)^2}{4} > 0$. Hence if $0 \le \overline{\alpha} < \frac{\pi}{2}$ and $0 \le u'(x) < 2$ positive definiteness is satisfied.

3.1 The finite-strain simple glide Cosserat problem

The geometrically exact variational problem for simple glide[5][6] with curvature exponent $q \equiv 2$ is given by

$$\int_0^1 \mu \, \| \operatorname{sym} \overline{R}^T F - 1\!\!1 \|^2 + \mu_c \, \| \operatorname{skew} \overline{R}^T F \|^2 + 2\mu \, L_c^2 |\overline{\alpha}'(x)|^2 \, \mathrm{dx} \mapsto \min . \quad \text{w.r.t. } (u, \overline{\alpha}). \tag{3.11}$$

$u(0) = 0, \; u(1) = \gamma$, Dirichlet boundary conditions for displacements,

$\overline{\alpha}(0) = \overline{\alpha}(1) = \overline{\alpha}_{\mathrm{d}}$, various rigid boundary conditions for microrotations,

$0 = \operatorname{skew}(\overline{R}^T F)_{\{0,1\}} \Leftrightarrow 2 \tan \overline{\alpha}(0) = u'(0), \; 2 \tan \overline{\alpha}(1) = u'(1), \quad |\overline{\alpha}| < \frac{\pi}{2}$,

weak/strong consistent coupling boundary conditions,

$\overline{\alpha}'(0) = \overline{\alpha}'(1) = 0$, Neumann boundary conditions for microrotations,

$$0 = \int_0^1 \cos \overline{\alpha}(x) \cdot u'(x) - 2 \sin \overline{\alpha}(x) \, \mathrm{dx}, \quad \textbf{first moment symmetry constraint} \; . \tag{3.12}$$

In terms of $(u', \overline{\alpha})$ the **finite energy expression** W_{finite} is given by

$$\begin{aligned} W_{\text{finite}}(u', \overline{\alpha}, \overline{\alpha}') &= \mu \left(2(\cos \overline{\alpha} - 1)^2 + \frac{u'^2}{2} + \frac{\sin^2 \overline{\alpha} \, u'^2}{2} + 2(\cos \overline{\alpha} - 1) \sin \overline{\alpha} \, u' \right) \\ &+ \mu_c \left(\frac{\cos^2 \overline{\alpha} \, u'^2}{2} - 2 \cos \overline{\alpha} \sin \overline{\alpha} \, u' + 2 \sin^2 \overline{\alpha} \right) + 2\mu \, L_c^2 |\overline{\alpha}'|^2 \\ &= \mu \left(2(\cos \overline{\alpha} - 1)^2 + \frac{u'^2}{2} + \frac{\sin^2 \overline{\alpha} \, u'^2}{2} + 2(\cos \overline{\alpha} - 1) \sin \overline{\alpha} \, u' \right) \\ &+ \frac{\mu_c}{2} \cos^2 \overline{\alpha} \, [2 \tan \overline{\alpha} - u']^2 + 2\mu \, L_c^2 |\overline{\alpha}'|^2 . \end{aligned} \tag{3.13}$$

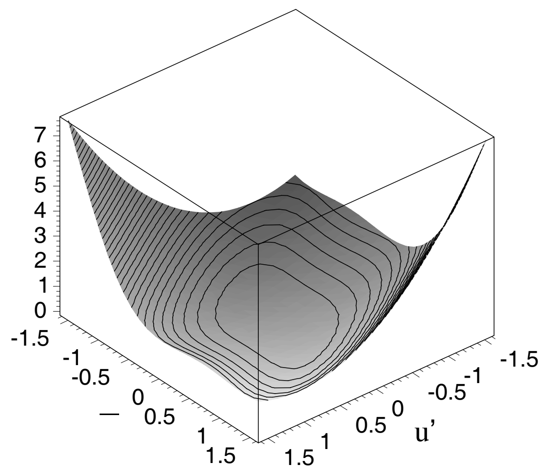

Figure 3.1: Plot of the **non-convex** energy $W_{\text{finite}}(u', \overline{\alpha}, \overline{\alpha}')$ (3.13) for $\mu_c = 0$ and $L_c = 0$.

[5]Note that by the analytical results recalled in section (2.4) we already know that minimum energy configurations in the finite-strain case exist for three types of boundary conditions: Dirichlet, pure Neumann and Neumann with first moment symmetry constraint. In the one-dimensional case the coercivity $|\overline{\alpha}'(x)|^2$ is enough to guarantee strong convergence of minimizing sequences of microrotations $(\sin \overline{\alpha}_k, \cos \overline{\alpha}_k)$ in the space of continuous functions due to Sobolev embedding theorems. These **existence results**, however, **do not cover automatically the consistent coupling condition**.

[6]As we will see subsequently, it is a delicate matter to specify independent boundary conditions for the microrotations $\overline{\alpha}$. Somehow it requires to know the solution of the boundary value problem in advance. In this sense a classical rigid boundary condition is nothing but a first guess, perhaps useful as start value in a numerical scheme.

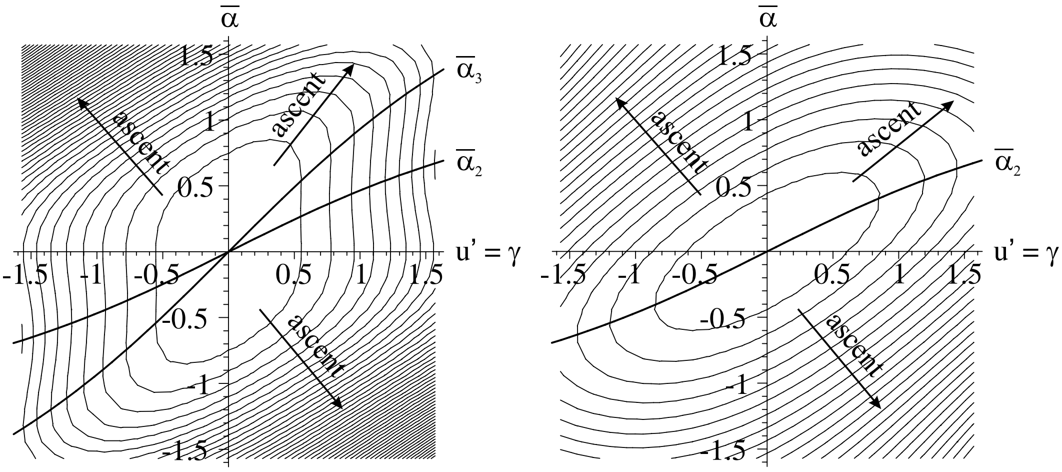

Figure 3.2: Contour plot of W_{finite} for $\mu_c = 0$ (left) and $\mu_c = \mu$ (right) with $L_c = 0$. For $\mu_c = 0$ one observes **non-convexity** of the local strain part of the energy (non-convex sub-levels), while large μ_c has a convexifying influence. Here, $\overline{\alpha}_2 = \arctan\frac{\gamma}{2}$ and $\overline{\alpha}_3 = 2\arctan\frac{\gamma}{2}$ are the possible homogeneous microrotations for homogeneous macroscopic deformation $u' = \gamma$ if $\mu_c = 0$. Vertical lines are tangent to contour-lines in the points $\overline{\alpha}_1 = 0$, $\overline{\alpha}_2$, $\overline{\alpha}_3$.

3.1.1 The finite-strain Euler-Lagrange equations

The equilibrium equations in the fully finite-strain case are obtained by taking free variations w.r.t. $(u, \overline{\alpha})$. **Balance of forces** in the finite-strain case results from taking free variations w.r.t. displacements u respecting the boundary conditions, hence

$$
\begin{aligned}
\forall \phi \in C_0^\infty([0,1],\mathbb{R}):\quad 0 &= \frac{\mathrm{d}}{\mathrm{dt}}_{|t=0} \int_0^1 W_{\text{finite}}(u'(x) + t\phi'(x), \overline{\alpha}(x), \overline{\alpha}'(x))\,\mathrm{dx} \;\Rightarrow \\
0 &= \int_0^1 \big[-\mu\, u''(x) - \mu\left(2\sin\overline{\alpha}(x)\cos\overline{\alpha}(x)\overline{\alpha}'(x)u'(x) + \sin^2\overline{\alpha}(x)\, u''(x)\right) \\
&\quad - 2\mu\left((\cos\overline{\alpha}(x) - 1)\cos\overline{\alpha}(x)\overline{\alpha}'(x) - \sin^2\overline{\alpha}(x)\overline{\alpha}'(x)\right) \\
&\quad - \mu_c\left(-2\cos\overline{\alpha}(x)\sin\overline{\alpha}(x)\overline{\alpha}'(x)u'(x) + \cos^2\overline{\alpha}(x)u''(x)\right) \\
&\quad -2\mu_c\left(-\sin^2\overline{\alpha}(x)\,\overline{\alpha}'(x) + \cos^2\overline{\alpha}(x)\,\overline{\alpha}'(x)\right)\big]\cdot\phi\,\mathrm{dx}\,, \qquad (3.14)
\end{aligned}
$$

where we already performed partial integration and used the zero boundary condition for the testfunction $\phi \in C_0^\infty([0,1],\mathbb{R})$. **Balance of angular momentum** is obtained from taking free variation w.r.t. microrotation angles $\overline{\alpha}$. We have

$$
\begin{aligned}
&\forall\, \delta\overline{\alpha} \in C^\infty([0,1],[0,2\pi)):\\
&0 = \frac{\mathrm{d}}{\mathrm{dt}}_{|t=0} \int_0^1 W_{\text{finite}}(u'(x), \overline{\alpha}(x) + t\,\delta\overline{\alpha}(x), \overline{\alpha}'(x) + t\,\delta\overline{\alpha}'(x))\,\mathrm{dx} \\
&= \int_0^1 -4\mu(\cos\overline{\alpha}(x) - 1)\,\sin\overline{\alpha}(x)\,\delta\overline{\alpha}(x) + \frac{\mu}{2}\,2\sin\overline{\alpha}(x)\,\cos\overline{\alpha}(x)u'(x)^2\,\delta\overline{\alpha} \\
&\qquad + 2\mu(\cos\overline{\alpha}(x) - 1)\,\cos\overline{\alpha}(x)\,u'(x)\,\delta\overline{\alpha}(x) \\
&\quad + 2\mu(-\sin\overline{\alpha}(x)\,\sin\overline{\alpha}(x)u'(x)\delta\overline{\alpha}(x) + 4\mu\,L_c^2\overline{\alpha}'(x)(\delta\overline{\alpha})'(x) \qquad (3.15)\\
&\quad + \mu_c\left(\frac{2\cos\overline{\alpha}(x)(-\sin\overline{\alpha}(x))}{2}\delta\overline{\alpha}(x)\,u'(x)^2 - 2\cos\overline{\alpha}(x)\cos\overline{\alpha}(x)\delta\overline{\alpha}(x)\,u'(x)\right. \\
&\quad +2\sin\overline{\alpha}(x)\sin\overline{\alpha}(x)\delta\overline{\alpha}(x)u'(x) + 4\sin\overline{\alpha}(x)\cos\overline{\alpha}(x)\delta\overline{\alpha}(x))\;\mathrm{dx} \\
&= \int_0^1 \mu\left[-4\,(\cos\overline{\alpha}(x) - 1)\,\sin\overline{\alpha}(x)\,\delta\overline{\alpha}(x) + \sin\overline{\alpha}(x)\,\cos\overline{\alpha}(x)u'(x)^2\,\delta\overline{\alpha}(x)\right. \\
&\qquad + 2\mu(\cos\overline{\alpha}(x) - 1)\,\cos\overline{\alpha}(x)\,u'(x)\,\delta\overline{\alpha}(x) \\
&\qquad +2\mu(-\sin\overline{\alpha}(x)\,\sin\overline{\alpha}(x)u'(x)\delta\overline{\alpha}(x)\;\;]
\end{aligned}
$$

$$+\mu_c \Big[-\cos\overline{\alpha}(x)\sin\overline{\alpha}(x)\delta\overline{\alpha}(x)\,u'(x)^2 - 2\cos\overline{\alpha}(x)\cos\overline{\alpha}(x)\delta\overline{\alpha}(x)\,u'(x)$$
$$+ 2\sin\overline{\alpha}(x)\sin\overline{\alpha}(x)\delta\overline{\alpha}(x)u'(x) + 4\sin\overline{\alpha}(x)\cos\overline{\alpha}(x)\delta\overline{\alpha}(x)\Big]$$
$$- 4\mu\,L_c^2\overline{\alpha}''(x)\delta\overline{\alpha}(x)\,\mathrm{dx} + 4\mu\,L_c^2\left[\overline{\alpha}'(1)\,\delta\overline{\alpha}(1) - \overline{\alpha}'(0)\,\delta\overline{\alpha}(0)\right] .$$

Since the values $\delta\overline{\alpha}(1), \delta\overline{\alpha}(0)$ can be chosen arbitrary, the last line shows that **natural boundary conditions for the microrotation angle** $\overline{\alpha}$ amount to $\overline{\alpha}'(0) = 0$, $\overline{\alpha}'(1) = 0$. The complete equilibrium system in strong form reads then

$$\begin{aligned}
0 &= u''\,\left[2\mu + (\mu-\mu_c)\,\cos^2\overline{\alpha}\right] + 2\,(\mu-\mu_c)\,\sin\overline{\alpha}\,\cos\overline{\alpha}\,\overline{\alpha}'\,u' \\
&\quad + 2(\mu+\mu_c)\left[\cos^2\overline{\alpha} - \sin^2\overline{\alpha}\right]\,\overline{\alpha}' - 2\mu\cos\overline{\alpha}\,\overline{\alpha}', \qquad \textbf{force balance}, \qquad (3.16)\\
0 &= \mu\,\cos\overline{\alpha}\,\left(2(\cos\overline{\alpha}-1) + \sin\overline{\alpha}\,u'\right)\,[u' - 2\tan\overline{\alpha}] \\
&\quad - \mu_c\left(-\cos\overline{\alpha}\,\sin\overline{\alpha}\,[2\tan\overline{\alpha} - u'] + 2\right)\,[u' - 2\tan\overline{\alpha}] - 4\mu\,L_c^2\,\alpha'', \quad \textbf{torque balance}.
\end{aligned}$$

The force balance equation $(3.16)_1$ can also be written as

$$\begin{aligned}
0 &= \frac{\mathrm{d}}{\mathrm{dx}}\left[\tau_{\text{finite}}(u'(x), \overline{\alpha}(x))\right], \quad \tau_{\text{finite}}(u', \overline{\alpha}) = D_{u'}W_{\text{finite}}(u', \overline{\alpha}, \overline{\alpha}'), \\
\tau_{\text{finite}}(u', \overline{\alpha}) &= \mu\,\left(u' + \sin^2\overline{\alpha}\,u' + 2(\cos\overline{\alpha}-1)\,\sin\overline{\alpha}\right) - \mu_c\,\cos^2\overline{\alpha}\,[2\tan\overline{\alpha} - u'] . \qquad (3.17)
\end{aligned}$$

Based on $(3.16)_1$ the following estimate (independent of $\mu_c \geq 0$) can be shown for weak solutions of (3.16) with $u' \in L^2((0,1),\mathbb{R})$:

$$\int_0^1 |u''(s)|\,\mathrm{ds} \leq K\,\left(1 + \|\overline{\alpha}'\|_{L^2((0,1))}\right) . \qquad (3.18)$$

Since for $L_c > 0$ minimizers of (3.11) are weak solutions of (3.16) with $u \in H^1((0,1),\mathbb{R})$ and $\overline{\alpha} \in H^1((0,1),[0,2\pi))$, estimate (3.18) implies that $u \in W^{2,1}((0,1),\mathbb{R}) \subset C^1([0,1],\mathbb{R})$. Hence u' is continuous up to the boundary and **consistent coupling is justified**.

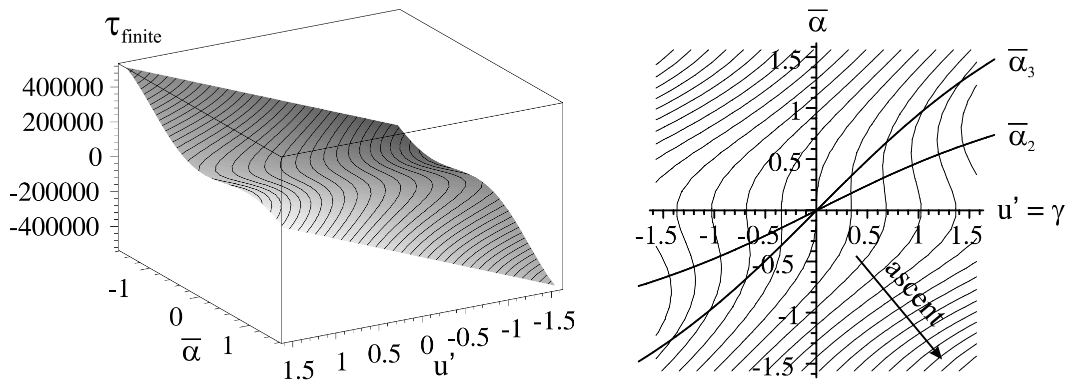

Figure 3.3: 3D and contour plot of τ_{finite} for $\mu_c = 0$. Force balance requires $\tau_{\text{finite}} = const.$. Balance of angular momentum for $\mu_c = 0$ and $L_c = 0$ requires additionally $\overline{\alpha}(x) \in \{0, \overline{\alpha}_2 = \arctan\frac{u'(x)}{2}, \overline{\alpha}_3 = 2\arctan\frac{u'(x)}{2}\}$.

3.1.2 Possible homogeneous solutions

Let us investigate in a first step the possible **homogeneous solutions** $(u,\overline{\alpha})$ of the coupled system (3.16) for $0 \leq \overline{\alpha} < \frac{\pi}{2}$ and $0 \leq u' < 2$. We observe that if the microrotation $\overline{\alpha}$ is homogeneous, then the problem for the macroscopic displacement u is a homogeneous, strictly convex minimization problem which implies that the homogeneous displacement $u(x) = \gamma\,x$ is the unique solution of (3.16).[7] It remains to determine those homogeneous microrotation

[7]This homogeneous response $u(x) = \gamma\,x$ is the unique minimizer in simple glide for any strictly Legendre-Hadamard elliptic finite elasticity formulation.

angles $\overline{\alpha}$ which are solutions of the balance of angular momentum equation. For $\mu_c = 0$ equation $(3.16)_2$ corresponds for homogeneous $\overline{\alpha}$ to

$$
\begin{aligned}
0 = &-4\mu\,(\cos\overline{\alpha} - 1)\sin\overline{\alpha} + \mu\,\sin\overline{\alpha}\,\cos\overline{\alpha}\,(u')^2 \\
&+ 2\mu\,(\cos\overline{\alpha} - 1)\,\cos\overline{\alpha}\,(u') - 2\mu\,\sin\overline{\alpha}\,\sin\overline{\alpha}\,(u')\,.
\end{aligned}
\tag{3.19}
$$

For $|u'| < 2$ and for $|\overline{\alpha}| < \frac{\pi}{2}$, this equation has no solution for $\overline{\alpha}$ with $\cos\overline{\alpha} = 0$, therefore we may divide by $\cos\overline{\alpha}$ to obtain (in the homogeneous case: $u' = \gamma$) after rearranging

$$0 = [2\,(\cos\overline{\alpha} - 1) + \sin\overline{\alpha}\,(u')] \cdot [(u') - 2\,\tan\overline{\alpha}]\ . \tag{3.20}$$

Equating again to zero the two brackets the first solution is obviously given by $\overline{\alpha} = \overline{\alpha}_1 = 0$. The second solution is $\overline{\alpha}_2 = \arctan\frac{\gamma}{2}$. For a third solution note the two well-known relations

$$\frac{1}{2}(1 - \cos\overline{\alpha}) = \sin^2\frac{\overline{\alpha}}{2}\,, \quad \sin\overline{\alpha} = 2\sin\frac{\overline{\alpha}}{2}\,\cos\frac{\overline{\alpha}}{2}\,. \tag{3.21}$$

Equating to zero the first bracket in (3.20) is equivalent to

$$\frac{\gamma}{4}\,\sin\overline{\alpha} = \frac{1}{2}(1 - \cos\overline{\alpha})\,. \tag{3.22}$$

Using (3.21) on both sides, we obtain

$$\frac{\gamma}{4}\left[2\sin\frac{\overline{\alpha}}{2}\,\cos\frac{\overline{\alpha}}{2}\right] = \sin^2\frac{\overline{\alpha}}{2} \quad \Rightarrow \quad \frac{\gamma}{2} = \frac{\sin\frac{\overline{\alpha}}{2}}{\cos\frac{\overline{\alpha}}{2}} = \tan\frac{\overline{\alpha}}{2}\,. \tag{3.23}$$

Hence, the third solution is given by $\overline{\alpha}_3 = 2\,\arctan\frac{\gamma}{2} = 2\,\overline{\alpha}_2$.

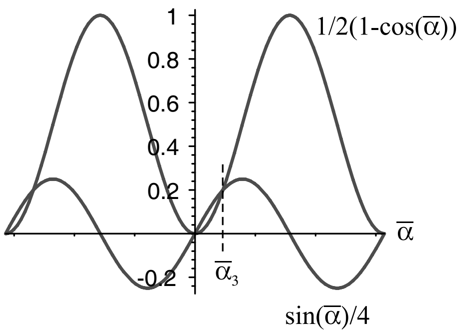

Figure 3.4: Graph for (3.22) with $\gamma = 1$.

Altogether,

$$\overline{\alpha}_1 = 0\,, \quad \overline{\alpha}_2 = \arctan\frac{\gamma}{2}\,, \quad \overline{\alpha}_3 = 2\,\arctan\frac{\gamma}{2}\,. \tag{3.24}$$

Each of these three possible homogeneous responses corresponds to physically distinguished situations. For general $\mu_c \geq 0$ it can be seen that three distinct homogeneous solutions of (3.16) cease to exist if $\mu_c \geq \mu_c^{\mathrm{crit}}$. For $\mu_c \geq \mu_c^{\mathrm{crit}}$ only $\overline{\alpha}_2$ survives, see Figure 3.5.

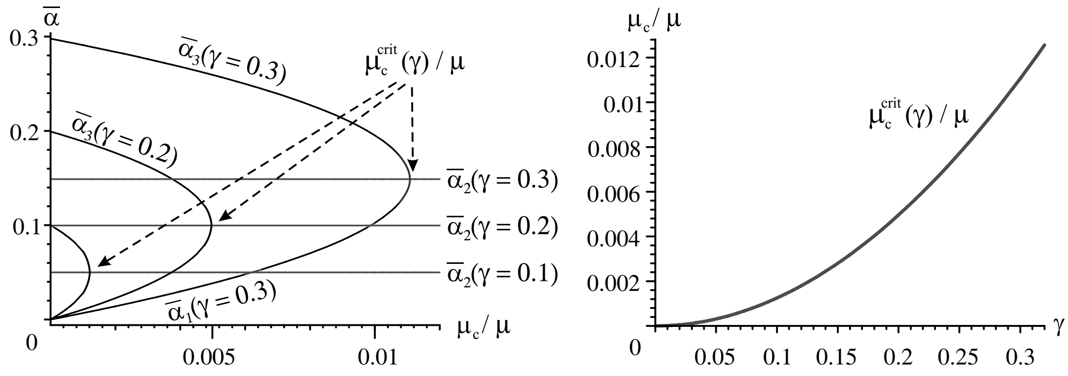

Figure 3.5: Solution for various μ_c/μ of the finite-strain torque-balance equation $(3.16)_2$ for homogeneous situations $u' = \gamma$ and applied shear $\gamma = 0.1$, $\gamma = 0.2$ and $\gamma = 0.3$. Three distinct solutions for $\overline{\alpha}$ cease to exist if $\mu_c < \mu_c^{\text{crit}} = \mu_c^{\text{crit}}(\gamma) = \mu\,\frac{\sqrt{4+\gamma^2}-2}{\sqrt{4+\gamma^2}}$. For $\mu_c \geq \mu_c^{\text{crit}}$ only $\overline{\alpha}_2 = \arctan\frac{\gamma}{2}$ survives as homogeneous solution. A typical **pitchfork bifurcation** at μ_c^{crit}. **This implies that in order to guarantee a unique microstructure homogeneous response of the finite-strain Cosserat model in simple glide for arbitrary applied shear $\gamma > 0$ (large) one must take $\mu_c \geq \mu$, provided no extra conditions on the microrotations are specified! Similarly, if three homogeneous solutions should exist for arbitrary applied shear $\gamma > 0$ (small), one must take $\mu_c = 0$.**

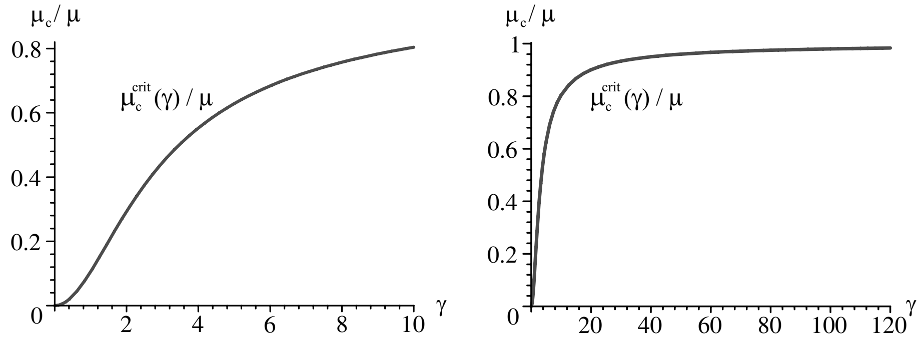

Figure 3.6: μ_c^{crit}/μ of the finite-strain torque-balance equation $(3.16)_2$ for homogeneous situations $u' = \gamma$ and various (large) γ.

3.1.3 Physical interpretation of different homogeneous response

Now we try to interpret the previously obtained non-uniqueness of the homogeneous solution in terms of assumed substructure properties.

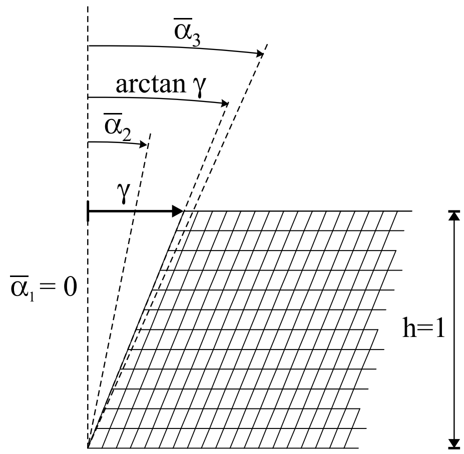

Figure 3.7: Graph for $\overline{\alpha}_1, \overline{\alpha}_2, \overline{\alpha}_3$. Homogeneous macroscopic deformation $u(x) = \gamma\, x$ and homogeneous microrotation $\overline{\alpha}(x) = \arctan \frac{\gamma}{2}$ should constitute the classical aligned homogeneous response.

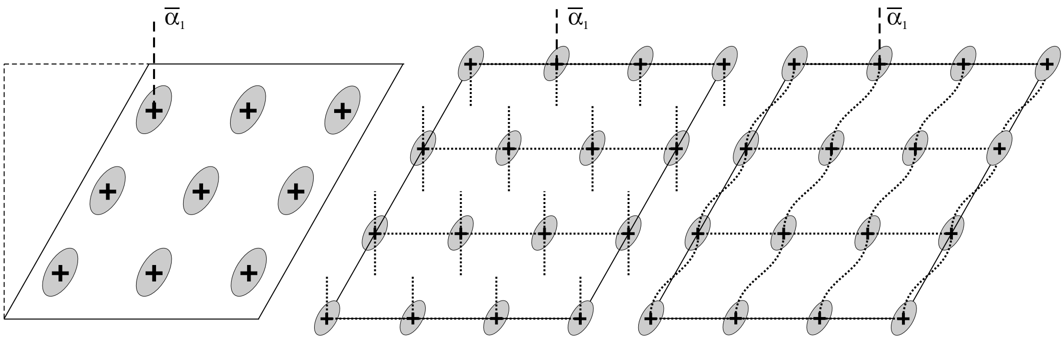

Figure 3.8: Different possibilities of the Cosserat problem (3.16) to realize homogeneous response. Left: Visualization of continuum deformation $\mathbf{F}$ (ellipsis) and microrotation $\overline{\alpha}_1 = 0$ corresponding to no rotation of the substructure. The "underwinded" case. Thinking in terms of a granular assembly the individual grains would be non-cohesive. Middle: Assumed vertical substructure (represented by broken lines) must tear up to follow this deformation. Right: Assumed vertical beams of a substructure must bend to follow this deformation. Note that classical continuum theory does not control angular momentum for these beams (and they would not be in angular equilibrium).

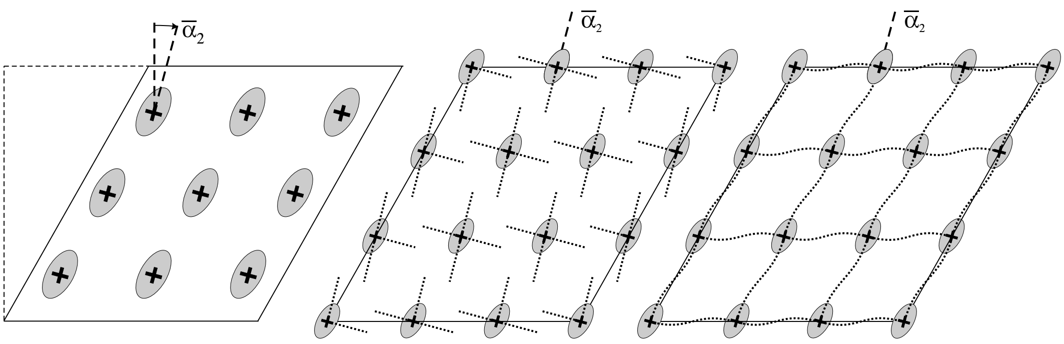

Figure 3.9: Different possibilities of the Cosserat problem (3.16) to realize homogeneous response. Left: Visualization of continuum deformation $\mathbf{F}$ (ellipsis) and microrotation $\overline{\alpha}_2 = \arctan \frac{\gamma}{2}$. Microrotations are **aligned** (coincide) with continuum rotations. Note that the continuum rotations themselves differ from the homogeneous deformation. Middle: Assumed vertical and horizontal substructure must tear up to follow this deformation. Right: Assumed vertical and horizontal beams of a substructure must bend to follow this deformation. Here, beams would be in angular equilibrium.

The right beam solution in Figure 3.9 represents the only solution in terms of a restricted interpretation of the Cosserat model as a beam model, which does not tear up and which satisfies in addition angular equilibrium in the knots. However, it has to be realized that **the Cosserat model is strictly more than a homogenized description of a beam structure**, e.g. allowing for discontinuities in the assumed beam structure and the microrotations cannot necessarily be identified with the rotations of the substructure. The next picture shows that the curvature energy acts like torsional springs between different material points: only gradients in microrotations are taken into account.

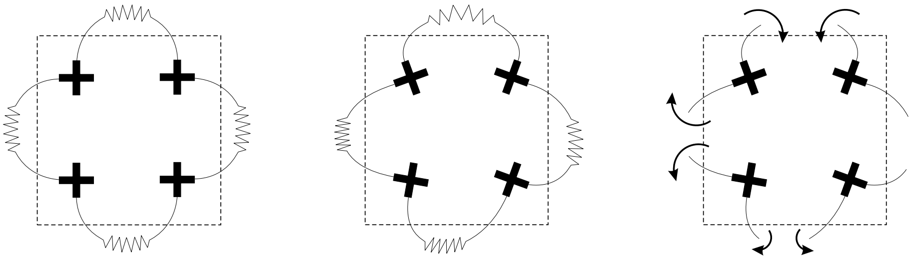

Figure 3.10: Left: Torsional springs (with spring parameter $\mu\, L_c^2 > 0$) inter-connect microrotations in the Cosserat model (note the distinction to beams). Middle: Under gradients in microrotation torsional springs begin to act and curvature effects take place. Right: Cosserat theory ensures equilibrium in angular momentum for these springs.

We are faced with the question whether $\mu_c > 0$ can prevent the previous tearing up as observed in Figure 3.9. The parameter $\mu_c > 0$ can be interpreted as an additional elastic spring connecting microrotations and continuum rotations.

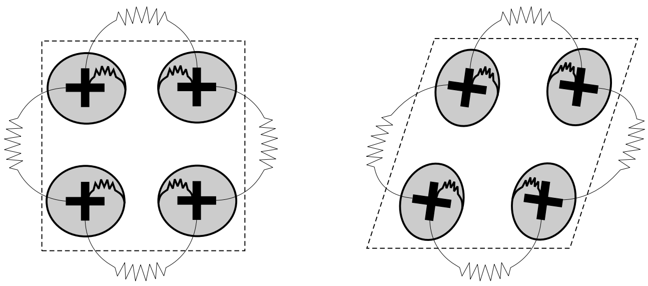

Figure 3.11: Left: Additional elastic springs corresponding to $\mu_c > 0$ connect microrotations with continuum rotation. Right: In simple glide this μ_c-connection leads automatically to the right continuous beam solution from Figure 3.9.

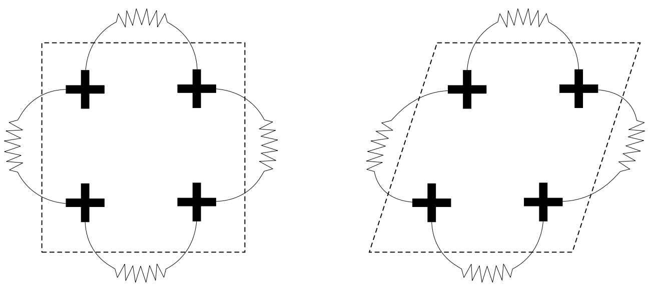

Figure 3.12: Left: For $\mu_c = 0$ the direct connection between microrotations and continuum rotations does not exist. Right: In simple glide $\mu_c = 0$ allows the discontinuous beam solution from Figure 3.8 or 3.13.

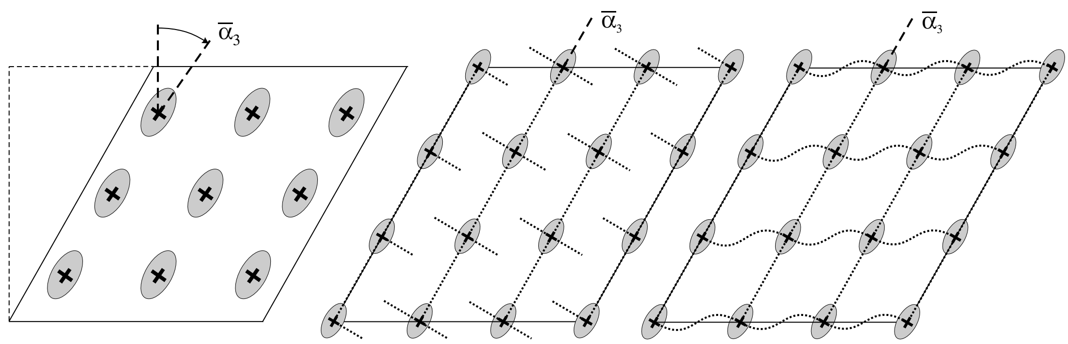

Figure 3.13: Different possibilities of the Cosserat problem (3.16) to realize homogeneous response. Left: Visualization of continuum deformation $\mathbf{F}$ (ellipsis) and microrotation $\overline{\alpha}_3 = 2\arctan\frac{\gamma}{2}$. The "overwinded" case. Difficult to interpret physically. Middle: Assumed horizontal substructure must tear up to follow this deformation. Right: Horizontal beams of an assumed substructure bend to follow this deformation. Once more, these beams would not be in angular equilibrium!

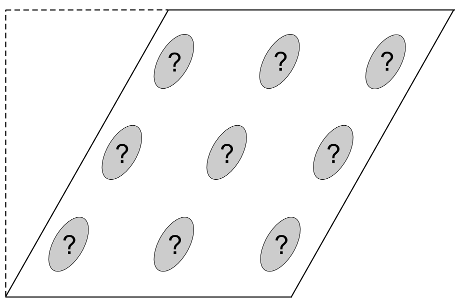

Figure 3.14: The classical continuum case in which microrotations are a priori indeterminate because they do not explicitly appear. In order to determine the microrotations nevertheless, one needs to supply additional constitutive requirements. We propose consistent coupling or the first moment symmetry constraint. This determines the microrotations to coincide with the continuum rotations for homogeneous response, the "aligned" solution.

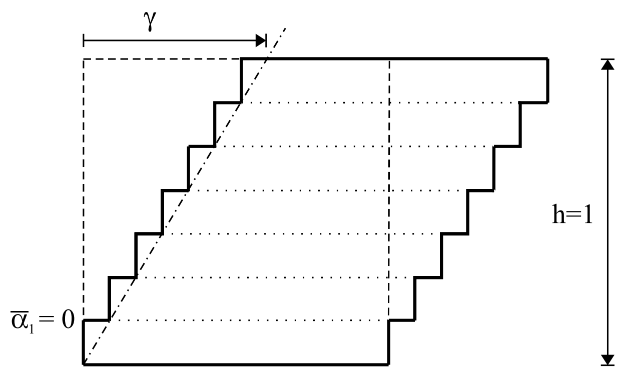

Figure 3.15: Macroscopic simple glide can be generated by different microscopic mechanisms: here "deck of cards solution" corresponding to **plastic slip** along horizontal glide planes. Dislocations pile up along the glide planes. The "substructure" does not rotate at all - this would suggest $\overline{\alpha}_1 = 0$ in the Cosserat model.

3.1.4 Shear stress response

In the finite-strain case, we evaluate the generated tangential shear stresses τ at the upper face where maximal shear occurs. They are given as

$$
\begin{aligned}
\tau_{\text{finite}} &= \langle S_1(F(1), \overline{R}(1)).e_3, e_1\rangle \\
&= \langle \overline{R}(1)\left(2\mu\, \mathrm{sym}(\overline{R}(1)^T F(1) - 1\!\!1) + 2\mu_c\, \mathrm{skew}(\overline{R}(1)^T F(1))\right).e_3, e_1\rangle\,.
\end{aligned}
\tag{3.25}
$$

For **consistent coupling** conditions, the **homogeneous deformation** $u(x) = \gamma\, x$ and $\tan\overline{\alpha}(0) = \tan\overline{\alpha}(x) = \frac{\gamma}{2}$ is always a solution and **leads to a nonlinear, strictly monotone** shear stress response at the upper face with

$$
\begin{aligned}
\tau_{\text{finite}}^{\text{cons,hom}} &= \mu u'(1) + \mu \sin^2\overline{\alpha}(1) u'(1) + 2\mu \sin\overline{\alpha}(1)(\cos\overline{\alpha}(1) - 1) \\
&= \mu\gamma + \mu \sin^2(\arctan\frac{\gamma}{2})\,\gamma + 2\mu \sin(\arctan\frac{\gamma}{2})\,(\cos(\arctan\frac{\gamma}{2}) - 1)\,.
\end{aligned}
$$

Using the well known relations $\arctan(x) = \arcsin(\frac{x}{\sqrt{1+x^2}})$ and $\arctan(x) = \arccos(\frac{1}{\sqrt{1+x^2}})$ shows

$$
\tau_{\text{finite}}^{\text{cons,hom}} = \mu\gamma + \frac{\mu\gamma^3}{4+\gamma^2} + \frac{2\mu\gamma\,(2-\sqrt{4+\gamma^2})}{4+\gamma^2} = 2\,\mu\,\frac{\left(\sqrt{4+\gamma^2}-1\right)}{\sqrt{4+\gamma^2}}\cdot\gamma\,.
\tag{3.26}
$$

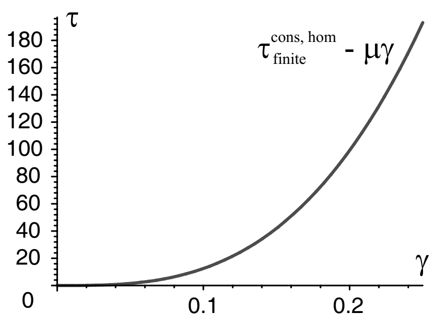

Figure 3.16: Difference of $\tau_{\text{finite}}^{\text{cons,hom}}$ to linear solution $\tau_{\text{small}} = \mu\,\gamma$. $\tau_{\text{finite}}^{\text{cons,hom}}\big|_{\gamma=0.2} = 20099.2562$.

It is obvious that for the consistent coupling condition and the Neumann-problem with first moment symmetry constraint, the homogeneous response with "aligned" substructure is the only possible homogeneous solution of (3.16) while the pure Neumann-response permits three homogeneous solutions. For the finite-strain problem (3.16), at this point, we do not know whether the classical homogeneous response for Neumann with first moment symmetry constraint or consistent coupling condition for all $\mu_c \geq 0$ is the only one possible or realizes the minimum energy. It may be that inhomogeneous equilibria exist! In order to approach this problem analytically, we investigate a simplification in the following.

3.2 The partially reduced Cosserat problem in simple glide

We consider a **fourth order reduction** of the energy and introduce for small microrotation angle $\overline{\alpha}$ the approximations $\cos\overline{\alpha} \sim 1 - \frac{\overline{\alpha}^2}{2}$, $\sin\overline{\alpha} \sim \overline{\alpha} - \frac{\overline{\alpha}^3}{3!}$. **Keeping terms up to order four** in the energy density (3.13) we get a **reduced energy density expression** W_{red}

$$
\begin{aligned}
W_{\text{red}}(u', \overline{\alpha}, \overline{\alpha}') &= \mu\left(\frac{1+\overline{\alpha}^2}{2}u'^2 + \frac{\overline{\alpha}^4}{2} - \overline{\alpha}^3\, u'\right) + 2\mu_c\left(\left(\frac{u'}{2} - \overline{\alpha}\right)^2 - \frac{\overline{\alpha}^2\, u'^2}{4} + \frac{2}{3}\overline{\alpha}^3 u' - \frac{\overline{\alpha}^4}{3}\right) \\
&\quad + 2\mu\, L_c^2 |\overline{\alpha}'|^2 \qquad\qquad (3.27) \\
&= \mu\left(\frac{1+\overline{\alpha}^2}{2}u'^2 + \frac{\overline{\alpha}^4}{2} - \overline{\alpha}^3\, u'\right) + 2\mu_c\left(\frac{u'}{2} - \overline{\alpha}\right)\left[\left(\frac{u'}{2} - \overline{\alpha}\right) - \frac{\overline{\alpha}^2}{6}\,(3u' - 2\overline{\alpha})\right] \\
&\quad + 2\mu\, L_c^2 |\overline{\alpha}'|^2\,.
\end{aligned}
$$

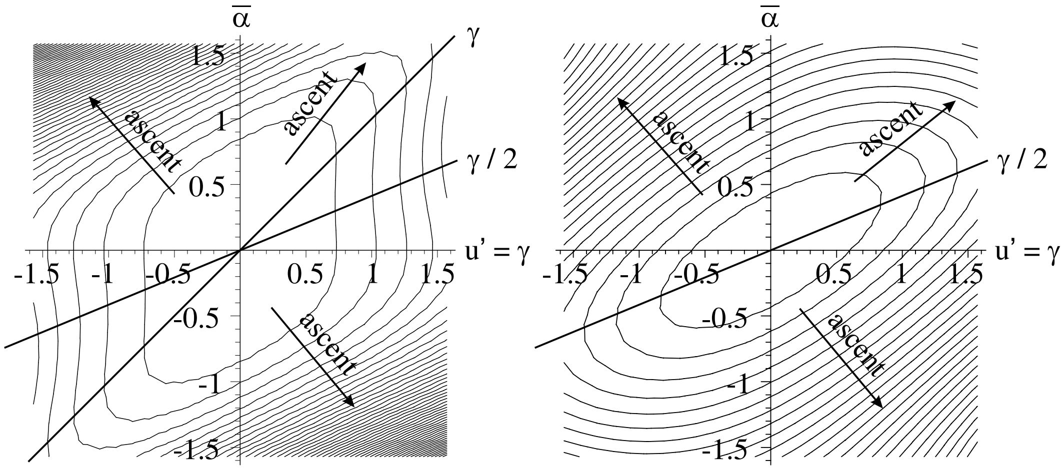

Figure 3.17: Contour plot of W_{red} (3.27) for $\mu_c = 0$ (left) and $\mu_c = \mu$ (right) with $L_c = 0$. Similar observation as in Figure 3.2: for $\mu_c = 0$ the energy W_{red} is **not convex** and large μ_c has a convexifying influence. Close quantitative agreement of W_{red} with W_{finite} in the considered range of parameters. For $\mu_c = 0$ possible homogeneous solutions for microrotations are $\overline{\alpha}_1^{\text{hom}} = 0$, $\overline{\alpha}_2^{\text{hom}} = \frac{\gamma}{2}$ or $\overline{\alpha}_3^{\text{hom}} = \gamma$.

The minimization problem based on W_{red} is coercive w.r.t. $\overline{\alpha} \in L^4((0,1),\mathbb{R})$ only if $3\mu - 4\mu_c > 0$ ($\mu = \mu_c$ excluded). In this case minimizers $u \in H^1((0,1),\mathbb{R})$ and $\overline{\alpha} \in H^1((0,1),\mathbb{R})$ exist.

3.2.1 The reduced finite-strain Euler-Lagrange equations

The corresponding equilibrium system may be obtained by free-variation of W_{red} w.r.t. u and $\overline{\alpha}$. The result coincides with the simplification of the two equilibrium equations in (3.16) based on W_{finite} by considering the second order expansions $\cos\overline{\alpha}(x) = 1 - \frac{\overline{\alpha}^2}{2} + \ldots$, $\sin\overline{\alpha} = \overline{\alpha} - \frac{\overline{\alpha}^3}{6} + \ldots$ and **keeping terms up to order three** in the variables $(u', \overline{\alpha})$. The corresponding weak consistent coupling condition is obtained by setting formally $\mu_c = \infty$ at the boundary and requiring that the reduced energy W_{red} remains finite there. This implies the **reduced consistent coupling condition**

$$\begin{aligned} 2\tan\overline{\alpha}(0) = u'(0) \quad &\Rightarrow \quad 2\,\overline{\alpha}(0) = u'(0)\,, \\ 2\tan\overline{\alpha}(1) = u'(1) \quad &\Rightarrow \quad 2\,\overline{\alpha}(1) = u'(1)\,, \end{aligned} \tag{3.28}$$

which coincides in fact with a simple linearization of the boundary condition.[8] The **reduced Euler-Lagrange equations** in strong form read[9]

$$\begin{aligned} 0 &= u'' + \frac{2(\mu-\mu_c)\,\overline{\alpha}\,\overline{\alpha}'u'}{\mu(1+\overline{\alpha}^2)+\mu_c(1-\overline{\alpha}^2)} + \frac{(-4\mu_c - 3\mu)\,\overline{\alpha}^2\overline{\alpha}'}{\mu(1+\overline{\alpha}^2)+\mu_c(1-\overline{\alpha}^2)} - \frac{2\mu_c\overline{\alpha}'}{\mu(1+\overline{\alpha}^2)+\mu_c(1-\overline{\alpha}^2)}\,, \\ 0 &= \mu\left(\frac{1}{2}\overline{\alpha}^3 + \frac{1}{4}\overline{\alpha}u'^2 - \frac{3}{4}\overline{\alpha}^2u' - L_c^2\overline{\alpha}''\right) - \mu_c\left(\frac{1}{4}\overline{\alpha}u'^2 + \frac{2}{3}\overline{\alpha}^3 - \overline{\alpha}^2u' + \left(\frac{u'}{2} - \overline{\alpha}\right)\right)\,, \\ & u(0) = 0,\ u(1) = \gamma, \quad \text{Dirichlet boundary conditions for displacements}\,, \\ & \overline{\alpha}(0) = \overline{\alpha}(1) = \overline{\alpha}_{\text{d}}, \quad \text{various rigid boundary conditions}\,, \\ & 2\,\overline{\alpha}(0) = u'(0),\ 2\,\overline{\alpha}(1) = u'(1), \quad \text{reduced consistent coupling}\,, \\ & \overline{\alpha}'(0) = \overline{\alpha}'(1) = 0, \quad \text{natural boundary conditions}\,, \\ 0 &= \int_0^1 2\overline{\alpha}(x) - u'(x)\,\text{dx}, \quad \text{reduced first moment symmetry constraint}\,. \end{aligned} \tag{3.29}$$

[8] This does not coincide with a third order approximation of the nonlinear consistent coupling condition! For us the variational structure is primordial. The same comment applies to the reduced first moment constraint: a simple third order reduction would be inconsistent with the possible homogeneous solutions for $\mu_c = 0$ and $L_c = 0$.

[9] $\tan x = x + \frac{x^3}{3} + \ldots$

Based on $(3.29)_1$ and the coercivity requirement $3\mu - 4\mu_c > 0$, the following estimate (independent of $\mu_c \geq 0$) can be shown for weak solutions of (3.29) with $u' \in L^2((0,1),\mathbb{R})$:

$$\int_0^1 |u''(s)|\, \mathrm{ds} \leq K\, \left(1 + \|\overline{\alpha}'\|_{L^2((0,1))}\right) . \tag{3.30}$$

Since for $L_c > 0$ minimizers of (3.27) are weak solutions of (3.29) with $u \in H^1((0,1),\mathbb{R})$ and $\overline{\alpha} \in H^1((0,1),\mathbb{R})$, estimate (3.30) implies that $u \in W^{2,1}((0,1),\mathbb{R}) \subset C^1([0,1],\mathbb{R})$. Hence u' is continuous up to the boundary and **consistent coupling is justified also for the reduced model**.

Observe that the "**aligned**" homogeneous deformation remains a solution of the reduced system for reduced consistent coupling and reduced first moment symmetry constraint if and only if $\mu_c = 0$.[10]

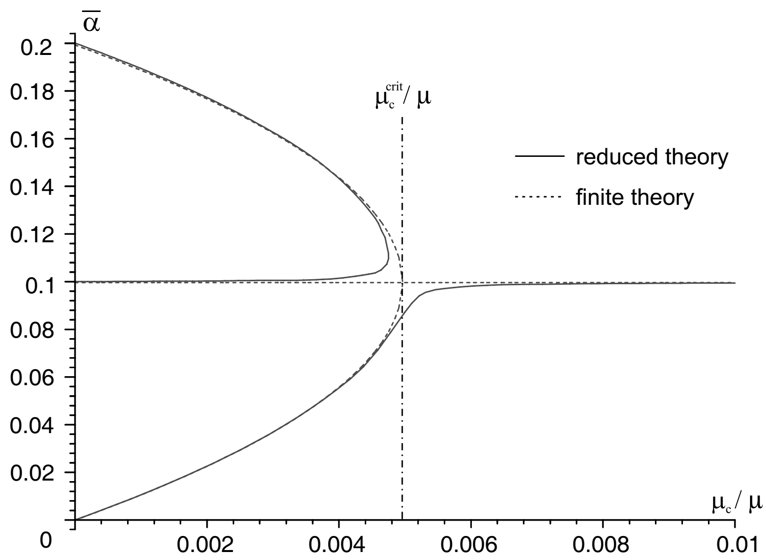

Figure 3.18: (Bifurcation diagram of homogeneous response) Solution for various μ_c/μ of the finite-strain torque-balance equation $(3.16)_2$ compared with the reduced torque-balance equation $(3.29)_2$ for homogeneous situation $u' = \gamma$ and $\gamma = 0.2$. Choosing $\mu_c \approx \mu_c^{\text{crit}}$ shows that the finite-strain aligned homogeneous solution $\overline{\alpha}_2 = \arctan\frac{\gamma}{2} \approx \frac{\gamma}{2}$ is not stable under approximation; this highlights again the critical influence of $\mu_c > 0$ on the model, compare with Figure 3.30

It seems to be natural to **require** that the solution of the reduced coupled boundary value problem (3.29), notably the **shear profile microrotation angle** $\overline{\alpha}$, is in fact **independent of** the **shear modulus** μ as it is the case in classical finite-strain elasticity or linear elasticity. This condition can only be met with $\mu_c = 0$.

For $\mu_c = 0$ the system of balance equations (3.29) reduces further to

$$\begin{aligned}
0 &= \frac{2\overline{\alpha}\,\overline{\alpha}'}{1+\overline{\alpha}^2}\,u' - \frac{3\overline{\alpha}^2\overline{\alpha}'}{1+\overline{\alpha}^2} + u'' \;\Leftrightarrow\; 0 = \frac{\mathrm{d}}{\mathrm{dx}}\left[\tau_{\text{red}}(u'(x),\overline{\alpha}(x))\right], \quad \tau_{\text{red}} = \mu\,\left(u' + \overline{\alpha}^2 u' - \overline{\alpha}^3\right),\\
0 &= \frac{1}{2}\overline{\alpha}^3 + \frac{1}{4}\overline{\alpha}u'^2 - \frac{3}{4}\overline{\alpha}^2 u' - L_c^2\overline{\alpha}'', \qquad (3.31)\\
&u(0) = 0,\; u(1) = \gamma, \quad \text{Dirichlet boundary conditions for displacements},\\
&\overline{\alpha}(0) = \overline{\alpha}(1) = \overline{\alpha}_{\mathrm{d}}, \quad \text{various rigid boundary conditions},\\
&2\,\overline{\alpha}(0) = u'(0),\; 2\,\overline{\alpha}(1) = u'(1), \quad \text{reduced consistent coupling},\\
&\overline{\alpha}'(0) = \overline{\alpha}'(1) = 0, \quad \text{natural boundary conditions},
\end{aligned}$$

[10]The factor of μ_c in equation $(3.29)_2$ cannot be factorized w.r.t. $(\frac{u'}{2} - \overline{\alpha})$. This means for $\mu_c > 0$ that $\overline{\alpha} = \frac{\gamma}{2}$ is not anymore a homogeneous solution, see Figure 3.18.

$$\int_0^1 \overline{\alpha}(x)\,\mathrm{dx} = \frac{\gamma}{2}, \quad \text{reduced first moment symmetry constraint}\,.$$

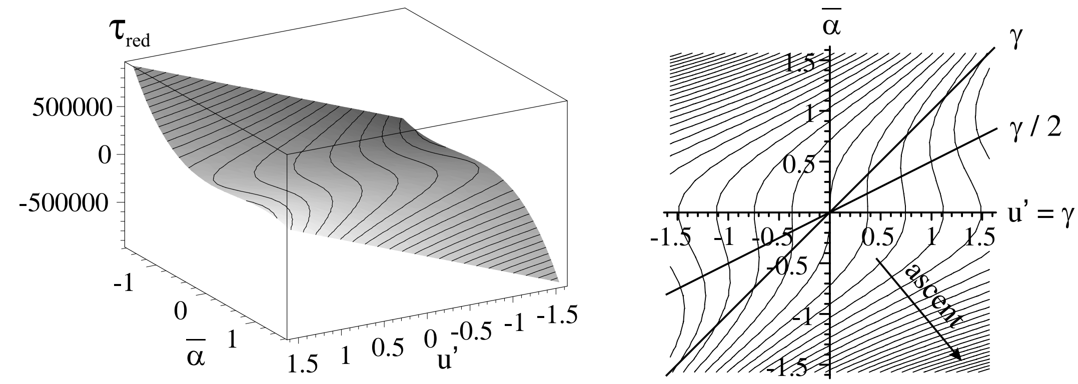

Figure 3.19: 3D and contour plot of $\tau_{\rm red}$ for $\mu_c = 0$. Lines $\overline{\alpha}_1 = 0$, $\overline{\alpha}_2 = \frac{u'}{2}$ and $\overline{\alpha}_3 = u'$. The balance equations for $\mu_c = 0$ and $L_c = 0$ require $\tau_{\rm red}(u', \overline{\alpha}) = const.$ and $\overline{\alpha}(x) \in \{0, \frac{u'(x)}{2}, u'(x)\}$. Homogeneous solutions are not necessarily unique and equilibria are not necessarily homogeneous!

Using $(3.31)_2$ and Neumann conditions for $\overline{\alpha}$ implies $0 = \int_0^1 \frac{\overline{\alpha}}{2}\,(\overline{\alpha} - u')\,(\overline{\alpha} - \frac{u'}{2})\,\mathrm{dx}$ which does not coincide with the first moment symmetry constraint. In this sense, the first moment symmetry constraint is an independent condition.

3.2.2 Microstructure solutions for $L_c = 0$

To gain more insight, we try to construct solutions to (3.31) for the the limit case of **vanishing internal length** $L_c = 0$, disregarding the possible boundary values for $\overline{\alpha}$ in a first approach. We call this the case with "**free rotations**" since the curvature terms are not involved. In any case solutions will satisfy $\tau_{\rm red}(u', \overline{\alpha}) = const.$ Let us integrate the first equation of (3.31) at given $\overline{\alpha}(x)$ by means of the variations of constants formula. This shows that for $u' > 0$

$$\begin{aligned} u'(x) &= e^{-\int_0^x \frac{2\overline{\alpha}(t)\overline{\alpha}'(t)}{1+\overline{\alpha}^2(t)}\,\mathrm{dt}} \cdot \left(u'(0) + \int_0^x \frac{3\overline{\alpha}^2\overline{\alpha}'(t)}{1+\overline{\alpha}^2(t)}\, e^{\int_0^t \frac{2\overline{\alpha}(s)\overline{\alpha}'(s)}{1+\overline{\alpha}^2(s)}\,\mathrm{ds}}\right)\mathrm{dt} \\ &= \frac{1+\overline{\alpha}^2(0)}{1+\overline{\alpha}^2(x)} \left(u'(0) + \frac{[\overline{\alpha}^3(x) - \overline{\alpha}^3(0)]}{1+\overline{\alpha}^2(0)}\right). \end{aligned} \tag{3.32}$$

The last equation is the **integrated form** of the **force balance** equation. This equation does not imply that u' is continuous if $\overline{\alpha}$ is not! The Dirichlet boundary conditions for u imply the additional integral condition

$$\gamma - 0 = u(1) - u(0) = \int_0^1 u'(x)\,\mathrm{dx} = \int_0^1 \frac{1+\overline{\alpha}^2(0)}{1+\overline{\alpha}^2(x)} \left(u'(0) + \frac{[\overline{\alpha}^3(x) - \overline{\alpha}^3(0)]}{1+\overline{\alpha}^2(0)}\right) \mathrm{dx}\,. \tag{3.33}$$

The second (now purely algebraic) equation of (3.31) (in fact the reduced Boltzmann-axiom (2.8))

$$0 = \frac{1}{2}\overline{\alpha}^3 + \frac{1}{4}\overline{\alpha}u'^2 - \frac{3}{4}\overline{\alpha}^2 u' = \frac{\overline{\alpha}}{2}\,(\overline{\alpha} - u')\left(\overline{\alpha} - \frac{u'}{2}\right), \tag{3.34}$$

can be solved locally for $\overline{\alpha}(x)$ at given $u'(x)$. The three distinct solutions $\overline{\alpha}$ are given by

$$\overline{\alpha}(x) \in \{0, \frac{u'(x)}{2}, u'(x)\} \qquad (\text{cf. } \overline{\alpha}_1, \overline{\alpha}_2, \overline{\alpha}_3 \text{ in } (3.24))\,. \tag{3.35}$$

For $x \in (0,1)$, reinserting the restriction (3.35) into (3.32) shows that we have **locally** altogether only **two different values** for $u'(x)$ at our disposition, determined by three equations (two coinciding)

$$\left[1+\overline{\alpha}^2(0)\right]u'(0)-\overline{\alpha}^3(0)=\begin{cases}u'(x) & \text{insert } \overline{\alpha}(x)=0\\ u'(x)+\frac{1}{8}\,u'(x)^3 & \text{insert } \overline{\alpha}(x)=\frac{u'(x)}{2}\\ u'(x) & \text{insert } \overline{\alpha}(x)=u'(x)\end{cases}. \tag{3.36}$$

Taking $\overline{\alpha}(0)=0$ or $\overline{\alpha}(0)=u'(0)$ leads to $const=u'(0)=u'(x)$ for all x, hence the classical macroscopic homogeneous response. In order to generate a non-trivial response we choose $u'(0)$, $\overline{\alpha}(0)$ such that the left hand side is

$$\left[1+\overline{\alpha}^2(0)\right]u'(0)-\overline{\alpha}^3(0)=\gamma+\delta^+,\quad \delta^+>0\,. \tag{3.37}$$

The value $\delta^+>0$ will be determined subsequently. Satisfying now the reduced consistent coupling condition $\overline{\alpha}(0)=\frac{u'(0)}{2}$ in (3.37) implies that $u'(0)+\frac{1}{8}\,u'(0)^3=\gamma+\delta^+$ and (3.36) turns for $u'(x)$ into two possible conditions

$$\gamma+\delta^+=\begin{cases}u'(x) & \text{with } \overline{\alpha}(x)=0\\ u'(x)+\frac{1}{8}\,u'(x)^3 & \text{with } \overline{\alpha}(x)=\frac{u'(x)}{2}\end{cases}. \tag{3.38}$$

In a first approach we determine the values of u' in the "**symmetric**" form

$$u'(x)=\begin{cases}\gamma+\delta^+\\ \gamma-\delta^+\end{cases}, \tag{3.39}$$

such that the second value $u'=\gamma-\delta^+$ is also satisfying (3.38). Therefore $\delta^+>0$ is the unique real solution of the equation

$$(\gamma-\delta^+)+\frac{1}{8}(\gamma-\delta^+)^3=\gamma+\delta^+\,. \tag{3.40}$$

This equality ensures that the stress $\tau_{\rm red}$ is constant, while u' and $\overline{\alpha}$ need not be constant. Writing $\delta^+=c^+\cdot\gamma$ instead, yields equivalently

$$(1-c^+)^3=\left(\frac{4}{\gamma}\right)^2 c^+\,. \tag{3.41}$$

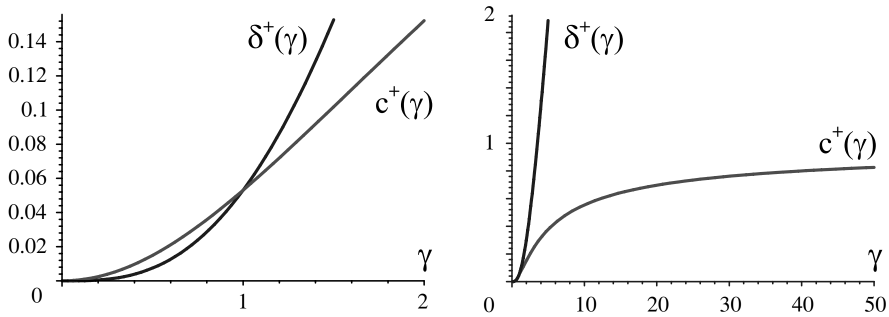

Figure 3.20: Graph for $c^+(\gamma)$ and $\delta^+(\gamma)$ for small γ (left) and large γ (right).

For $\gamma\to\infty$ we have $\delta^+(\gamma)\to\gamma$, $c^+(\gamma)\to 1$ and $\delta^+=\delta^+(\gamma)$ is a monotone increasing function of γ. This implies

$$u'(x)=\begin{cases}\gamma_2=\gamma+\delta^+(\gamma)\\ \gamma_1=\gamma-\delta^+(\gamma)\end{cases}, \tag{3.42}$$

and notably $u'(0)=\gamma-\delta^+(\gamma)=\gamma_1$. Now consider the four straight lines

$$v_1(x)=\gamma_1\,x,\quad v_2(x)=\gamma_1\,x+(\gamma-\gamma_1),\quad v_3(x)=\gamma_2\,x,\quad v_4(x)=\gamma_2\,x+(\gamma-\gamma_2)\,. \tag{3.43}$$

The lines v_1 and v_4 intersect at $x = \frac{1}{2}$, the same for v_2 and v_3.

A **family of weak solutions** of (3.31) with $L_c = 0$ and $\overline{\alpha}(0) = \frac{u'(0)}{2}$, $u'(0) = \gamma - \delta^+$ is given as a **continuous combination of piecewise affine functions with slopes parallel to** $v_i, i = 1, \ldots, 4$, satisfying $u(0) = 0$, $u(1) = \gamma$. This is the expected **microstructure**. The constructed displacements u are **absolutely continuous**, but do not belong to $H^2((0,1), \mathbb{R})$. The microstructure family and the classical aligned homogeneous solution ($\alpha' = 0$, $u'' = 0$) both satisfy

$$\begin{aligned}
u'(x) &= \frac{1+\overline{\alpha}^2(0)}{1+\overline{\alpha}^2(x)}\left(u'(0) + \frac{[\overline{\alpha}^3(x) - \overline{\alpha}^3(0)]}{1+\overline{\alpha}^2(0)}\right) \quad \text{and} \quad \tau_{\text{red}}(u', \overline{\alpha}) = const.\,, \\
0 &= \frac{1}{2}\overline{\alpha}^3 + \frac{1}{4}\overline{\alpha}u'^2 - \frac{3}{4}\overline{\alpha}^2 u'\,, \\
u(0) &= 0,\ u(1) = \gamma, \quad \text{Dirichlet boundary conditions for displacements}\,, \\
2\overline{\alpha}(0) &= u'(0), \quad 2\overline{\alpha}(1) = u'(1)\,, \quad \text{linearized consistent coupling}\,, \\
\overline{\alpha}'(0) &= \overline{\alpha}'(1) = 0, \quad \text{pure Neumann boundary conditions}\,.
\end{aligned} \tag{3.44}$$

Any symmetric solution (3.5) w.r.t. $x = \frac{1}{2}$ must have $\overline{\alpha}(1) = \frac{u'(1)}{2}$, $u'(1) = \gamma - \delta^+$ and satisfies the linearized consistent coupling condition. Symmetry, however, is not enough to single out a unique response. We may consider different solutions, e.g. that one which has the **least number of weak discontinuity points**. It is given by

$$u_\flat(x) = \begin{cases} (\gamma - \delta^+)\,x & 0 \le x \le \frac{1}{2} - \frac{1}{4} \\ (\gamma + \delta^+)\,x - \frac{\delta^+}{2} & \frac{1}{2} - \frac{1}{4} \le \frac{1}{2} + \frac{1}{4} \\ (\gamma - \delta^+)\,x + \delta^+ & \frac{1}{2} + \frac{1}{4} \le x \le 1 \end{cases}, \quad \overline{\alpha}_\flat(x) = \begin{cases} \frac{\gamma - \delta^+}{2} & 0 \le x \le \frac{1}{2} - \frac{1}{4} \\ 0 & \frac{1}{2} - \frac{1}{4} \le \frac{1}{2} + \frac{1}{4} \\ \frac{\gamma - \delta^+}{2} & \frac{1}{2} + \frac{1}{4} \le x \le 1 \end{cases}, \tag{3.45}$$

showing the (expected?, sharp) S-type symmetric shear profile.[11] [12]

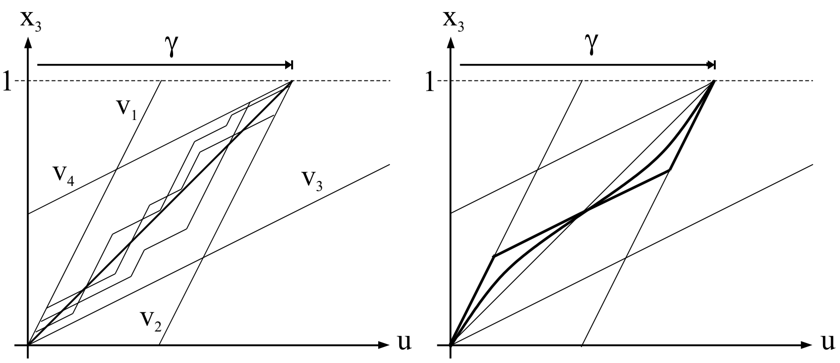

Figure 3.21: Left: Constructed family of equilibrium microstructure solutions (3.43) in simple glide for $\mu_c = 0$, $L_c = 0$ under **reduced consistent coupling conditions and for pure Neumann-conditions** since $\overline{\alpha}'(0) = \overline{\alpha}'(1) = 0$. Right: Point symmetric microstructure with least number of weak discontinuities (3.45) and expected regularized profile for $L_c > 0$ with linearized consistent coupling. Slopes of v_i are magnified.

For this solution of the reduced formulation we evaluate the generated shear force response at the upper face. They are

$$\begin{aligned}
\tau_{\text{red}} &= D_{u'}W_{\text{red}}(u'(1), \overline{\alpha}(1), \overline{\alpha}'(1)) = \mu\,\left(u'(1) + \overline{\alpha}^2(1)u'(1) - \overline{\alpha}^3(1)\right) \\
&= \mu\left(u'(1) + \left(\frac{u'(1)}{2}\right)^2 u'(1) - \left(\frac{u'(1)}{2}\right)^3\right).
\end{aligned} \tag{3.46}$$

[11]The constructed solution satisfies the reduced Boltzmann axiom yet the solution does not coincide with the classical homogeneous solution.

[12]Taking $\overline{\alpha} = u' = \gamma + \delta^+$ instead of $\overline{\alpha} = 0$ will give a higher energy and is therefore excluded.

This implies for the homogeneous and the microstructure solution (3.45), respectively

$$\tau_{\text{red}}^{\text{cons,hom}} = \mu\,(1+\frac{1}{8}\gamma^2)\,\gamma, \qquad \tau_{\text{red}}^{\text{cons,micro},\flat} = \mu\,(1+c^+(\gamma))\,\gamma\,, \tag{3.47}$$

with $c^+(\gamma) \in (0,1)$ from (3.41). This result suggests (cf. Figure 3.22) that the response with **microstructure** due to free rotations is always **weaker** (energetically favourable) than the still possible homogeneous response.[13]

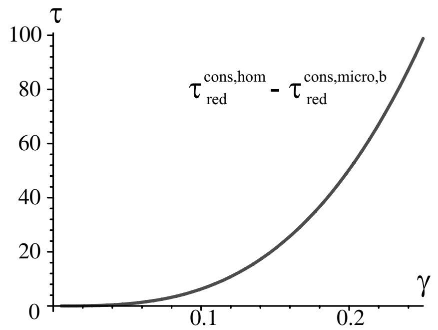

Figure 3.22: Difference of $\tau_{\text{red}}^{\text{cons,hom}}$ and $\tau_{\text{red}}^{\text{cons,micro},\flat}$. $\tau_{\text{red}}^{\text{cons,hom}}{}_{|\gamma=0.2} = 20100$ and $\tau_{\text{red}}^{\text{cons,micro},\flat}{}_{|\gamma=0.2} = 20049.6287$.

Whether the "symmetric" microstructure solution represents a minimizer under reduced consistent coupling conditions is not immediately clear. To investigate this let us compare the corresponding energy levels. It holds

$$\begin{aligned}
I_{\text{red}}^{\text{hom}}(\gamma) &= \int_0^1 W_{\text{red}}(u'(x),\overline{\alpha}(x),\overline{\alpha}'(x))\,\mathrm{dx}_{|_{u'=\gamma,\,\overline{\alpha}=\frac{u'}{2}=\frac{\gamma}{2}}}\\
&= \int_0^1 \mu\left(\frac{1+\overline{\alpha}(x)^2}{2}\,(u'(x))^2 + \frac{\overline{\alpha}(x)^4}{2} - \overline{\alpha}(x)^3\,u'(x)\right)\,\mathrm{dx}_{|_{u'=\gamma,\,\overline{\alpha}=\frac{u'}{2}=\frac{\gamma}{2}}}\\
&= \mu\int_0^1\left[\frac{\gamma^2}{2}+\frac{\gamma^4}{32}\right]\,\mathrm{dx} = \frac{\mu}{2}\,\gamma^2\left[1+\frac{\gamma^2}{16}\right]\,, && (3.48)\\
I_{\text{red}}^{\text{micro},\flat}(\gamma) &= \int_0^1 W_{\text{red}}(u'(x),\overline{\alpha}(x),\overline{\alpha}'(x))\,\mathrm{dx}\\
&= \int\limits_{u'=\gamma_1,\,\overline{\alpha}=\frac{\gamma_1}{2}} W_{\text{red}}(u'(x),\overline{\alpha}(x),\overline{\alpha}'(x))\,\mathrm{dx} + \int\limits_{u'=\gamma_2,\,\overline{\alpha}=0} W_{\text{red}}(u'(x),\overline{\alpha}(x),\overline{\alpha}'(x))\,\mathrm{dx}\\
&= \frac{1}{2}\left[\frac{\mu}{2}(u'(x))^2\left[1+\frac{(u'(x))^2}{16}\right]\right]_{u'=\gamma-\delta^+} + \frac{1}{2}\left[\frac{\mu}{2}(u'(x))^2\right]_{u'=\gamma+\delta^+}\\
&= \frac{\mu}{4}\left((u'(x))^2\left[1+\frac{(u'(x))^2}{16}\right]_{|_{u'=\gamma-\delta^+}} + (u'(x))^2_{|_{u'=\gamma+\delta^+}}\right)\,. && (3.49)
\end{aligned}$$

Figure 3.24 shows that the "symmetric" microstructure with least number of weak discontinuities energetically already beats the homogeneous solution. Let us consider also another, geometrically different equilibrium-microstructure solution. Consider the parallelogram given by (3.43). Choose a number $n \in \mathbb{N}$ and subdivide the edge starting with v_1 in $n+1$ equal parts and subdivide the other edge consisting of a part of v_2 into n equal parts. Draw a corresponding grid covering the parallelogram. The **"lamination"** solution is a continuous curve having alternating slopes in each box, starting and ending with slope $\gamma_1 = \gamma - \delta^+$, i.e. parallel to v_1.

[13]The weak discontinuities inherent in this microstructure might be seen as a precursor to **fracture**. The road to fracture starts with homogeneous solutions, which turn into smooth inhomogeneous solutions $u \in H^2$, which degenerate into solutions with weak discontinuities $u \in H^1 \setminus H^2$, which finally fail along glide planes with $u \notin W^{1,1}$.

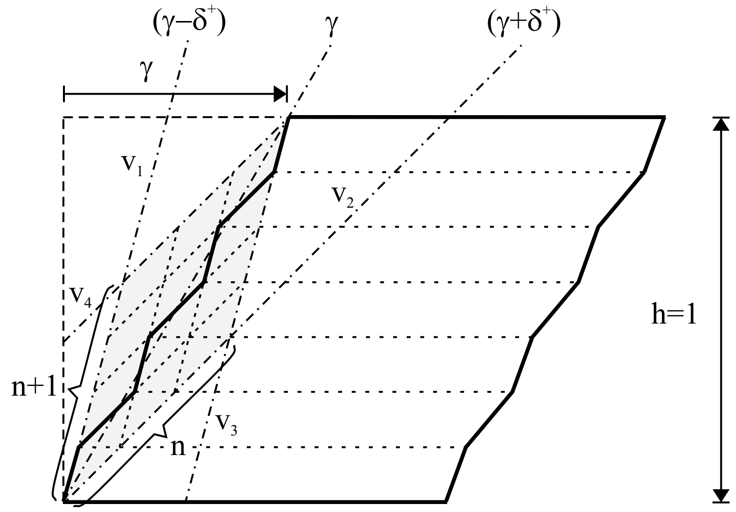

Figure 3.23: Macroscopic simple glide can be generated by different microscopic mechanisms: here periodic elastic "lamination" of layers. The homogeneous solution is a pointwise limit of the lamination response as the number of laminates tends to infinity. It is clear that a numerical algorithm with $L_c > 0$ has difficulties to find this lamination equilibrium solution for $L_c = 0$: the homogeneous response with curvature seems computationally to be locally stable.

The corresponding energy level of the lamination solution is given as

$$
\begin{aligned}
I_{\text{red}}^{\text{lam}}(\gamma) &= \int_0^1 W_{\text{red}}(u'(x), \overline{\alpha}(x), \overline{\alpha}'(x))\, \mathrm{dx} \\
&= \int\limits_{u'=\gamma_1,\, \overline{\alpha}=\frac{\gamma_1}{2}} W_{\text{red}}(u'(x), \overline{\alpha}(x), \overline{\alpha}'(x))\, \mathrm{dx} + \int\limits_{u'=\gamma_2, \overline{\alpha}=0} W_{\text{red}}(u'(x), \overline{\alpha}(x), \overline{\alpha}'(x))\, \mathrm{dx} \\
&= \frac{1}{2}\left[\frac{\mu}{2}(u'(x))^2\left[1+\frac{(u'(x))^2}{16}\right]\right]_{u'=\gamma-\delta+} + \frac{1}{2}\left[\frac{\mu}{2}(u'(x))^2\right]_{u'=\gamma+\delta+} \\
&= \frac{\mu}{4}\left((u'(x))^2\left[1+\frac{(u'(x))^2}{16}\right]_{|_{u'=\gamma-\delta+}} + (u'(x))^2_{|_{u'=\gamma+\delta+}}\right). \qquad (3.50)
\end{aligned}
$$

In effect, as far as energy levels are concerned, all members of the "symmetric" microstructure response have the same energy level. We observe that the graph of the lamination solution is pointwise arbitrarily close to the homogeneous response for $n \to \infty$.

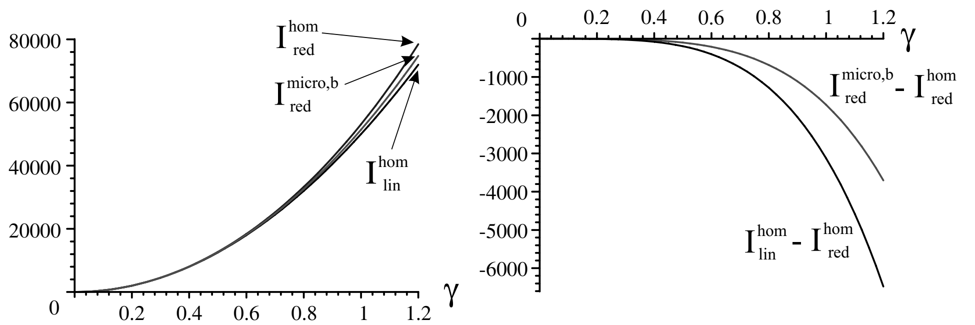

Figure 3.24: Left: $I_{\text{red}}^{\text{hom}}$ and $I_{\text{red}}^{\text{micro},\flat}$ for various γ are very close. Right: Difference of $I_{\text{red}}^{\text{hom}}$ and $I_{\text{red}}^{\text{micro},\flat}$. The microstructure response energetically beats the aligned homogeneous response! $I_{\text{red}}^{\text{hom}}(\gamma = 0.2) = 2005$, $I_{\text{red}}^{\text{micro},\flat}(\gamma = 0.2) = 2002.487592$ and $I_{\text{lin}}^{\text{hom}}(\gamma = 0.2) = 2000$.

The construction to obtain microstructure solutions can be generalized by giving up the "symmetry", i.e. by splitting δ^+ into to different values δ_1 and δ_2 such that u' is allowed to take the two values $\gamma - \delta_1 < \gamma + \delta_2$.[14] The corresponding energy is then given as

$$I^\sharp_{\rm red} = \frac{\mu}{2}\left(\frac{\delta_2}{\delta_1+\delta_2}(u'(x))^2\left[1+\frac{(u'(x))^2}{16}\right]_{|u'=\gamma-\delta_1} + \frac{\delta_1}{\delta_1+\delta_2}(u'(x))^2_{|u'=\gamma+\delta_2}\right), \tag{3.51}$$

where δ_2 is chosen such that

$$(\gamma+\delta_2) = (\gamma-\delta_1) + \frac{1}{8}(\gamma-\delta_1)^3, \tag{3.52}$$

replacing (3.40). The parallelogram construction in conjunction with (3.52) demands $0 < \delta_1 < \gamma$ and $0 < \delta_2$. Choosing δ_1 and δ_2 appropriately it is possible to beat the homogeneous response and be also better than the "symmetric" microstructure. The infimum of the energy levels of $I^\sharp_{\rm red}$ in the admissible range for δ_1 and δ_2 is given by $I^{\rm hom}_{\rm lin} = \mu\frac{\gamma^2}{2}$, see Figure 3.25. The infimum energy level is realized, however, only as solution of the minimizing (non-aligned) homogeneous Neumann problem, i.e. as $u(x) = \gamma\, x$ and $\overline{\alpha}(x) = 0$ or $\overline{\alpha}(x) = u'(x) = \gamma$. Both minimizing (non-aligned) homogeneous Neumann solutions do not satisfy consistent coupling (nor the first moment symmetry constraint). The reader should note that the microstructure solution incidentally also represents an equilibrium under pure Neumann conditions ($\overline{\alpha}$ is constant at the boundary). Hence, while consistent coupling allows for non-trivial equilibrium solutions it is not stable w.r.t energy minimization! **There do not exist energy minimizers for consistent coupling with $\mu_c = 0$ and $L_c = 0$.** After all, this is not surprising since the **energy** $W_{\rm red}$ is **not convex** in the joint argument $(u', \overline{\alpha})$ and the consistent coupling condition requires a higher level of smoothness for the evaluation of u' at the boundary than implied a priori in the variational formulation.

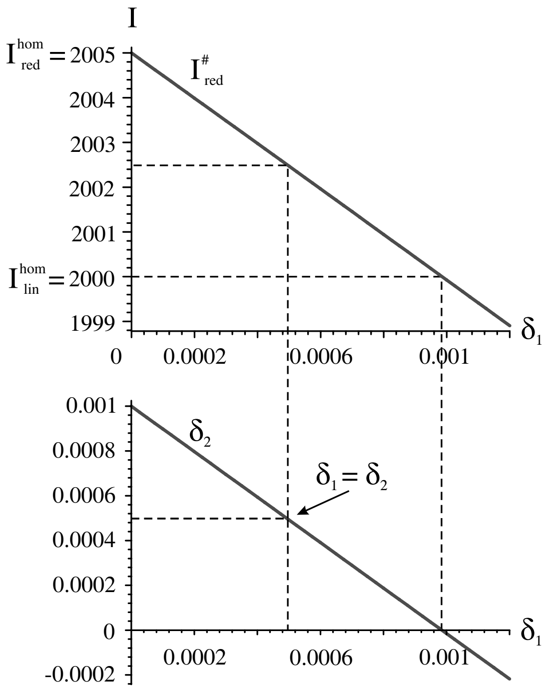

Figure 3.25: Graphics for $\gamma = 0.2$. Above: $I^{\rm hom}_{\rm red}$ and $I^\sharp_{\rm red}$ for various δ_1. Below: Constraint (3.52) for δ_2 as function of δ_1 and γ.

Remark 3.1 (Pure Neumann conditions with first moment symmetry constraint)
For $\mu_c = 0$ and $L_c = 0$ it is easy to see that one has only three possible homogeneous solutions for (3.44) of which only $\overline{\alpha}_2 = \frac{\gamma}{2}$ satisfies the first moment symmetry constraint. The same holds for consistent coupling. However, both sets of additional conditions do not single out a unique overall response: inhomogeneous equilibria exist for consistent coupling and first

[14] This is not in conflict with the symmetry requirement (3.5).

moment symmetry constraint. For the first moment symmetry constraint, the microstructure construction can be generalized to satisfy $\int_0^1 \overline{\alpha}(x)\,\mathrm{dx} = \frac{\gamma}{2}$. We cannot presently answer the question whether for $\mu_c = 0$ and $L_c > 0$ the classical aligned homogeneous response is the (unique? local?) minimizer for both conditions. In any case, choosing $L_c \gg 1$ large will favour a constant microrotation angle $\overline{\alpha}$ and should therefore provide at least a potential well around the classical "aligned" homogeneous response. The computational results in Figure 3.26 indicate non-trivial minimizing solutions for consistent coupling conditions.

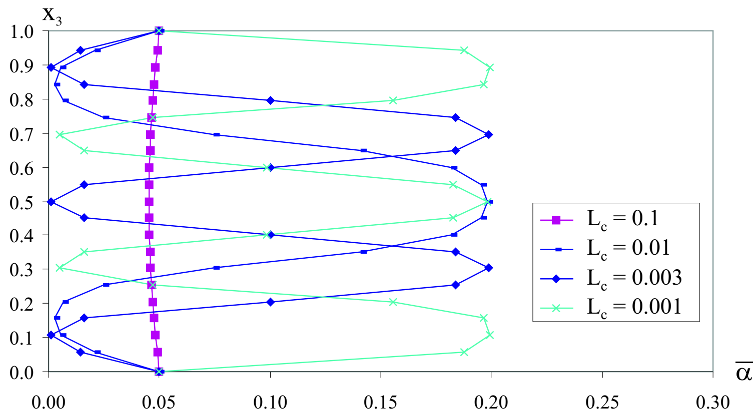

Figure 3.26: Non-trivial "microstructure" solutions for small L_c showing higher oscillations in $\overline{\alpha}$ as L_c gets smaller. The numerical solution is triggered by disturbing the faces with $\overline{\alpha}_{\mathrm{d}} = 0.05$ and requiring nevertheless consistent coupling.

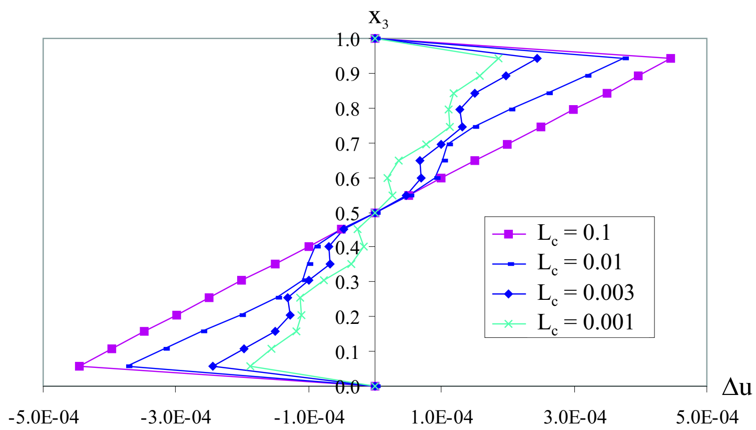

Figure 3.27: Non-trivial microstructure solutions for small L_c caused by disturbances on faces. Apart from a boundary layer the numerical response is consistent with the lamination solution in Figure 3.23. Here, $\Delta u = u(x) - \gamma\, x$.

3.3 The linearized Cosserat problem in simple glide

Now we contrast the nonlinear development with a similar analysis of the infinitesimal linear elastic Cosserat model with necessarily $\mu_c > 0$. This problem with a view towards the description of boundary layer effects has already been discussed in [10]. First, we recall the variational formulation in the infinitesimal case:

$$
\begin{aligned}
&\int_0^1 \mu\,\|\,\mathrm{sym}\,F - 1\!\!1\|^2 + \mu_c\,\|\,\mathrm{skew}\,F - \overline{A}\|^2 + 2\mu\,L_c^2|\overline{\alpha}'(x)|^2\,\mathrm{dx} \mapsto \min. \quad \text{w.r.t. } (u,\overline{\alpha})\,,\\
&\quad u(0)=0,\ u(1)=\gamma, \quad \text{Dirichlet boundary conditions for displacements}\,, \qquad (3.53)\\
&\quad \overline{\alpha}(0)=\overline{\alpha}(1)=\overline{\alpha}_{\mathrm{d}}=\overline{\alpha}_{\mathrm{d}}, \quad \text{various rigid boundary conditions}\,,\\
&\quad 0=\left(\mathrm{skew}(F)-\overline{A}\right)_{\{0,1\}} \Leftrightarrow 2\overline{\alpha}(0)=u'(0),\ 2\overline{\alpha}(1)=u'(1),\\
&\qquad \textbf{linearized consistent coupling}\ \text{boundary conditions}\,,\\
&\quad \overline{\alpha}'(0)=\overline{\alpha}'(1)=0, \quad \text{natural boundary conditions}\,,\\
&\int_0^1 \overline{\alpha}(x)\,\mathrm{dx}=\frac{\gamma}{2}\,, \quad \textbf{linearized first moment symmetry constraint}\,.
\end{aligned}
$$

The corresponding system of balance equations is given by

$$
\begin{aligned}
u''(x) &= 2\frac{\mu_c}{\mu+\mu_c}\,\overline{\alpha}'(x) = 2\,N^2\,\overline{\alpha}'(x)\,,\\
\mu\,L_c^2\overline{\alpha}''(x) &= \mu_c\left(\overline{\alpha}(x)-\frac{u'(x)}{2}\right)\,, \qquad (3.54)\\
&u(0)=0,\ u(1)=\gamma, \quad \text{Dirichlet boundary conditions for displacements}\,,\\
&\overline{\alpha}(0)=\overline{\alpha}(1)=\overline{\alpha}_{\mathrm{d}}, \quad \text{various rigid boundary conditions}\,,\\
&2\overline{\alpha}(0)=u'(0),\ 2\overline{\alpha}(1)=u'(1), \quad \text{linearized consistent coupling boundary conditions}\,,\\
&\overline{\alpha}'(0)=\overline{\alpha}'(1)=0, \quad \text{natural boundary conditions}\,,\\
&\int_0^1 \overline{\alpha}(x)\,\mathrm{dx}=\frac{\gamma}{2}\,, \quad \text{linearized first moment symmetry constraint}\,,
\end{aligned}
$$

with the traditional **Cosserat coupling number** $N^2=\frac{\mu_c}{\mu_c+\mu}$. The force balance equation can also be written as

$$
0=\frac{\mathrm{d}}{\mathrm{dx}}\left[\tau_{\mathrm{small}}(u'(x),\overline{\alpha}(x))\right]\,, \qquad \tau_{\mathrm{small}}(u',\overline{\alpha})=(\mu+\mu_c)\,u'-2\mu_c\,\overline{\alpha}\,. \qquad (3.55)
$$

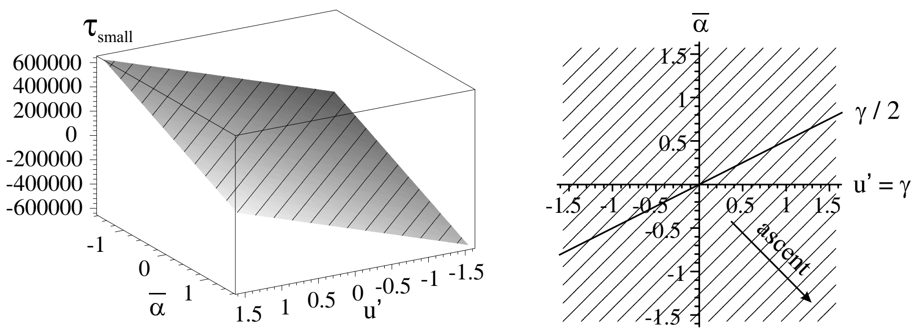

Figure 3.28: 3D and contour plot of τ_{small} for $\mu_c=\mu$.

The corresponding **infinitesimal energy expression** W_{small} in terms of u' and $\overline{\alpha}$ is

$$
\begin{aligned}
W_{\mathrm{small}}(u',\overline{\alpha},\overline{\alpha}') &= \mu\,\frac{u'^2}{2}+\mu_c\left(\frac{u'^2}{2}-2\overline{\alpha}\cdot u'+2\overline{\alpha}^2\right)+2\mu\,L_c^2|\overline{\alpha}'|^2\\
&= \mu\,\frac{u'^2}{2}+2\mu_c\left(\frac{u'}{2}-\overline{\alpha}\right)^2+2\mu\,L_c^2|\overline{\alpha}'|^2\,. \qquad (3.56)
\end{aligned}
$$

Remark 3.2 (First moment symmetry constraint in the linear case)
In the linear case with $\mu_c>0$ the first moment symmetry constraint is not an independent requirement but is a consequence of $(3.54)_2$ and natural boundary conditions on $\overline{\alpha}$. Only for the degenerated classical linear case with $\mu_c=0$ this is a constraint which singles out the aligned homogeneous response.

Inspection of (3.54) immediately shows that $u \in W^{2,1}((0,1),\mathbb{R}) \subset C^1([0,1],\mathbb{R})$ if $\overline{\alpha} \in H^1((0,1),\mathbb{R})$, hence **consistent coupling is well defined, also for other Dirichlet-data on** u.

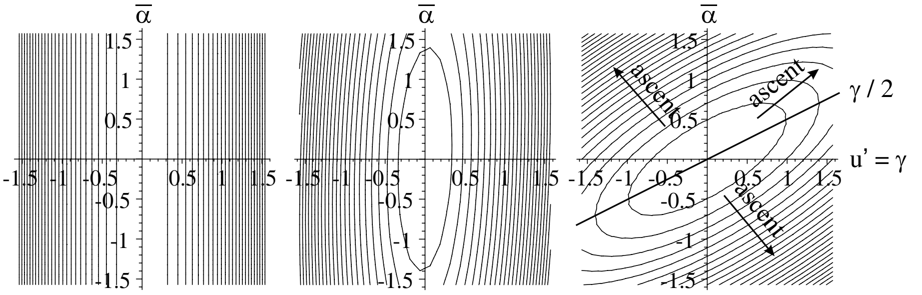

Figure 3.29: Contour plot of W_{small} (3.56) for $\mu_c = 0$ (left), $\mu_c > 0$ small (middle) and $\mu_c = \mu$ (right) with $L_c = 0$. For $\mu_c = 0$ the energy W_{small} is independent of $\overline{\alpha}$ and the **microrotations are left indeterminate.** W_{small} is **uniformly convex** for $\mu_c > 0$. Vertical lines are tangent to contour lines in a unique point if $\mu_c > 0$. For $\mu_c = 0$ but $L_c > 0$ the microrotations are only determined up to two integration constants. Both consistent coupling and the first moment symmetry constraint determine $\overline{\alpha} \equiv \frac{\gamma}{2}$, while rigid Dirichlet-data $\overline{\alpha}_{\text{d}} = 0$ sets $\overline{\alpha} \equiv 0$. Pure Neumann conditions leave one additive constant free, as usual.

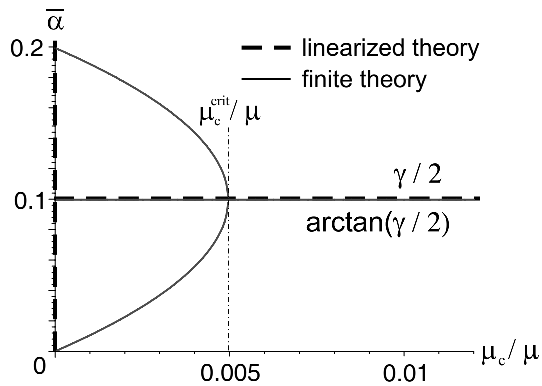

Figure 3.30: Solution for various μ_c/μ of the linearized torque-balance equation (3.54) for homogeneous situations $u' = \gamma$ and $\gamma = 0.2$. For $\mu_c = 0$ the microrotations $\overline{\alpha}$ remain indeterminate (vertical axes).

3.3.1 Unqualified uniqueness for $\mu_c > 0$

The second derivative of the energy W_{small} in the infinitesimal case for $\mu_c > 0$ w.r.t. $(u', \overline{\alpha})$ is given by

$$
\begin{aligned}
D^2_{(u',\overline{\alpha})} W_{\text{small}}(u',\overline{\alpha}).((\delta u, \delta\overline{\alpha}),(\delta u, \delta\overline{\alpha})) &= \mu\,|(\delta u)'|^2 + 4\mu_c\,|\frac{(\delta u)'}{2} - \delta\overline{\alpha}|^2 + 4\mu\, L_c^2 |(\delta\overline{\alpha})'|^2 \\
&= \mu\,|(\delta u)'|^2 + 4\mu_c \left[\left(\frac{(\delta u)'}{2}\right)^2 - (\delta u)'\,\delta\overline{\alpha} + (\delta\overline{\alpha})^2\right] + 4\mu\, L_c^2 |(\delta\overline{\alpha})'|^2 \\
&\quad \text{using Young's inequality we obtain} \qquad (3.57) \\
&\geq \mu\,|(\delta u)'|^2 + \mu_c |(\delta u)'|^2 - \frac{2\mu_c}{\varepsilon}|(\delta u)'|^2 + (4\mu_c - 2\mu_c\varepsilon)(\delta\overline{\alpha})^2 + 4\mu\, L_c^2 |(\delta\overline{\alpha})'|^2 \\
&= (\mu + \mu_c - \frac{2\mu_c}{\varepsilon})\,|(\delta u)'|^2 + 2\mu_c\,(2-\varepsilon)(\delta\overline{\alpha})^2 + 4\mu\, L_c^2 |(\delta\overline{\alpha})'|^2 \\
&\quad \text{taking } 2N^2 = \frac{2\mu_c}{\mu + \mu_c} < \varepsilon < 2 \text{ yields for some positive constant } c^+ > 0 \\
&\geq c^+\,|(\delta u)'|^2 + c^+\,(\delta\overline{\alpha})^2 + 4\mu\, L_c^2 |(\delta\overline{\alpha})'|^2\,,
\end{aligned}
$$

which shows, after integration on $(0,1)$ and using Poincare's inequality for δu, that for **classical Dirichlet boundary conditions** on the displacement u and for **linearized consistent coupling conditions** or **classical rigid Dirichlet boundary conditions** or **pure Neumann conditions** the **solution** $(u, \overline{\alpha})$ of the **infinitesimal Cosserat problem is unique for** $\mu_c > 0$. Since the homogeneous deformation $u(x) = \gamma \cdot x$ together with constant microrotation angle $\overline{\alpha}(x) = \frac{\gamma}{2}$ is an equilibrium solution for consistent coupling or prescribed $\overline{\alpha}_{\rm d} = \frac{\gamma}{2}$ or pure Neumann conditions on the microrotations ($\mu_c > 0$), it is the unique solution coinciding with the unique solution of the classical infinitesimal elasticity problem with shear stress at the upper face $\tau_{\rm lin} = \mu\,\gamma$. **Pure Neumann or consistent coupling** for the microrotations predict therefore the "aligned" homogeneous response if $\mu_c > 0$. As for the homogeneous solution for consistent coupling: The tangential stresses are given by

$$\begin{aligned}
\tau^{\rm cons}_{\rm small} &= \langle \sigma.e_3, e_1\rangle = \langle [2\mu\, \mathrm{sym}(F - 1\!\!1) + 2\mu_c(\mathrm{skew}(F - 1\!\!1) - \overline{A})].e_3, e_1\rangle \qquad (3.58)\\
&= (\mu + \mu_c)\cdot u'(1) - 2\mu_c\,\overline{\alpha}(1) = (\mu + \mu_c)\cdot u'(0) - 2\mu_c\,\overline{\alpha}(0) = \mu\,\gamma = \tau^{\rm Neum}_{\rm small} = \tau^{\rm Sym}_{\rm small}\,.
\end{aligned}$$

In order to predict inhomogeneous response in simple glide, the linear Cosserat model needs boundary conditions which make the previous homogeneous response impossible. This is achieved e.g. for rigid Dirichlet conditions $\overline{\alpha}_{\rm d} \neq \frac{\gamma}{2}$.

3.3.2 Analytical solution for rigid data

In order to find the unique nontrivial solution for rigid Dirichlet conditions $\overline{\alpha}(1) = \overline{\alpha}(0) = \overline{\alpha}_{\rm d} \neq \frac{\gamma}{2}$ on the microrotations, we integrate the first equation of (3.54) and get

$$2\,N^2[\overline{\alpha}(x) - \overline{\alpha}(0)] = u'(x) - u'(0)\,. \qquad (3.59)$$

Further integration of (3.59) shows

$$2\,N^2\int_0^1 \overline{\alpha}(x)\,\mathrm{dx} - 2\,N^2\overline{\alpha}(0) = u(1) - u(0) - u'(0) = \gamma - u'(0)\,, \qquad (3.60)$$

where we have used the Dirichlet boundary conditions for the displacement u. This shows

$$u'(0) = \gamma - 2\,N^2\int_0^1 \overline{\alpha}(x)\,\mathrm{dx} + 2N^2\overline{\alpha}_{\rm d}\,. \qquad (3.61)$$

Reinserting into (3.59) yields

$$u'(x) = \gamma + 2\,N^2\left(\overline{\alpha}(x) - \int_0^1 \overline{\alpha}(x)\,\mathrm{dx}\right)\,. \qquad (3.62)$$

Inserting the result for $u'(x)$ into balance of angular momentum and rearranging yields the linear second order differential equation

$$\overline{\alpha}''(x) - \frac{N^2}{L_c^2}\overline{\alpha}(x) = -\frac{\mu_c}{\mu\,L_c^2}\frac{\gamma}{2} + \frac{N^2\,\mu_c}{L_c^2\mu}\int_0^1 \overline{\alpha}(s)\,\mathrm{ds}\,. \qquad (3.63)$$

Differentiation w.r.t. x once more yields the linear third order ODE

$$\overline{\alpha}'''(x) = \frac{N^2}{L_c^2}\overline{\alpha}'(x)\,, \qquad (3.64)$$

The general solution of this differential equation in view of the expected point symmetry of $\overline{\alpha}$ w.r.t. $x = \frac{1}{2}$ is given by[15]

$$\overline{\alpha}(x) = \beta_1\cdot\cosh\left(\frac{N}{L_c}[x - \frac{1}{2}]\right) + \beta_2\,. \qquad (3.65)$$

[15]Since the solution is unique anyway this symmetry assumption constitutes no loss of generality at this point.

Since

$$\overline{\alpha}_{\rm d} = \overline{\alpha}(0) = \beta_1 \cdot \cosh\left(\frac{N}{L_c}[-\frac{1}{2}]\right) + \beta_2\,,$$
$$\overline{\alpha}_{\rm d} = \overline{\alpha}(1) = \beta_1 \cdot \cosh\left(\frac{N}{L_c}[\frac{1}{2}]\right) + \beta_2 \;\Rightarrow$$
$$\beta_2 = \overline{\alpha}_{\rm d} - \beta_1 \cdot \cosh\left(\frac{N}{L_c}[-\frac{1}{2}]\right) \;\Rightarrow$$
$$\overline{\alpha}(x) = \beta_1 \left[\cosh\left(\frac{N}{L_c}[x-\frac{1}{2}]\right) - \cosh\left(\frac{N}{L_c}[-\frac{1}{2}]\right)\right] + \overline{\alpha}_{\rm d}\,. \tag{3.66}$$

We calculate

$$\overline{\alpha}''(x) = \beta_1 \cdot \frac{N^2}{L_c^2}\cosh\left(\frac{N}{L_c}[x-\frac{1}{2}]\right)\,, \tag{3.67}$$
$$\begin{aligned}\int_0^1 \overline{\alpha}(x)\,{\rm dx} &= -\beta_1 \cosh\left(\frac{N}{L_c}[-\frac{1}{2}]\right) + \beta_1 \frac{L_c}{N}\left[\sinh\left(\frac{N}{L_c}[\frac{1}{2}]\right) - \sinh\left(\frac{N}{L_c}[-\frac{1}{2}]\right)\right] + \overline{\alpha}_{\rm d} \\ &= 2\beta_1 \frac{L_c}{N}\sinh\left(\frac{N}{L_c}[\frac{1}{2}]\right) - \beta_1\cosh\left(\frac{N}{L_c}[-\frac{1}{2}]\right) + \overline{\alpha}_{\rm d} \\ &= \beta_1\left[2\frac{L_c}{N}\sinh\left(\frac{N}{L_c}[\frac{1}{2}]\right) - \cosh\left(\frac{N}{L_c}[-\frac{1}{2}]\right)\right] + \overline{\alpha}_{\rm d}\,.\end{aligned}$$

Inserting this result into (3.63) we obtain

$$\beta_1 = \frac{2\,\mu_c\,\overline{\alpha}_{\rm d} - (\mu+\mu_c)\,\gamma}{2\,\mu_c\cosh\left(\frac{N}{L_c}[\frac{1}{2}]\right) - 4\,\mu_c\,L_c\,\sinh\left(\frac{N}{L_c}[\frac{1}{2}]\right)}\,, \tag{3.68}$$

which yields the micropolar microrotation angle

$$\overline{\alpha}(x) = \frac{\left[\cosh\left(\frac{N}{L_c}[x-\frac{1}{2}]\right) - \cosh\left(\frac{N}{L_c}[-\frac{1}{2}]\right)\right](2\,\mu_c\,\overline{\alpha}_{\rm d} - (\mu+\mu_c)\,\gamma)}{2\,\mu_c\cosh\left(\frac{N}{L_c}[\frac{1}{2}]\right) - 4\,\mu_c\,L_c\,\sinh\left(\frac{N}{L_c}[\frac{1}{2}]\right)} + \overline{\alpha}_{\rm d}\,. \tag{3.69}$$

The micropolar displacement for rigid Dirichlet data is given by

$$u(x) = \int_0^x u'(s)\,{\rm ds} = \int_0^x (\gamma + 2N^2\overline{\alpha}(s))\,{\rm ds} - 2N^2\int_0^x \left(\int_0^1 \overline{\alpha}(x)\,{\rm dx}\right)\,{\rm ds}\,, \tag{3.70}$$

which turns for $\overline{\alpha}_{\rm d} = 0$ into

$$u(x) = \gamma\left(\frac{\cosh\left(\frac{N}{L_c}[\frac{1}{2}]\right)}{\cosh\left(\frac{N}{L_c}[\frac{1}{2}]\right) - 2NL_c\sinh\left(\frac{N}{L_c}[\frac{1}{2}]\right)}\,x - NL_c\frac{\sinh\left(\frac{N}{L_c}[x-\frac{1}{2}]\right) - \sinh\left(\frac{N}{L_c}[-\frac{1}{2}]\right)}{\cosh\left(\frac{N}{L_c}[\frac{1}{2}]\right) - 2NL_c\sinh\left(\frac{N}{L_c}[\frac{1}{2}]\right)}\right)\,.$$

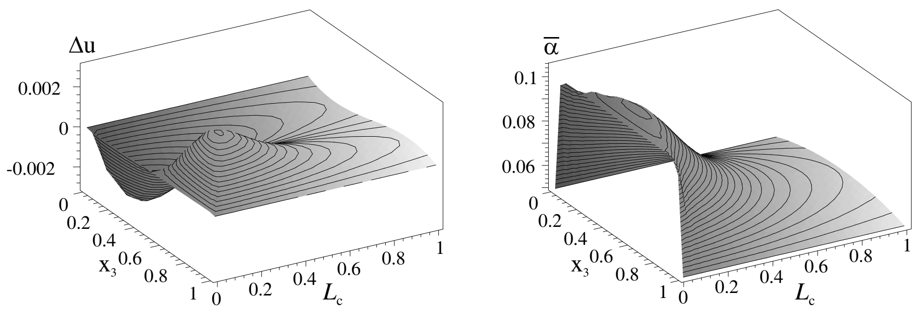

Figure 3.31: 3-D plot of shear difference $\Delta u = u(x) - \gamma\,x$ from (3.70) and of $\overline{\alpha}(x)$ from (3.69) for the linearized Cosserat problem, maximal shear $\gamma = 0.2$, $\overline{\alpha}_{\rm d} = 0.05$ and various L_c.

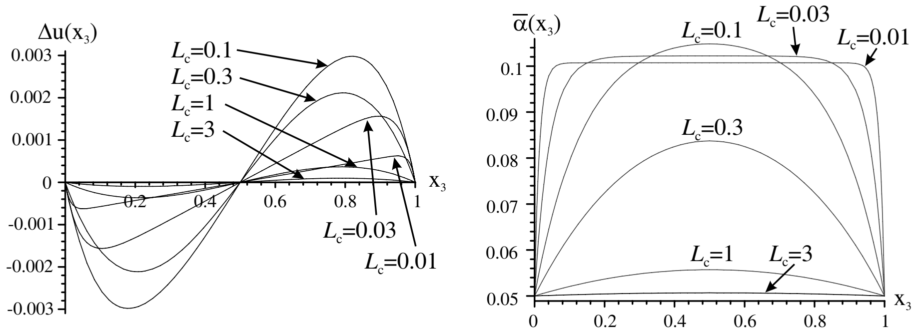

Figure 3.32: Plot of shear difference $\Delta u = u(x) - \gamma\, x$ from (3.70) and of $\overline{\alpha}(x)$ from (3.69) for the linearized Cosserat problem, maximal shear $\gamma = 0.2$, $\overline{\alpha}_{\mathrm{d}} = 0.05$ and various L_c.

The tangential shear stresses for $\overline{\alpha}_{\mathrm{d}} = 0$ are given by (cf. [10, 3.17])

$$\begin{aligned}
\tau^{\text{rigid}}_{\text{small}} &= \langle \sigma.e_3, e_1\rangle = \langle [2\mu\, \mathrm{sym}(F - 1\!\!1) + 2\mu_c(\mathrm{skew}(F - 1\!\!1) - \overline{A})].e_3, e_1\rangle \\
&= (\mu + \mu_c)\cdot u'(1) - 2\mu_c\, \overline{\alpha}(1) = (\mu + \mu_c)\cdot u'(0) - 2\mu_c\, \overline{\alpha}_{\mathrm{d}} \\
&= (\mu + \mu_c)\left(\gamma - 2N^2 \int_0^1 \overline{\alpha}(x)\,\mathrm{dx}\right) = \mu \left(\frac{1}{1 - 2NL_c \tanh\left(\frac{N}{L_c}[\frac{1}{2}]\right)}\right)\cdot \gamma\,. \qquad (3.71)
\end{aligned}$$

Expansion shows that for $N > 0, L_c \to \infty$ (ever smaller samples)[16] it results in the limit $\tau^{\text{rigid}}_{\text{small}} = \mu\left(\frac{1}{1-N^2}\right)\cdot\gamma = (\mu + \mu_c)\cdot\gamma$ for a homogeneous deformation $u(x) = \gamma\, x$ and homogeneous microrotation $\overline{\alpha} = 0$; the evaluated stresses $\tau^{\text{rigid}}_{\text{small}}$ are increased due to $\mu_c > 0$ and the (incompatible) rigid boundary prescription $\overline{\alpha}_{\mathrm{d}} = 0$. For $0 < N \ll 1$, $L_c > 0$ we observe that $\tau^{\text{rigid}}_{\text{small}} \approx (\mu + \mu_c)\cdot\gamma$ and $u(x) \approx \gamma\, x$. In this case, it can be seen that the **Cosserat couple modulus** $\mu_c > 0$ is in fact **a measure of the influence of boundary conditions for microrotations on the solution** and therefore **not a material parameter.**[17] Similarly, it can be shown that $N \to 0$, $L_c > 0$ is possible and results in the classical response $\tau^{\text{rigid}}_{\text{small}} = \mu\cdot\gamma$. Finally, $N > 0$, $L_c \to 0$ approaches the classical result as well. In all cases the micropolar response for rigid Dirichlet data $\overline{\alpha}_{\mathrm{d}} = 0$ is **stiffer** than the corresponding homogeneous classical response, this is a typical boundary layer effect.

3.3.3 Only Dirichlet conditions on the microrotations $\overline{\alpha}$

Since we want to understand the influence of boundary conditions on the microrotations $\overline{\alpha}_{\mathrm{d}}$ better we study as well the case of Dirichlet conditions on $\overline{\alpha}$ only without prescribing the macroscopic displacement. The boundary conditions are $\overline{\alpha}(1) = \overline{\alpha}(0) = \overline{\alpha}_{\mathrm{d}} \neq 0$ and Neumann conditions on the displacement, which turn out to be $u'(0) = 2\,N^2\,\overline{\alpha}(0) = 2\,N^2\,\overline{\alpha}_d = u'(1)$.[18] In addition one needs to assume the normalization condition $\int_0^1 u(x)\,\mathrm{dx} = 0$.

[16] Only a formal limit in the linear Cosserat model: the smallest sample size should be larger than the chosen $L_c > 0$ of the unit cube, i.e. the smallest sample size must be larger than the smallest constituents of the material given as unit cube. Hence, if L_c has any physical meaning, we should have $0 \leq L_c < 1$.

[17] Consider any other independent (artificial) Dirichlet boundary condition for the microrotation angle $0 \leq \overline{\alpha}(0) = \overline{\alpha}(1) = \overline{\alpha}_{\mathrm{d}} < \frac{\gamma}{2}$. The solution u will produce a different shear stress response $\tau^{\text{rigid}}_{\text{small}} = \mu\, u'(1) + 2\mu_c\,(\frac{u'(1)}{2} - \overline{\alpha}_{\mathrm{d}})$ which, for different L_c, necessitates a modification of μ_c for the same material. In our example, this inconsistency can be avoided for consistent coupling and first moment constraint but persists in the general case.

[18] Consistent coupling is only consistent with $\overline{\alpha}_{\mathrm{d}} = 0$ in this formulation.

The system of balance equations for the linear problem reads

$$
\begin{aligned}
u''(x) &= 2\frac{\mu_c}{\mu+\mu_c}\,\overline{\alpha}'(x) = 2\,N^2\,\overline{\alpha}'(x)\,,\\
\mu\,L_c^2\overline{\alpha}''(x) &= \mu_c\left(\overline{\alpha}(x) - \frac{u'(x)}{2}\right)\,, \qquad (3.72)\\
&u'(0) = 2\,N^2\,\overline{\alpha}(0) = 2\,N^2\,\overline{\alpha}_d = u'(1) \quad \text{Neumann boundary conditions for displacements}\,,\\
&\overline{\alpha}(0) = \overline{\alpha}(1) = \overline{\alpha}_{\mathrm{d}} \neq 0, \quad \text{Dirichlet boundary conditions for microrotations}\,,\\
&\int_0^1 u(x)\,\mathrm{dx} = 0, \quad \text{normalization condition}\,.
\end{aligned}
$$

Integrating $(3.72)_1$ w.r.t. x shows

$$
u'(x) = u'(0) + 2\,N^2\,\left[\overline{\alpha}(x) - \overline{\alpha}(0)\right] = 2\,N^2\,\overline{\alpha}_{\mathrm{d}} + 2\,N^2\,\left[\overline{\alpha}(x) - \overline{\alpha}_{\mathrm{d}}\right] = 2\,N^2\,\overline{\alpha}(x)\,. \qquad (3.73)
$$

Inserting this result in $(3.72)_2$ leads to the homogeneous ODE

$$
\mu\,L_c^2\,\overline{\alpha}''(x) = \mu_c\left(\overline{\alpha}(x) - N^2\,\overline{\alpha}(x)\right) \;\Leftrightarrow\; \overline{\alpha}''(x) = \frac{N^2}{L_c^2}\,\overline{\alpha}(x)\,, \qquad (3.74)
$$

with a general solution given by

$$
\overline{\alpha}(x) = \beta_1\,\cosh(\frac{N}{L_c}(x-\frac{1}{2}))\,. \qquad (3.75)
$$

Using the boundary condition $(3.72)_4$ $\overline{\alpha}(1) = \overline{\alpha}_d$ determines β_1, thus

$$
\overline{\alpha}(x) = \frac{\overline{\alpha}_d}{\cosh(\frac{N}{L_c}\frac{1}{2})}\,\cosh(\frac{N}{L_c}(x-\frac{1}{2}))\,. \qquad (3.76)
$$

Reinserting (3.76) into (3.73) leads to

$$
u'(x) = \frac{2\,N^2\,\overline{\alpha}_d}{\cosh(\frac{N}{L_c}\frac{1}{2})}\,\cosh(\frac{N}{L_c}(x-\frac{1}{2}))\,, \qquad (3.77)
$$

and integrating (3.77) w.r.t. x results in

$$
u(x) = \frac{2\,N\,L_c\,\overline{\alpha}_d}{\cosh(\frac{N}{L_c}\frac{1}{2})}\,\sinh(\frac{N}{L_c}(x-\frac{1}{2})) + C_1\,. \qquad (3.78)
$$

The normalization condition for displacements $\int_0^1 u(x)\,\mathrm{dx} = 0$ shows $C_1 = 0$ and such that finally

$$
u(x) = \frac{2\,N\,L_c\,\overline{\alpha}_d}{\cosh(\frac{N}{L_c}\frac{1}{2})}\,\sinh(\frac{N}{L_c}(x-\frac{1}{2}))\,. \qquad (3.79)
$$

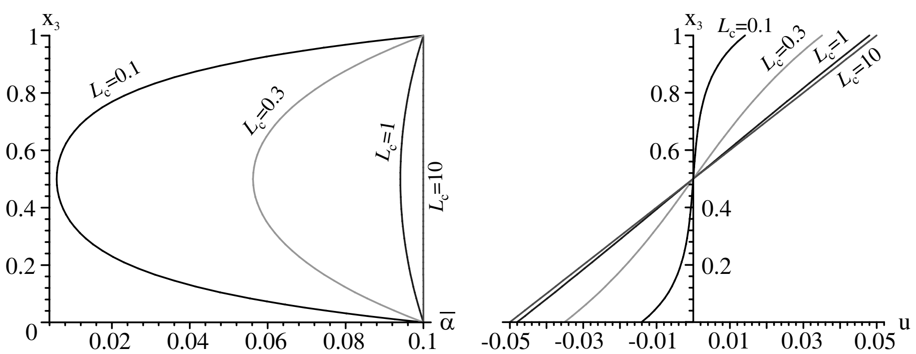

Figure 3.33: Analytical results for only Dirichlet conditions on the microrotations $\overline{\alpha} = 0.1$, $\mu_c = \mu$ and various L_c.

It can be seen that by applying rotations at the upper and lower face, the structure will respond with nonzero displacement in general. We can interpret this result in the following way: the structure is responding to nonzero Dirichlet conditions on the microrotation **as if** an imaginary shear force had been applied. From a mechanical point of view, surface moments m must be applied to prescribe microrotations $\overline{\alpha}_{\mathrm{d}} \neq 0$ and the expended outer work $m \cdot \overline{\alpha}_{\mathrm{d}}$ causes deformation as shown in Figure 3.33. In the combined case with applied shear γ and prescribed microrotations $\overline{\alpha}_{\mathrm{d}}$, this individual effect of the microrotations leads to an increase or decrease of the computed shear force τ depending on the sign of the applied rotations. In our example $\overline{\alpha}_{\mathrm{d}} > 0$ leads to a decreasing shear force τ and vice versa. Nevertheless, in this example, classical shear forces on faces are zero, since $\tau = (\mu + \mu_c)\, u'(1) - 2\mu_c\, \overline{\alpha}(1) = 0$. The solution for the special case $N \equiv 0$, $L_c > 0$ is easily obtained as $u(x) = 0$ and $\overline{\alpha}(x) = 0$ if $\overline{\alpha}_d = 0$, otherwise, no solution exists. Similarly for $L_c = 0\,, N > 0$. Finally, $L_c = 0$, $N \equiv 0$ yields $u(x) = 0$ and $\overline{\alpha}$ is not determined.

Looking at the reduced formulation for $\mu_c = 0$ and $L_c = 0$ we see that it does not have a solution for $\overline{\alpha}_{\mathrm{d}} \neq 0$, otherwise the unique solution is $u(x) = 0$ and $\overline{\alpha}(x) = 0$.

The influence of μ_c on the solution of the linear problem is given qualitatively in the next picture ($\mu_c \to 0$ decouples).

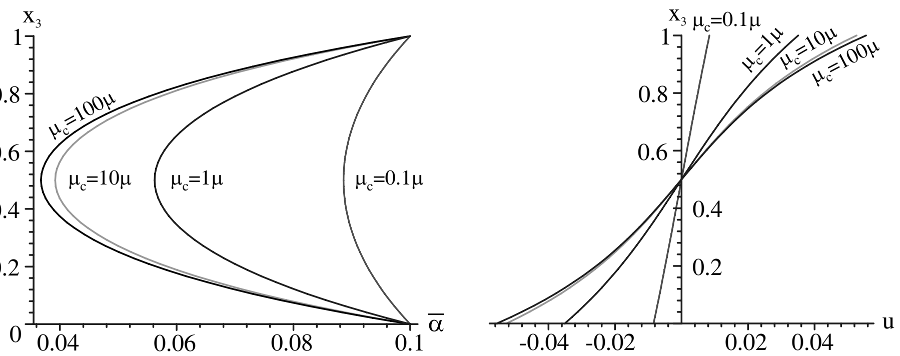

Figure 3.34: Analytical results for only Dirichlet conditions on the microrotations $\overline{\alpha}_{\mathrm{d}} = 0.1$, $L_c = 0.3$ and various μ_c.

3.4 The linear indeterminate couple stress model

Now we consider the **infinitesimal indeterminate couple stress** response in simple glide. The variational problem is easily obtained from (3.53) by identifying $\overline{\alpha}(x) = \frac{u'(x)}{2}$ throughout and taking free variations w.r.t. u only. This is formally equivalent to setting $\mu_c = \infty$ in (3.54). It results in the problem

$$\int_0^1 \mu\, \| \operatorname{sym} F - 1\!\!1 \|^2 + \frac{\mu}{2}\, L_c^2 |u''(x)|^2 \,\mathrm{dx} \mapsto \min . \quad \text{w.r.t. } u\,, \quad u(0) = 0,\, u(1) = \gamma\,, \tag{3.80}$$
$$\sigma = \sigma^{\mathrm{loc}} + \sigma^{\mathrm{hyper}}, \quad \tau^{\mathrm{indet}}_{\mathrm{small}} = \mu\, u'(x) - \mu\, L_c^2\, u'''(x)\,.$$

The indeterminate couple stress model identifies the microrotations with the continuum rotations apriori, an additional condition like the consistent coupling requirement etc. is therefore not needed. The first moment constraint and the consistent coupling condition are satisfied a priori. The corresponding **infinitesimal indeterminate energy expression** W_{indet} in terms of u' and u'' is

$$W_{\mathrm{indet}}(u', u'') = \frac{\mu}{2}\, \left(|u'|^2 + L_c^2 |u''|^2 \right)\,, \tag{3.81}$$

and the Euler-Lagrange equation of **fourth order** reads

$$
\begin{aligned}
-u''(x) + L_c^2\, u^{(4)}(x) = 0 \;\Leftrightarrow\; 0 = \frac{\mathrm{d}}{\mathrm{dx}}\left[\tau^{\text{indet}}_{\text{small}}(u'(x), u'''(x))\right]\,, \\
u(0) = 0,\; u(1) = \gamma\,, \quad \text{Dirichlet boundary conditions for displacements}\,, \\
u'(0) = u'(1) = 2\,\overline{\alpha}_{\mathrm{d}}\,, \quad \text{various rigid conditions}\,, \\
u''(0) = u''(1) = 0\,, \quad \text{or natural boundary condition}\,.
\end{aligned} \tag{3.82}
$$

This equation coincides with equation (3.64) if we identify again $\frac{u'}{2} = \overline{\alpha}$ and take $N \equiv 1$. The general solution of (3.82) is

$$
u(x) = b_1 \sinh\left(\frac{1}{L_c}[x - \frac{1}{2}]\right) + b_2 \cosh\left(\frac{1}{L_c}[x - \frac{1}{2}]\right) + b_3\,(x - \frac{1}{2}) + b_4\,. \tag{3.83}
$$

Natural boundary conditions imply effectively $u(x) = \gamma\, x$ as unique homogeneous solution with shear stress response $\tau^{\text{indet,hom}}_{\text{small}} = \mu\,\gamma$. For rigid boundary conditions on the other hand we have to satisfy

$$
\begin{aligned}
0 = u(0) &= b_1 \sinh\left(\frac{1}{L_c}[-\frac{1}{2}]\right) + b_2 \cosh\left(\frac{1}{L_c}[-\frac{1}{2}]\right) + b_3\,(-\frac{1}{2}) + b_4\,, \\
\gamma = u(1) &= b_1 \sinh\left(\frac{1}{L_c}[\frac{1}{2}]\right) + b_2 \cosh\left(\frac{1}{L_c}[\frac{1}{2}]\right) + b_3\,\frac{1}{2} + b_4\,, \\
2\,\overline{\alpha}_{\mathrm{d}} = u'(0) &= \frac{b_1}{L_c} \cosh\left(\frac{1}{L_c}[-\frac{1}{2}]\right) + \frac{b_2}{L_c} \sinh\left(\frac{1}{L_c}[-\frac{1}{2}]\right) + b_3\,, \\
2\,\overline{\alpha}_{\mathrm{d}} = u'(1) &= \frac{b_1}{L_c} \cosh\left(\frac{1}{L_c}[\frac{1}{2}]\right) + \frac{b_2}{L_c} \sinh\left(\frac{1}{L_c}[\frac{1}{2}]\right) + b_3\,,
\end{aligned} \tag{3.84}
$$

which implies

$$
\begin{aligned}
b_1 &= \frac{L_c(2\,\overline{\alpha}_{\mathrm{d}} - \gamma)}{\cosh\left(\frac{1}{L_c}[\frac{1}{2}]\right) - 2L_c \sinh\left(\frac{1}{L_c}[\frac{1}{2}]\right)}, \qquad b_2 = 0, \\
b_3 &= \frac{\gamma \cosh\left(\frac{1}{L_c}[\frac{1}{2}]\right) - 4\,L_c\,\overline{\alpha}_{\mathrm{d}} \sinh\left(\frac{1}{L_c}[\frac{1}{2}]\right)}{\cosh\left(\frac{1}{L_c}[\frac{1}{2}]\right) - 2L_c \sinh\left(\frac{1}{L_c}[\frac{1}{2}]\right)}, \quad b_4 = \frac{\gamma}{2}\,,
\end{aligned} \tag{3.85}
$$

and the unique solution of the rigid indeterminate couple stress problem for given $\overline{\alpha}_{\mathrm{d}}$ is

$$
\begin{aligned}
u(x) &= \gamma \left(\frac{\cosh\left(\frac{1}{L_c}[\frac{1}{2}]\right)}{\cosh\left(\frac{1}{L_c}[\frac{1}{2}]\right) - 2L_c \sinh\left(\frac{1}{L_c}[\frac{1}{2}]\right)}\, x - L_c \frac{\sinh\left(\frac{1}{L_c}[x - \frac{1}{2}]\right) - \sinh\left(\frac{1}{L_c}[-\frac{1}{2}]\right)}{\cosh\left(\frac{1}{L_c}[\frac{1}{2}]\right) - 2L_c \sinh\left(\frac{1}{L_c}[\frac{1}{2}]\right)} \right) \\
&\quad + 2\,\overline{\alpha}_{\mathrm{d}}\, L_c \left(\frac{-2 \sinh\left(\frac{1}{L_c}[\frac{1}{2}]\right)}{\cosh\left(\frac{1}{L_c}[\frac{1}{2}]\right) - 2L_c \sinh\left(\frac{1}{L_c}[\frac{1}{2}]\right)}\, x + \frac{\sinh\left(\frac{1}{L_c}[x - \frac{1}{2}]\right) - \sinh\left(\frac{1}{L_c}[-\frac{1}{2}]\right)}{\cosh\left(\frac{1}{L_c}[\frac{1}{2}]\right) - 2L_c \sinh\left(\frac{1}{L_c}[\frac{1}{2}]\right)} \right), \\
u'(x) &= \gamma \left(\frac{\cosh\left(\frac{1}{L_c}[\frac{1}{2}]\right) - \cosh\left(\frac{1}{L_c}[x - \frac{1}{2}]\right)}{\cosh\left(\frac{1}{L_c}[\frac{1}{2}]\right) - 2L_c \sinh\left(\frac{1}{L_c}[\frac{1}{2}]\right)} \right) \\
&\quad + 2\,\overline{\alpha}_{\mathrm{d}}\, L_c \left(\frac{-2 \sinh\left(\frac{1}{L_c}[\frac{1}{2}]\right) + \frac{1}{L_c} \cosh\left(\frac{1}{L_c}[x - \frac{1}{2}]\right)}{\cosh\left(\frac{1}{L_c}[\frac{1}{2}]\right) - 2L_c \sinh\left(\frac{1}{L_c}[\frac{1}{2}]\right)} \right).
\end{aligned} \tag{3.86}
$$

The term $\frac{u'(x)}{2}$ does coincide with $\overline{\alpha}(x)$ in (3.69) for $N \equiv 1$. The limit $L_c \to 0$ (ever larger samples) is possible, the solution **converges pointwise** in the interior $(0, 1)$ **to the homogeneous solution**, but the convergence is not uniform due to the appearance of a strong **boundary layer** caused by the incompatible rigid boundary prescription. For large L_c the solution converges to a smooth S-type shear profile.

The shear stress response for $\overline{\alpha}_{\rm d} = 0$ is given by

$$\begin{aligned}\tau_{\rm small}^{\rm indet,rigid} &= \mu\, u'(1) - \mu\, L_c^2 u'''(1) = -\mu L_c^2 \left(\frac{b_1}{L_c^3}\cosh\left(\frac{1}{L_c}[1-\frac{1}{2}]\right) + \frac{b_2}{L_c^3}\cosh\left(\frac{1}{L_c}[1-\frac{1}{2}]\right)\right) \\ &= -\mu \frac{b_1}{L_c}\cosh\left(\frac{1}{L_c}[1-\frac{1}{2}]\right) = \mu\, \frac{\cosh\left(\frac{1}{L_c}[\frac{1}{2}]\right)}{\cosh\left(\frac{1}{L_c}[\frac{1}{2}]\right) - 2L_c \sinh\left(\frac{1}{L_c}[\frac{1}{2}]\right)}\,\gamma \qquad (3.87) \\ &= \mu\left(\frac{1}{1-2L_c\tanh\left(\frac{1}{L_c}[\frac{1}{2}]\right)}\right)\cdot\gamma\,,\end{aligned}$$

coinciding with the **stiffer** shear stress response of the infinitesimal micropolar model for $N \equiv 1$. Passage to the limit $L_c \to \infty$ (ever smaller samples) in the stresses is not possible for rigid Dirichlet conditions. [19] This point highlights again our understanding that boundary conditions should be such that in principal homogeneous solutions remain possible. The boundary conditions in a three-dimensional problem should not be the cause for nonhomogeneous response.[20]

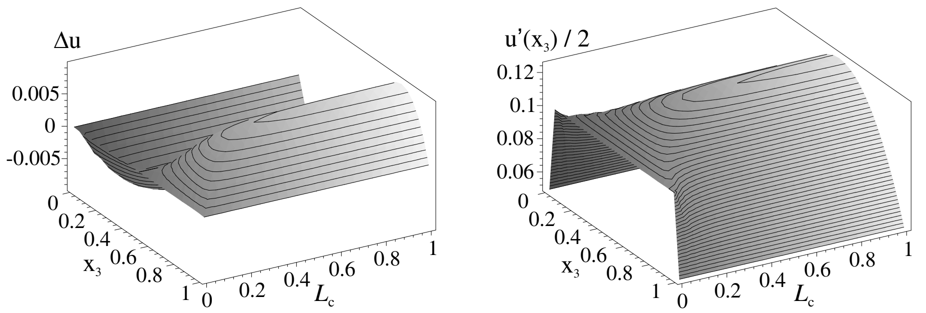

Figure 3.35: 3-D plot of shear difference $\Delta u = u - \gamma\, x$ and of $\frac{u'}{2}$ for the indeterminate couple stress model (3.86), maximal shear $\gamma = 0.2$, $\overline{\alpha}_{\rm d} = 0.05$ and various L_c.

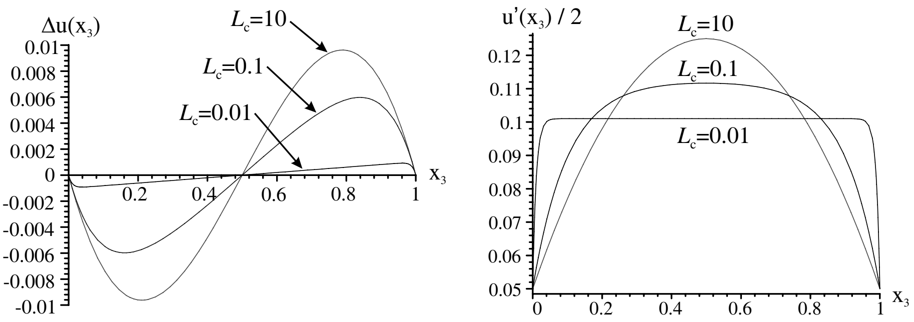

Figure 3.36: Plot of shear difference $\Delta u = u - \gamma\, x$ and of $\frac{u'}{2}$ for the indeterminate couple stress model (3.86), maximal shear $\gamma = 0.2$, $\overline{\alpha}_{\rm d} = 0.05$ and various L_c. Curves for $L_c = 0.01$ and $L_c = 10$ represent lower and upper limits. $L_c \to 0$ shows a strong boundary layer.

[19] Since $\tanh x = x - \frac{x^3}{3} + \ldots$, for $L_c \to \infty$, then $\tau_{\rm small}^{\rm indet,rigid} \to \infty$, a severe shortcoming of the indeterminate couple stress model due, in essence, to boundary layer stiffening. This underlines the objections of Koiter [28] against this model.

[20] This principle does not apply to plates and shells where boundary conditions appear naturally by a dimensional reduction process and carry physical information. In the Cosserat bulk model the boundary conditions for microrotations are in principal unknown.

3.5 Complement: the elastic Biot-material in simple glide

In order to complement our exposition we consider simple glide in a nonlinear classical elasticity context. The energy of the elastic Biot material is assumed to be of the form

$$\int_\Omega \mu\,\|U-1\!\!1\|^2+\frac{\lambda}{4}\left[(\det[U]-1)^2+\left(\frac{1}{\det[U]}-1\right)^2\right]\mathrm{dV}\,. \tag{3.88}$$

For small classical Biot-strains $\|U-1\!\!1\|\ll 1$, this is consistent with

$$\int_\Omega \mu\,\|U-1\!\!1\|^2+\frac{\lambda}{2}\,\mathrm{tr}\,[U-1\!\!1]^2\,\mathrm{dV}\,, \tag{3.89}$$

which reduces in simple glide (incompressibility) to

$$\begin{aligned}\int_0^1 \mu\,\|U-1\!\!1\|^2\,\mathrm{dx}&=\int_0^1 \mu\,\|R^TF-1\!\!1\|^2\,\mathrm{dx}\\&=\int_0^1 \mu\,\|F-R\|^2\,\mathrm{dx}=\int_0^1 \mu\left(\|F\|^2-2\langle F,R\rangle+3\right)\,\mathrm{dx}\,,\end{aligned} \tag{3.90}$$

where $R\in\mathrm{SO}(3,\mathbb{R})$ represents now the **continuum rotation**, while $U=\sqrt{F^TF}$ is the **classical symmetric stretch tensor** such that $F=R\,U$ from the **polar decomposition** theorem. For the assumed kinematics in simple glide, the continuum rotation has the form

$$R(x_1,x_2,x_3)=\begin{pmatrix}\cos\alpha(x_3)&0&\sin\alpha(x_3)\\0&1&0\\-\sin\alpha(x_3)&0&\cos\alpha(x_3)\end{pmatrix}\,, \tag{3.91}$$

with **continuum rotation angle** $\alpha\in[0,2\pi)$. A simple calculation shows that

$$\sin\alpha(x)=\frac{u'(x)}{\sqrt{4+(u'(x))^2}},\quad R(x)=\frac{1}{\sqrt{4+(u'(x))^2}}\begin{pmatrix}2&0&u'(x)\\0&\sqrt{4+u'(x)^2}&0\\-u'(x)&0&2\end{pmatrix}\,, \tag{3.92}$$

this yields

$$\int_0^1 \mu\left(\|F\|^2-2\langle F,R(u')\rangle+3\right)\,\mathrm{dx}=\int_0^1 \mu\,\left(\sqrt{4+u'(x)^2}-1\right)^2-\mu\,\mathrm{dx}\,. \tag{3.93}$$

Let us analyze this **convex** minimization problem

$$\begin{aligned}&\int_0^1 W_{\mathrm{Biot}}(u'(x))\,\mathrm{dx}=\int_0^1 \mu\left[\left(\sqrt{4+u'(x)^2}-1\right)^2-1\right]\,\mathrm{dx}\mapsto\ \min.\mathrm{w.r.t.}\ u,\\&\qquad u(0)=0,\ u(1)=\gamma\,.\end{aligned} \tag{3.94}$$

The Euler-Lagrange equation is

$$\forall\,\phi\in C_0^\infty([0,1],\mathbb{R}):\quad \int_0^1 \frac{\left(\sqrt{4+u'(x)^2}-1\right)}{\sqrt{4+u'(x)^2}}\,u'(x)\,\phi'(x)\,\mathrm{dx}=0,\qquad \textbf{weak form}$$

$$\frac{\mathrm{d}}{\mathrm{dx}}\left[\tau_{\mathrm{Biot}}(u'(x))\right]=0\,,\quad \tau_{\mathrm{Biot}}(u')=2\mu\left(\frac{\left(\sqrt{4+(u')^2}-1\right)}{\sqrt{4+(u')^2}}\,u'\right),\qquad \textbf{strong form}$$

$$\tau_{\mathrm{Biot}}=2\mu\left(\frac{\left(\sqrt{4+(u'(x))^2}-1\right)}{\sqrt{4+(u'(x))^2}}\,u'(x)\right)=\mathrm{const.},\qquad \textbf{integrated form}$$

$$\begin{aligned}u''(x)\cdot\left(1-\frac{1}{\sqrt{4+u'(x)^2}}+\frac{u'(x)^2}{\left(4+u'(x)^2\right)^{(3/2)}}\right)&=0,\qquad \textbf{differentiated form}\,,\\u(0)=0,\ u(1)&=\gamma,\end{aligned} \tag{3.95}$$

showing that the homogeneous deformation is always a solution and hence, by strict convexity, the **unique solution** with **nonlinear, strictly-monotone** shear stress response

$$\tau_{\text{Biot}} = 2\,\mu\,\frac{\left(\sqrt{4+\gamma^2}-1\right)}{\sqrt{4+\gamma^2}}\cdot\gamma = \tau^{\text{cons}}_{\text{finite}} \quad (= \mu\,\gamma + o(\gamma))\ , \tag{3.96}$$

which **coincides** in fact with the shear stress response of the finite-strain Cosserat model with weak consistent coupling evaluated for this homogeneous response in (3.26).

Finally, it should be noted that from a three-dimensional viewpoint, the used shear energy $\mu\,\|U-1\!\!1\|^2$ is **not quasiconvex** and **not Legendre-Hadamard elliptic** [2] but satisfies still the **seperate convexity requirement in the principal stretches**. This loss of ellipticity is due to the continuum rotations inherent in $U = R^T(F)\,F$. A more refined analysis shows that the **Baker-Ericksen inequalities** (necessary for ellipticity) are violated if $\lambda_i + \lambda_j < 1$, where λ_i are the eigenvalues of U. The natural idea to overcome the non-ellipticity of W_{Biot} in a classical elasticity context is to consider its quasiconvexification. However, the analytical form of the quasiconvex hull $QW_{\text{Biot}}(F)$ is not known explicitly. The Cosserat model with small $L_c > 0$ provides an alternative means of regularization.

Let us gather the obtained stress/strain behaviour in simple glide for small amounts of shear γ. For consistent coupling we have:

$$\mu\,\gamma = \tau_{\text{lin}} = \tau^{\text{cons}}_{\text{small}} = \tau^{\text{indet}}_{\text{small}}, \qquad \mu\,\gamma = \tau_{\text{lin}} < \tau^{\text{micro}}_{\text{red}} < \tau^{\text{hom}}_{\text{finite}} < \tau^{\text{hom}}_{\text{red}}\ , \tag{3.97}$$

where $\tau_{\text{lin}} < \tau^{\text{micro}}_{\text{red}} < \tau^{\text{hom}}_{\text{finite}} < \tau^{\text{hom}}_{\text{red}}$ have the same tangent in 0. For rigid Dirichlet data $\overline{\alpha}_{\text{d}} = 0$ we obtain

$$\mu\,\gamma = \tau_{\text{lin}} < \tau^{\text{rigid}}_{\text{small}} < \tau^{\text{indet,rigid}}_{\text{small}}\ , \tag{3.98}$$

with artificially stiffer behaviour for arbitrary small shear due to boundary layer effects.

4 Numerical treatment

In our non-linear finite element formulation we apply the consistent linearization as it has been treated in [30, p.226] since the numerical algorithm solves locally linearized equations in the sense of Newtons-method. Thus, we introduce the Gateaux differentiation

$$D\{\,\cdot\}(\mathbf{a})\cdot\mathbf{b} := \frac{d}{d\varepsilon}\{\,\cdot\}(\mathbf{a}+\varepsilon\mathbf{b})|_{\varepsilon=0} \tag{4.1}$$

of a tensor-valued function $\{\,\cdot\}(\mathbf{a})$ at the vector $\mathbf{a}$ into the direction of a vector $\mathbf{b}$ and we use the short notation $\Delta\{\,\cdot\}(\mathbf{a},\Delta\mathbf{b}) := D\{\,\cdot\}(\mathbf{a})\cdot\mathbf{b}$.

The deformation of a body Ω_0 from reference configuration into actual configuration Ω_t is primarily described by a displacement field $\mathbf{u}(\mathbf{X},t)$ connecting reference coordinates $\mathbf{X}\in\Omega_0$ and actual coordinates $\mathbf{x}\in\Omega_t$ through $\mathbf{x}(t) = \mathbf{X}(t_0) + \mathbf{u}(t)$ and a microrotation field $\overline{\alpha}(\mathbf{X},t)$ defining the microrotation tensor $\bar{\mathbf{R}}$. For compact notation a vector of primary unknown variables $\mathbf{p}(\mathbf{X},t) := \{\mathbf{u}(\mathbf{X},t),\overline{\alpha}(\mathbf{X},t)\}$ (Lagrangean description) is introduced. In the same spirit we define the variational vector $\delta\mathbf{p}(\mathbf{X},t) := \{\delta\mathbf{u}(\mathbf{X},t),\delta\overline{\alpha}(\mathbf{X},t)\}$ and the incremental vector $\Delta\mathbf{p}(\mathbf{X},t) := \{\Delta\mathbf{u}(\mathbf{X},t),\Delta\overline{\alpha}(\mathbf{X},t)\}$ of primary unknown variables.

The two-field variational principle reads in the quasistatic case

$$0 = \delta I(\varphi,\bar{\mathbf{R}}) =: G(\mathbf{p},\delta\mathbf{p})\,. \tag{4.2}$$

Local linearization of $G(\mathbf{p},\delta\mathbf{p})$ at $\mathbf{p}=\bar{\mathbf{p}}$ gives us

$$LG(\bar{\mathbf{p}},\delta\mathbf{p},\Delta\mathbf{p}) = G(\bar{\mathbf{p}},\delta\mathbf{p}) + \Delta G(\bar{\mathbf{p}},\delta\mathbf{p},\Delta\mathbf{p}) \tag{4.3}$$

and thus, the equation to be solved within a Newton iteration is

$$\Delta G(\bar{\mathbf{p}},\delta\mathbf{p},\Delta\mathbf{p}) = -G(\bar{\mathbf{p}},\delta\mathbf{p})\,. \tag{4.4}$$

For a standard isoparametric 8-node brick element with trilinear shape functions (4.4) can be converted to a system of algebraic equations expressed in discrete nodal point vectors $\bar{\mathbf{p}}^I$, $\delta\mathbf{p}^I$ and $\Delta\mathbf{p}^I$ by

$$< \delta\mathbf{p}^I, \mathbf{K}(\bar{\mathbf{p}}^I), \Delta\mathbf{p}^I >= - < \delta\mathbf{p}^I, \mathbf{F}(\bar{\mathbf{p}}^I) > \tag{4.5}$$

During Newtons iteration process the stiffness matrix $\mathbf{K}$ and the nodal force vector $\mathbf{F}$ are generated for actual vectors $\bar{\mathbf{p}}^I$. The result of solving (4.5) is the incremental vector $\Delta\mathbf{p}^I$ of discrete displacements $\mathbf{u}^I$ and microrotations $\overline{\alpha}^I$ at nodes. Note that the update of nodal displacements $\mathbf{u}^I$ is simply additive $\mathbf{u}^I_{i+1} = \mathbf{u}^I_i + \Delta\mathbf{u}^I$. For the multiplicative update of microrotations we refer to [44]. A completely general 3D-nonlinear Cosserat formulation is available and already used for more complicated tests as shown in Figure 4.1.

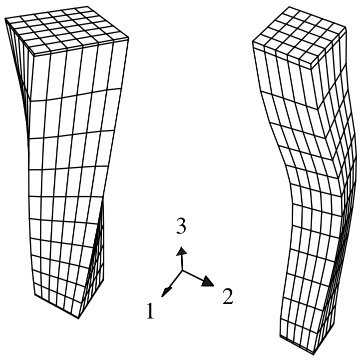

Figure 4.1: Completely general 3D-nonlinear Cosserat tests (left: torsion; right: compression with twist and buckling).

The finite element code is validated by the analytical solutions for both the linear and nonlinear Cosserat model. The consistent coupling boundary condition is numerically treated by introducing a boundary layer with μ_c very large there - this ensures algorithmically consistent coupling.

5 Computational results

First we specify the sample and its material parameters for the numerical investigations. Then we vary the prescribed microrotation angle $\overline{\alpha}_\mathrm{d}$ at upper and lower face for given shear $\gamma = 0.2$. At last the possibility and influence of various boundary conditions for microrotations $\overline{\alpha}$ are discussed.

5.1 Specification of the test

As shown in Figure (5.1) the investigated sample is a squared cube with height=1, width=1 and length=1. The material parameters are $\mu = 1 \cdot 10^5$ and $\lambda = 1.5 \cdot 10^5$, internal length $L_c = 0.05$ and curvature exponent $q = 6$. It has been checked that the computational results for simple glide are independent of λ, as they must be in view of the kinematics which leads to $\det[F] = 1$.

Remark 5.1 (Simple glide and torsion)
The simple glide problem is often compared with the torsion test. But an important difference is: simple glide allows for homogeneous response for certain boundary conditions, while torsion never does, not in the linear case nor in the nonlinear case.

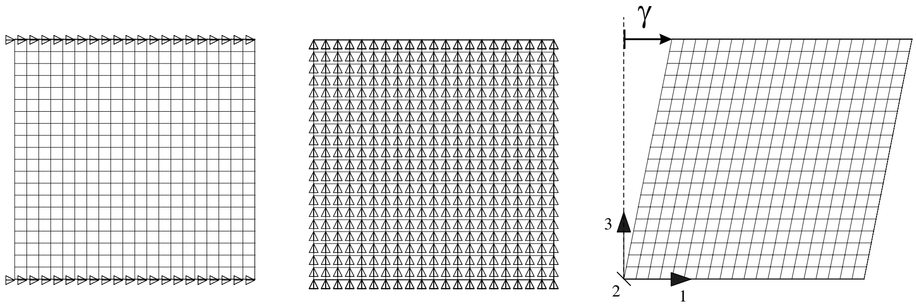

Figure 5.1: Undeformed mesh with boundaries in e_1- and e_3- direction and deformed mesh with axis

We block displacements in e_2- and e_3-direction. Additionally, displacements in e_1-direction are linked in each e_1-e_2-plane. Microrotations around e_1- and e_3-direction are blocked, too. Additionally, microrotations around e_2-direction are linked in each e_1-e_2-plane. Thus we simulate the simple glide problem.

5.2 Variation of prescribed microrotations at upper and lower face

In the following, we investigate the equilibrium solution for given shear $\gamma = 0.2$ and prescribed microrotations at upper and lower face between $\overline{\alpha}_{\mathrm{d}} = -0.1$ and $\overline{\alpha}_{\mathrm{d}} = 0.3$ as Dirichlet boundary condition. The solution depends sensitivly on the Cosserat couple modulus μ_c. Four situations with μ_c between 0 and μ show these effects. One situation with weak consistent coupling boundary condition and prescribed microrotations at upper and lower face is also considered. The first moment symmetry constraint determines the unique classical solution.

5.2.1 Results for the linear elastic Cosserat model

Due to the unqualified uniqueness of the linear Cosserat model in simple glide for $\mu_c > 0$ the computational response is easily understood and serves mainly the validation of our algorithm.

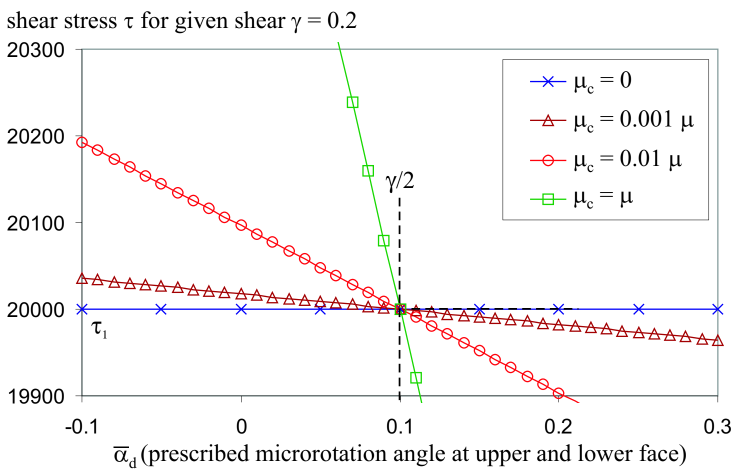

Figure 5.2: Shear stress τ for various Cosserat couple modulus μ_c

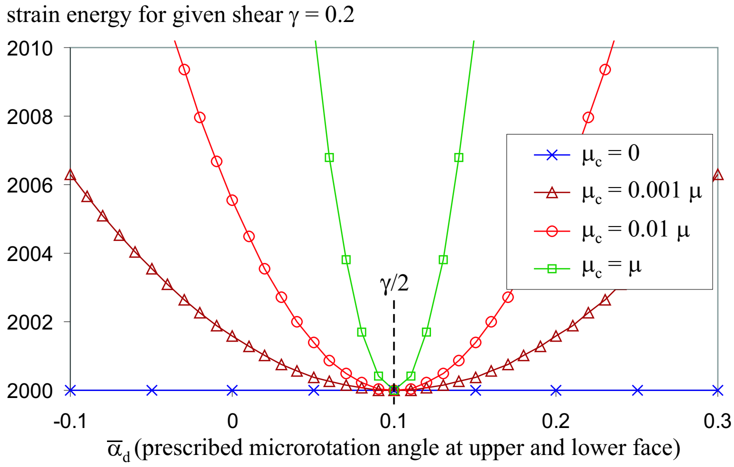

Figure 5.3: Strain energy for various Cosserat couple modulus μ_c

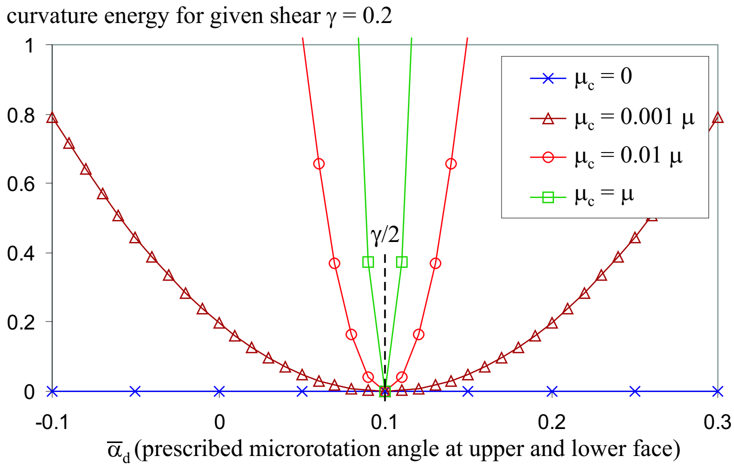

Figure 5.4: Curvature energy for various Cosserat couple modulus μ_c

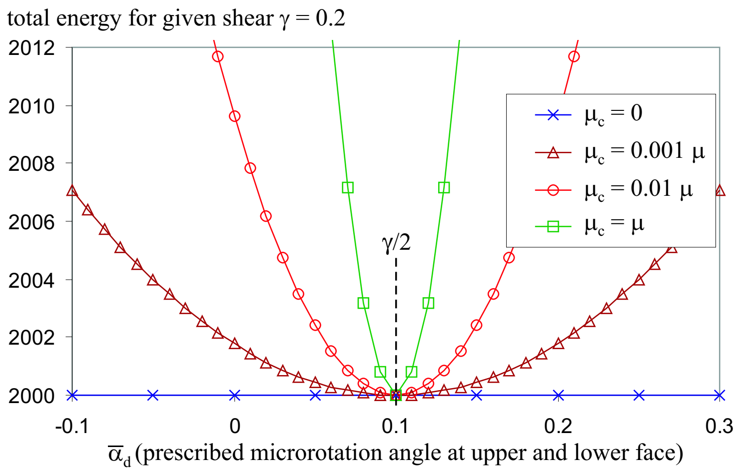

Figure 5.5: Total energy of equilibrium solutions for various Cosserat couple modulus μ_c

Remark that in the linear case, pure Neumann, consistent coupling and first moment symmetry constraint determine the unique aligned homogeneous response $\overline{\alpha} = \frac{\gamma}{2} = 0.1$, so nothing is to be plotted here.

5.2.2 Results for the nonlinear elastic Cosserat theory

At prescribed $\overline{\alpha}_{\mathrm{d}}$ at the upper and lower face and for $L_c > 0$ our computations suggest that the nonlinear equilibria are unique for simple glide. For pure Neumann conditions on the rotations we have three equilibria $\overline{\alpha}_1 = 0$, $\overline{\alpha}_2 = \arctan\frac{\gamma}{2}$, $\overline{\alpha}_3 = 2\arctan\frac{\gamma}{2}$, two of them $(\overline{\alpha}_1, \overline{\alpha}_3)$ minimizers. For consistent coupling the computational results suggest that the classical homogeneous solution is the unique energy minimizer while adjacent equilibria are found. Whether this is really the case remains open. The first moment symmetry constraint again provides only the aligned homogeneous solution $\overline{\alpha}_2 = \arctan\frac{\gamma}{2} = 0.0996687$.

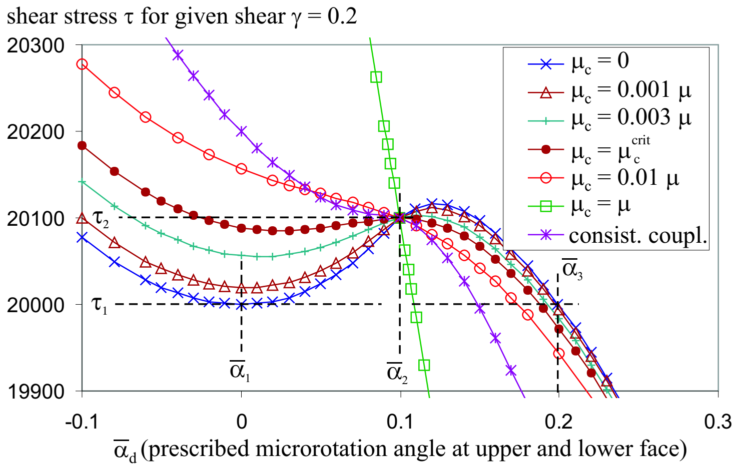

Figure 5.6: Shear stress τ for various Cosserat couple modulus μ_c.

For $\mu_c = \mu$ Figure 5.6 indicates the dramatic dependence of the shear stress τ on the value of the Dirichlet microrotational boundary condition $\overline{\alpha}_{\mathrm{d}}$. Only for $\overline{\alpha}_{\mathrm{d}} = \alpha_2$ we obtain the same result τ_2 for all situations. It is the **trivial** homogeneous solution and a prominent point in all diagrams. The difference between τ_1 and τ_2 can be easily explained: the shear stress response is given for the specific value $\gamma = 0.2$, at which already nonlinear effects take place. Choosing γ smaller, removes this difference.

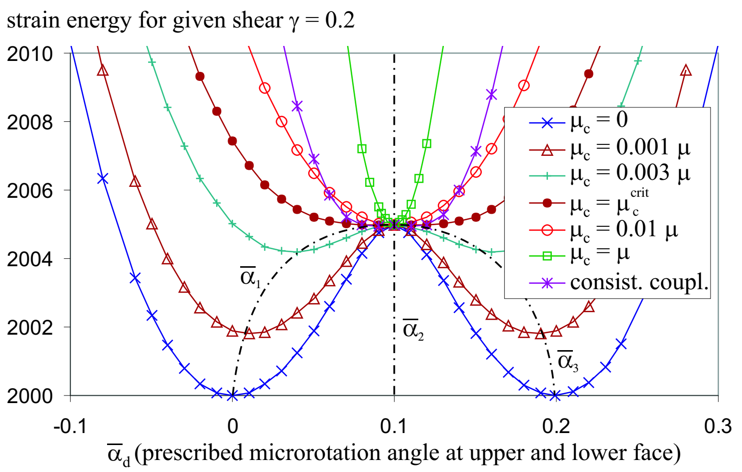

Figure 5.7: Strain energy for various Cosserat couple modulus μ_c. Here $\overline{\alpha}_1 = 0$, $\overline{\alpha}_2 = \arctan\frac{\gamma}{2} = 0.0996687$, $\overline{\alpha}_3 = 2\overline{\alpha}_2 = 0.1993373$. The intersection of the parabola with the response curve gives the possible homogeneous solutions for $\gamma = 0.2$, compare with (3.5). Here, $\mu_c^{\mathrm{crit}} > 0.00496\,\mu$.

For $\mu_c = 0$ the strain energy W_{mp} reaches a minimal value of 2000 in Figure 5.7, choosing $\overline{\alpha}_{\mathrm{d}} = \alpha_1$ or $\overline{\alpha}_{\mathrm{d}} = \overline{\alpha}_3$. For small μ_c or consistent coupling boundary condition the strain energy possesses minimal points different from $\overline{\alpha}_{\mathrm{d}} = \overline{\alpha}_2$, which means inhomogeneous situations for the microrotation field $\overline{\alpha}$ and consequently non-vanishing curvature energy.

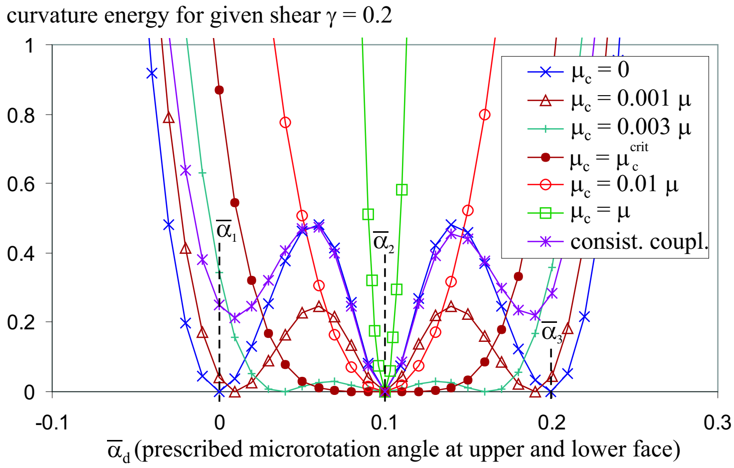

Figure 5.8: Curvature energy for various Cosserat couple modulus μ_c. Qualitative change if μ_c passes μ_c^{crit}!

The graph of $\mu_c = 0$ with and without consistent coupling boundary condition seems to be identical for the curvature energy. But the numerical values at $\overline{\alpha}_1$ and $\overline{\alpha}_3$ for consistent coupling boundary condition differ slightly from zero.

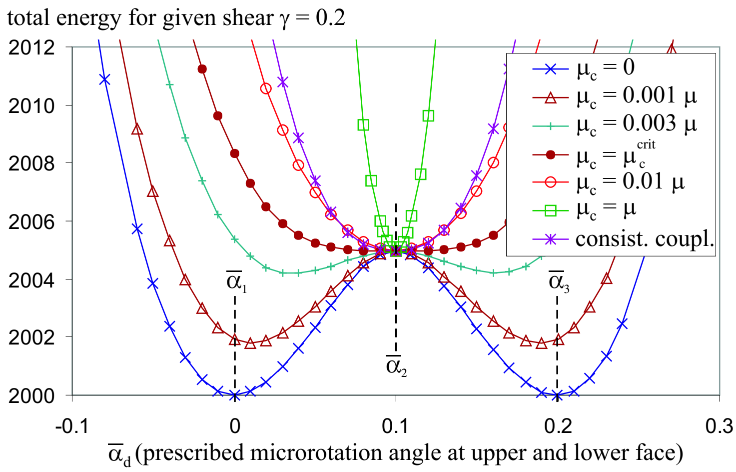

Figure 5.9: Total energy of equilibrium solutions for various Cosserat couple modulus μ_c

The total energy as sum of strain and curvature energy represents a flat graph around $\overline{\alpha}_2$ for consistent coupling boundary condition with minimal points $\overline{\alpha}_{\mathrm{d}} = 0.06$ and $\overline{\alpha}_{\mathrm{d}} = 0.14$ in the vicinity of the homogeneous response.

It can bee seen that for pure Neumann boundary conditions three equilibria exist (roughly if $\mu_c < \mu_c^{\mathrm{crit}}$) of which two are minimizers. For $\mu_c = 0$ the two minimizers are the two non-trivial homogeneous responses corresponding to $\overline{\alpha}_1 = 0$ and $\overline{\alpha}_3 = 2\arctan\frac{\gamma}{2}$. Moreover, $\overline{\alpha}_1 = 0$ corresponds to the linear response: it can easily be understood by noting that $\overline{\alpha}_1 \equiv 0$ implies $\overline{R} \equiv 1\!\!1$, which then yields exactly linear elasticity for the deformation as remaining problem to be solved in the variational context.

5.3 Dependence of $\overline{\alpha}$ on the Dirichlet boundary condition $\overline{\alpha}_{\mathrm{d}}$

Here we depict the response of the finite-strain Cosserat model in simple glide as far as microrotations are concerned. The solution is plotted for different μ_c and various Dirichlet data.

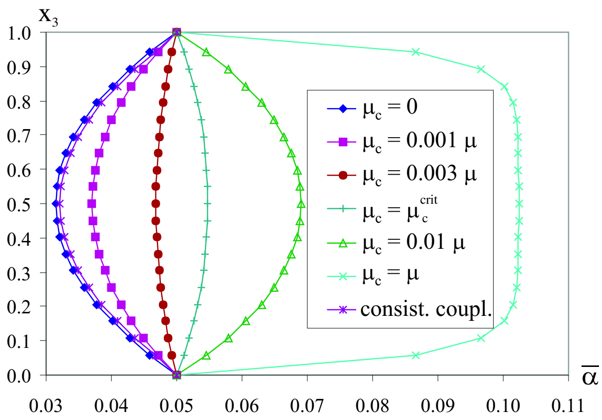

Figure 5.10: Microrotation $\overline{\alpha}$ for various μ_c with $L_c = 0.05$ and $\overline{\alpha}_{\rm d} = 0.05 < \overline{\alpha}_2$.

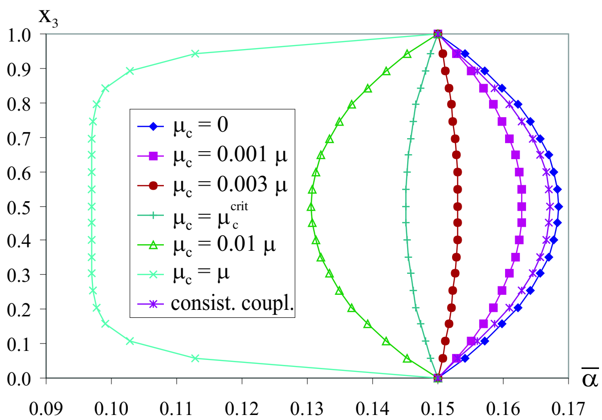

Figure 5.11: Microrotation $\overline{\alpha}$ for various μ_c with $L_c = 0.05$ and $\overline{\alpha}_{\rm d} = 0.15 > \overline{\alpha}_2$.

In both pictures it can be seen that the qualitative behaviour of the solution depends sensitively on whether μ_c is bigger or smaller than $\mu_c^{\rm crit}$.

In the following we discuss the two-dimensional shear problem.

5.4 Boundary layer stiffening and identification of moduli

With a simple glide test it is not possible to specify the Cosserat couple modulus μ_c unambiguously, since then the value of μ_c depends on the boundary condition for $\overline{\alpha}$ and the height of the structure. In Diebels [10] e.g. a two-dimensional beam structure with height $h > 0$ and length $b > 0$ has been numerically exposed to simple shear using the fourth-order Bernoulli-beam theory (conceptually similar to the indeterminate couple stress model) and the corresponding macroscopic (effective) shear modulus G_c, relating average shear force at the upper face $\overline{\tau} = \frac{1}{b}\int_{x_1} \tau(x_1, h)\, dx_1$ versus average shear per unit height $\overline{\gamma} = \frac{u(x_1,h)}{h}$ has been determined. It is numerically found that G_c is systematically larger than the classical shear modulus μ determined from computational tension data for the same beam structure. The difference being the larger the smaller the height h of the beam structure. Diebels et al. propose that this systematic deviation can be modelled with a linear Cosserat model for which then $G_c := \mu + \mu_c$, $\mu_c > 0$. For their numerical experiment it has been assumed that the beams adjacent to the upper and lower face are rigidly connected to the translated faces. Conceptually, the rotation of beam elements is viewed as the microrotation in the Cosserat model and therefore, rigid Dirichlet conditions $\overline{\alpha}_{\rm d} = 0$ lead to higher stiffness caused by micro bending moments.

The next picture shows that in a one layer honeycomb structure beams on faces rotate, but in strong dependence of the beam cross section area A and the moment of inertia I.

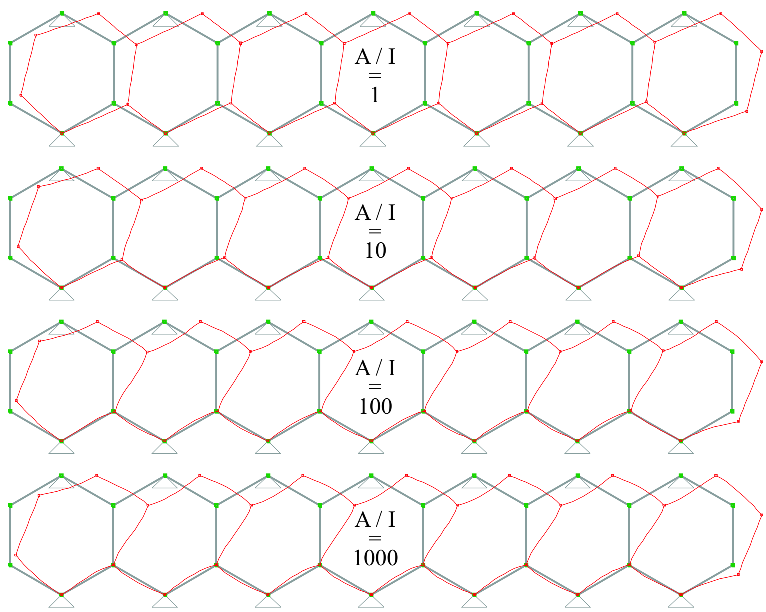

Figure 5.12: Undeformed and deformed meshes of a one layer honeycomb structure with beams under shear loading for different ratios A/I. Results obtained from Bernoulli-beam theory.

The question arises, what kind of ratio A/I can be taken for realistic investigations. Considering a beam structure with circular members of radius r, cross-section area $A = \pi r^2$ and moment of inertia $I = \pi r^4/4$ leads to $A/I = 4/r^2$. This ratio is not a dimensionless function, so we take a squared sample cube of length 1 cm. It is not possible to talk about (one-dimensional) beams in this sample if e.g. $r > 0.2$ cm, since then the simplifications provided by the Bernoulli beam theory do not any more apply. Next diagram shows that if we assume $A/I > 100$, then the corresponding radius is small enough for Bernoulli theory to apply.

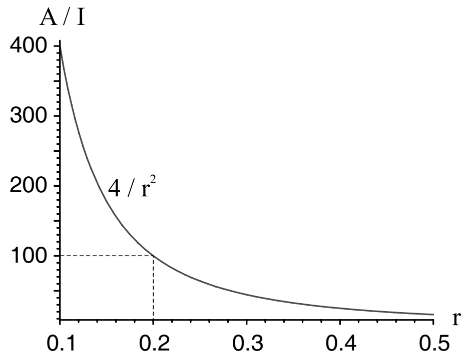

Figure 5.13: Ratio A/I as function of radius r for circular cross section.

In the following, we take $A/I = 1000$ and compute the horizontal reaction forces on the boundaries.

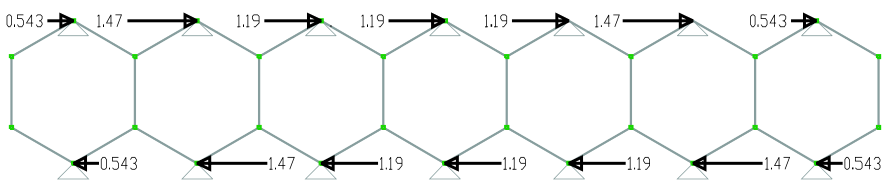

Figure 5.14: Horizontal reaction forces on boundaries (rotations free), plotted on reference configuration.

The same test, but now with fixed rotations on boundaries.

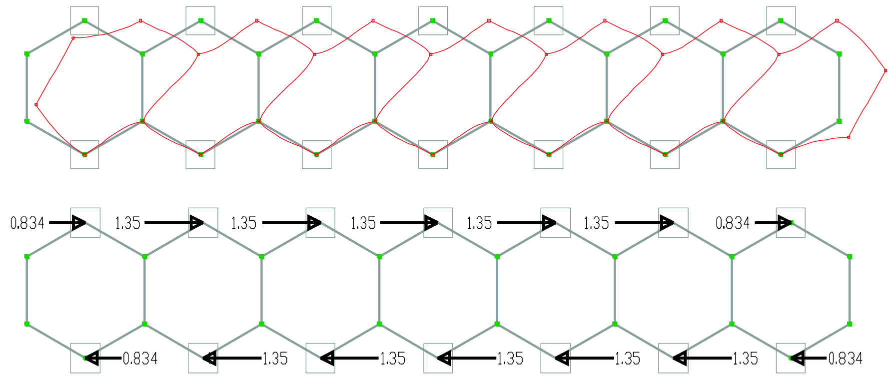

Figure 5.15: Up: Undeformed and deformed mesh with fixed rotations on boundaries (rigid Dirichlet condition $\overline{\alpha}_{\mathrm{d}} = 0$). Down: Horizontal reaction forces on boundaries (rotations fixed), plotted on reference configuration.

The sum of horizontal reaction forces in Figure 5.15 compared to Figure 5.14 shows clearly that fixing rotations leads to a higher stiffness by a factor $8.418/7.596 = 1.108$. This effect is especially marked in a one layer honeycomb structure and decreases with more layers (higher sample, see Figure 5.16 and Figure 5.17), as it has been observed in [10].

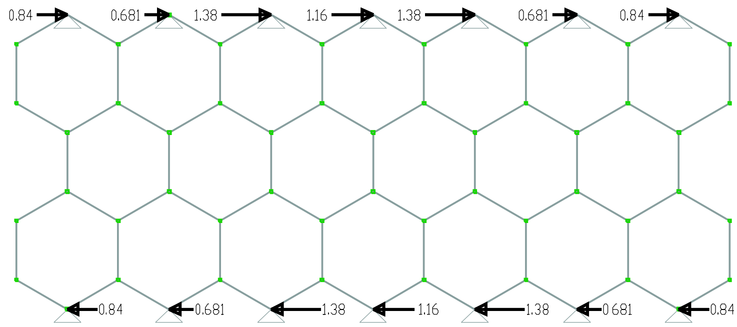

Figure 5.16: Horizontal reaction forces on boundaries (rotations free), plotted on reference configuration.

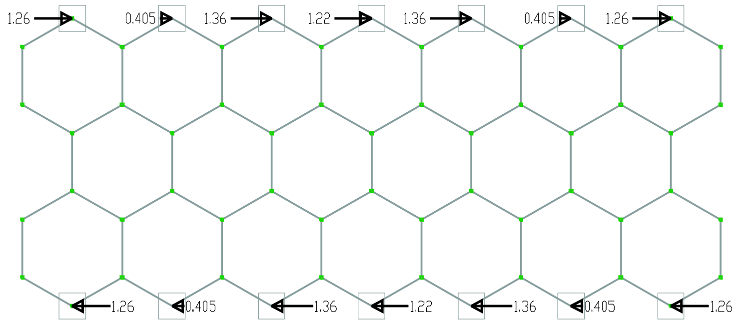

Figure 5.17: Horizontal reaction forces on boundaries (rotations fixed), plotted on reference configuration.

Again, the sum of horizontal reaction forces in Figure 5.17 compared to Figure 5.16 shows that fixing rotations leads to higher stiffness but now by a smaller factor $7.27/6.962 = 1.044$. Further it can be seen, that influences from the left and right border of the structure increase with its height.

In summary, an exhausting continuum description for the shear problem of a beam structure does need detailed information on how beams behave at the boundary. We note: the parameter $\mu_c > 0$, accounting here for the stiffness increase, is a property of the boundary value problem (how boundary conditions are applied) but not a property of the material, as μ and λ are. ¿From the derived analytical representation we infer that the complete solution of the linear Cosserat problem in terms of the displacement u is a function of γ, $\frac{N}{L_c}$ and $N \cdot L_c$. Consider the same material given in different sample sizes of cubes with edge length $L_i > 1$. Due to scaling relations, we may transform the different sample sizes to the unit cube resulting in a modified internal length $\frac{L_c}{L_i}$ but identical values (γ, N) by the assumption that μ_c, hence $N = \sqrt{\frac{\mu_c}{\mu+\mu_c}}$ is a dimensionless **material parameter independent of size**. Performing a corresponding shear experiment on each sample size we obtain best-fitting values of $\frac{N}{(L_c/L_i)} = \hat{C}_i$ and $N\,\frac{L_c}{L_i} = \hat{D}_i$ for every size. If the infinitesimal micropolar model would be physically consistent this implies that $N^2 = \hat{C}_i \cdot \hat{D}_i$, independent[21] of i. A striking consequence of this development is that **the assumed size-independent material parameter N cannot be determined without prior knowledge of the characteristic length L_c in contrast to the other classical elastic constants μ and λ and vice-versa: the characteristic internal length L_c can only be determined once N is known. This is a problematic feature shared by all micropolar models with $\mu_c > 0$.**

5.5 Planar shear of a long layer

Let us extend the previous computations to cover also the planar shear of a layer with unit height. The calculations are now fully two-dimensional, displacements in e_2-direction remain blocked. Of interest are the influences of μ_c and of various boundary conditions. We consider a long sample (ratio $4:1$) with the intention to obtain a zone in the middle of the specimen which behaves like in the simple glide test (far enough away from disturbing effects of the free left and right edges). The next picture shows the finite element mesh in the undeformed and deformed state, indicating different zones of deformation:

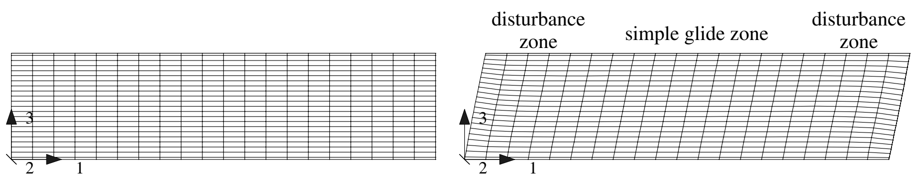

Figure 5.18: Undeformed and deformed mesh with indicated deformation-zones.

A honeycomb structure under planar shear also indicates different zones of deformation.

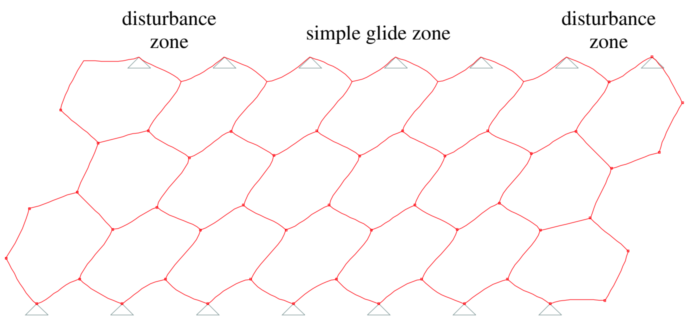

Figure 5.19: Different zones of deformation for a honeycomb structure under planar shear and free rotations at the boundary. High inhomogeneity at left and right corners.

It is possible to obtain classical material behaviour by using the nonlinear Cosserat theory and special material parameters. The first possibility is using $\mu_c = 0$ and $L_c \to \infty$ (this results

[21] It appears as if $N^2 = \hat{C}_i \cdot \hat{D}_i$ independent of i for different sizes is questionable.

in constant microrotations and leads to classical linear elasticity), the second is using $\mu_c = \mu$ and $L_c = 0$ (evaluation of the Boltzmann-axiom shows that microrotations must coincide with the polar decomposition of the deformation gradient, the classical geometrically nonlinear Biot model).

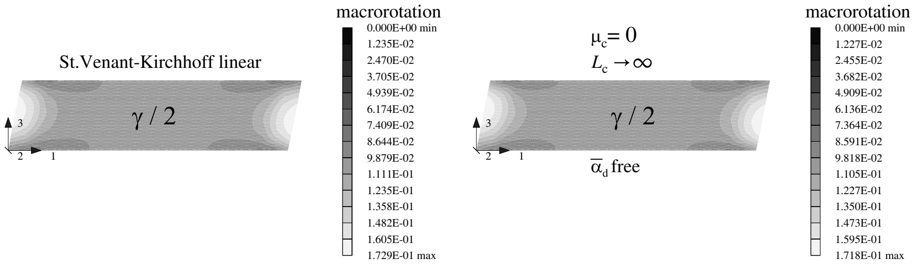

Figure 5.20: Macrorotation for classical linear elastic material (left) and nonlinear Cosserat theory with $\mu_c = 0$ and $L_c \to \infty$ (right) together with $\overline{\alpha}_{\rm d} = 0$. Both computations practically coincide.

Macro- and microrotation coincide for Biot model as Figure 5.21 shows.

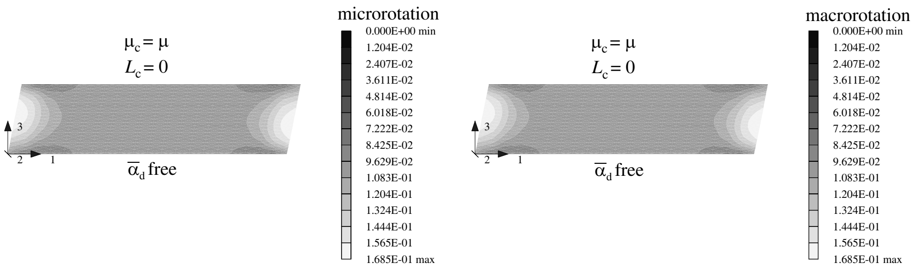

Figure 5.21: Macro- and microrotation for Biot model using nonlinear Cosserat theory with $\mu_c = \mu$ and $L_c = 0$.

By using the linear Cosserat theory, we can compare our results with [10]. The next figure clearly shows that μ_c influences the shape and height of boundary layers.

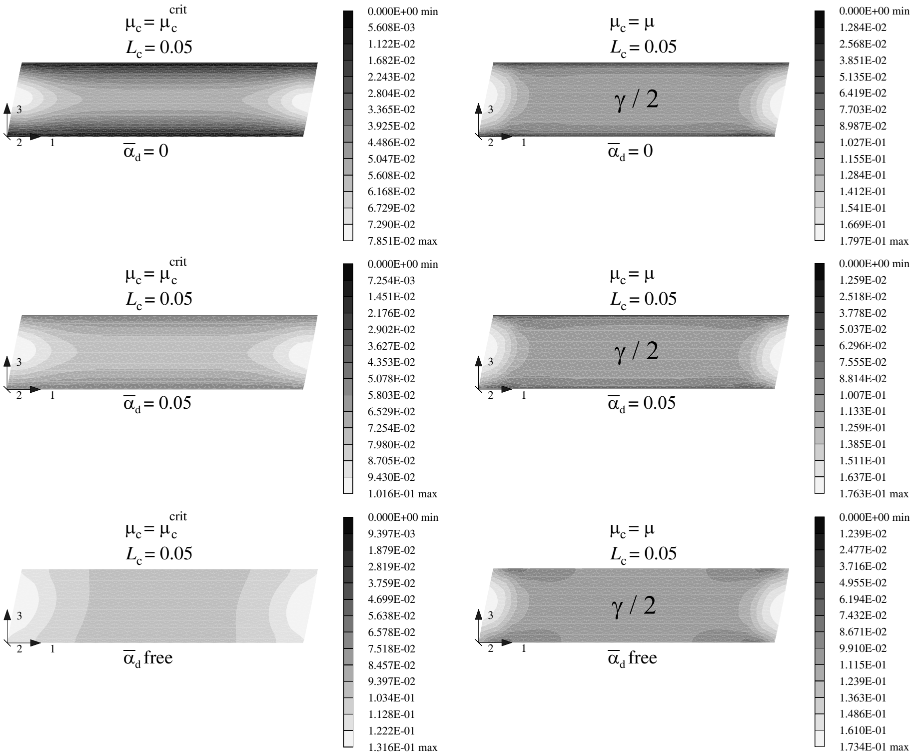

Figure 5.22: Microrotation $\overline{\alpha}$ for linear Cosserat theory, various boundary conditions and various μ_c. The microrotations remain throughout positive.

The Nonlinear computation gives us the possibility to set $\mu_c = 0$. In this case it is interesting to note that microrotations become non-trivial solutions $\overline{\alpha} \neq \overline{\alpha}_1$ at left and right edges. The behaviour in the middle of the specimen is consistent with our previous results from simple glide tests.

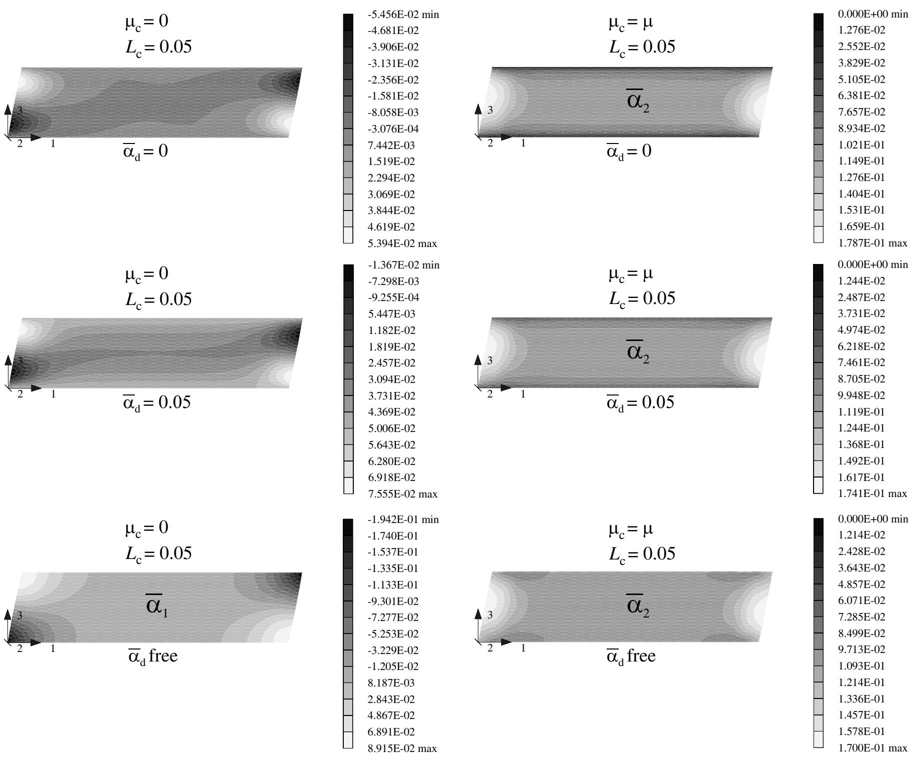

Figure 5.23: Microrotation $\overline{\alpha}$ for nonlinear Cosserat theory, various boundary conditions and various μ_c. Observe that for $\mu_c = 0$ microrotations may become negative. This effect shows the relative freedom microrotations have when choosing $\mu_c = 0$.

Negative values in microrotations do not imply that macrorotations become also negative! On the contrary, observe that negative microrotations lead to an increasing positive value in macrorotations along edges (compare with Figure 5.26). This shows that microrotations are not necessarily a structural object (like the rotation of beam elements) but rather hidden (internal variables) acting where the material responds inhomogeneously.

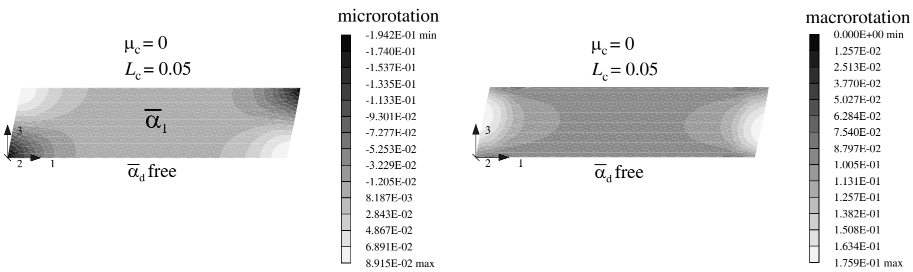

Figure 5.24: Micro- and macrorotation for nonlinear Cosserat theory, $\mu_c = 0$ and Neumann boundary conditions.

Now we investigate the numerical behaviour around the critical value of $\mu_c = \mu_c^{\mathrm{crit}}$.

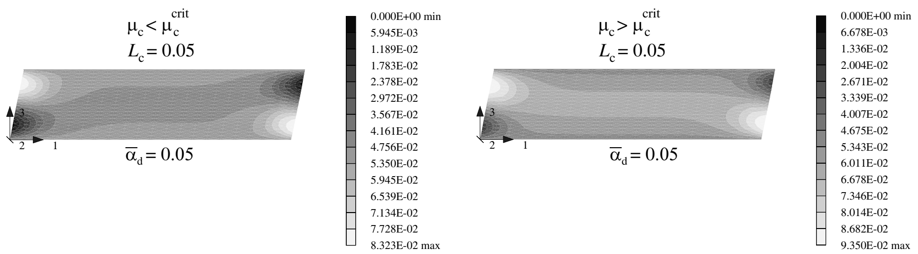

Figure 5.25: Microrotation $\overline{\alpha}$ for nonlinear Cosserat theory, boundary condition $\overline{\alpha}_d = 0.05$ and μ_c around μ_c^{crit}. Qualitative change of response, consistent with the analytical and numerical results for simple glide.

In both Figure 5.23 and Figure 5.25 it can be seen, that microrotations for small μ_c tend to zero in the middle of the sample: the non-aligned $\overline{\alpha}_1$ solution from simple glide.

At last we present the solution for $\mu_c = 0$ and consistent coupling boundary condition.

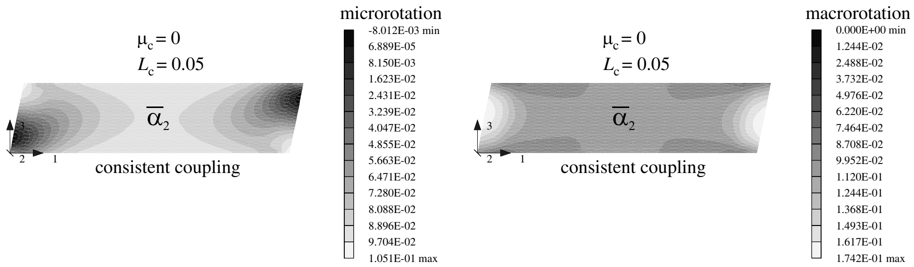

Figure 5.26: Microrotation $\overline{\alpha}$ for nonlinear Cosserat theory and consistent coupling. Observe that macrorotations remain positive throughout!

Microrotation and shear difference $\Delta u = u - \gamma\, x_3$ at left free edge show the inhomogeneous situation at free boundaries.

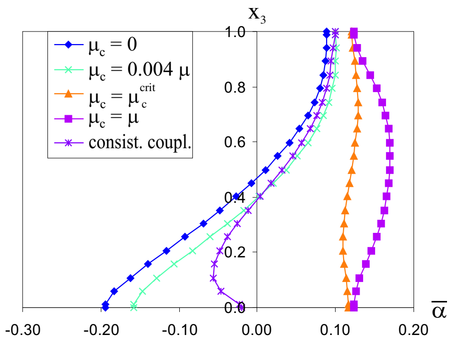

Figure 5.27: Plot of $\overline{\alpha}$ for nonlinear Cosserat theory at left free edge for various μ_c.

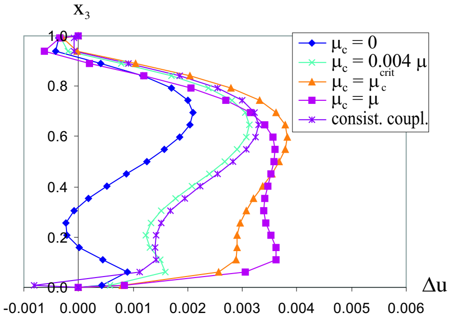

Figure 5.28: Plot of shear difference $\Delta u = u - \gamma\, x_3$ for nonlinear Cosserat theory at left free edge for various μ_c. Precise measurements of the edge-profile of an actual sample in a shear experiment might be of use in determining boundary conditions and parameters for the Cosserat model.

5.6 Discussion of boundary conditions for microrotations

We have seen that the highly non-unique response in the geometrically exact case necessitates to discuss and define boundary or side-conditions for microrotations, if these microrotations are supposed to represent independent degrees of freedom within the boundary value problem.

For the choice of $\mu_c = \mu$ the microrotation angles $\overline{\alpha}$ are coupled with the continuum rotations nearly one to one (through a strong elastic spring with elasticity constant μ_c) in both the linear and the nonlinear problem. Thus, the prescription of additional independent boundary conditions on the microrotations $\overline{\alpha}$ in this case affect the solution in a doubtful way. A decrease of the shear stress τ as represented in Figure 5.6 excludes the principle of local effects, which a boundary condition should have according to **St.Venant's principle**. In effect, the linear analysis following (3.71) shows that $\mu_c > 0$ in the simple glide problem is rather a measure of the influence of Dirichlet boundary conditions for microrotations on the displacement solution! This effect becomes the weaker the smaller we chose μ_c. Further, the solution for small μ_c offers two minimal points for $\overline{\alpha}$ and simultaneously causes an inhomogeneous microrotational field.

The consistent coupling boundary condition has no marked minimum for $\overline{\alpha}_2$ as it is the case for $\mu_c = \mu$. This indicates that a (nearly?) homogeneous solution can be found by the numerical algorithm, but neighbouring solutions with lower potential might be found as well, as suggested by the "laminate" microstructure solution in the partially simplified reduced problem (3.50). The consistent coupling condition is well-suited for smooth equilibrium solutions, however, it fails to be stable under energy minimization for $L_c = 0$ as has been argued in (3.52).

It still remains to find a boundary condition on the microrotations (or side-condition) which ensures that minimizers to homogeneous boundary conditions on the deformation are homogeneous within the body **and** coincide with the classical solution. A candidate, allowing for existence results in the finite-strain case could be the first moment symmetry constraint

$$\int_\Omega \overline{U}(x)\,\mathrm{dV} = \int_\Omega \overline{R}^T(x) F(x)\,\mathrm{dV} \in \mathrm{PSym}\,,$$

which translates into

$$0 = \int_0^1 \cos\overline{\alpha}(x)\cdot u'(x) - 2\sin\overline{\alpha}(x)\,\mathrm{dx}, \quad 0 \le \overline{\alpha} < \frac{\pi}{2}, \quad 0 \le u'(x) < 2\,,$$

for simple glide. It singles out the preferred aligned homogeneous solution, also in the degenerate linear Cosserat case with $\mu_c = 0$ and $L_c > 0$. The computational handling of this nonlocal condition seems to be technically challenging, here we have implemented it through a penalty formulation.

5.7 Boundary and side conditions for microrotations under $L_c \to \infty$

Let us switch back to the three-dimensional problem. If we consider $L_c \to \infty$ (arbitrary small structures) then the variational problem determines the microrotations $\overline{R}$ automatically to be constant in the limit.

In this case the **classical rigid Dirichlet condition** (at some part of the boundary $\Gamma \subset \partial\Omega$) implies $\overline{R} = \overline{R}_{\mathrm{d}} \equiv 1\!\!1$ and the remaining variational problem for the deformation φ is precisely linear elasticity. The limit $L_c \to \infty$ for other rigid Dirichlet data $\overline{R}_{\mathrm{d}}$ is only possible for a constant prescription of $\overline{R}_{\mathrm{d}}$.

The **consistent coupling condition** turns for $L_c \to \infty$ into

$$const. = \overline{R} = \mathrm{polar}(\nabla\varphi(x)), \quad x \in \Gamma,$$

which requires that the orthogonal part of $\nabla\varphi$ at the boundary Γ be constant. This can become a source of inconsistency if non-homogeneous Dirichlet conditions for φ are prescribed. For homogeneous boundary conditions $\varphi(x) = B.x$, with a constant matrix $B \in \mathrm{GL}^+(3,\mathbb{R})$ one has $\overline{R} = \mathrm{polar}(B)$ and the deformation response in the interior will be $\varphi(x) = B.x$, due to strict convexity of the formulation w.r.t. $F = \nabla\varphi$ at given constant microrotation $\overline{R}$.

Computationally, we have implemented a **consistent boundary layer requirement**, i.e. requiring $\overline{R}(x) = \mathrm{polar}(\nabla\varphi(x))$ in a thin boundary layer adjacent to Γ by setting μ_c very high in this layer and otherwise $\mu_c = 0$. However, this condition has a similar problem as the original formulation.

For **pure Neumann conditions** the constant microrotation $\overline{R} = const.$ is not uniquely determined, as has already be seen in the simple glide problem if $0 \leq \mu_c < \mu_c^{\mathrm{crit}}$. Note again that this fundamental indeterminacy is not a problem related to $\mu_c = 0$.

For **pure Neumann conditions in conjunction with first moment symmetry constraint** we obtain for a constant microrotation $\overline{R}$

$$\int_\Omega \overline{R}(x)^T \nabla\varphi(x)\,\mathrm{dV} = \overline{R}^T \int_\Omega \nabla\varphi(x)\,\mathrm{dV} = \overline{R}^T \int_\Omega \begin{pmatrix} \mathrm{Div}\,(\varphi_1(x)\,1\!\!1) \\ \mathrm{Div}\,(\varphi_2(x)\,1\!\!1) \\ \mathrm{Div}\,(\varphi_3(x)\,1\!\!1) \end{pmatrix} \mathrm{dV} = \overline{R}^T \int_{\partial\Omega} \varphi(x) \otimes \vec{n}\,\mathrm{dS}.$$

Assume that

$$\det \int_\Omega \nabla\varphi(x)\,\mathrm{dV} = \det \int_{\partial\Omega} \varphi(x) \otimes \vec{n}\,\mathrm{dS} > 0.$$

The symmetry constraint requires

$$\overline{R}^T \int_{\partial\Omega} \varphi(x) \otimes \vec{n}\,\mathrm{dS} \in \mathrm{PSym}.$$

According to the polar decomposition theorem this defines $\overline{R} \in \mathrm{SO}(3,\mathbb{R})$ uniquely for all boundary conditions on φ as

$$\overline{R} = \mathrm{polar}\left(\frac{1}{|\Omega|} \int_{\partial\Omega} \varphi(x) \otimes \vec{n}\,\mathrm{dS}\right),$$

compare to [49, Lem4.4] for a similar condition for the pure Neumann problem in classical nonlinear elasticity. Hence the first moment symmetry constraint seems to remain a useful condition also in the limit $L_c \to \infty$.

It is also possible to **relax the first moment symmetry constraint** into a symmetry condition in one connected **boundary layer** $\Gamma_h \subset \Omega$, adjacent to Γ. We may require

$$\int_{\Gamma_h} \overline{U}(x)\,\mathrm{dV} \in \mathrm{PSym}.$$

This condition is already enough to provide a unique aligned homogeneous response and is stable under minimization. Computationally, the smaller $h > 0$, the simpler its implementation by a penalty formulation.

Finally, the **weakest possible condition** fixing the microrotations $\overline{R}$ for homogeneous situations is given by arbitrarily choosing one point $x_0 \in \Omega \cup int(\Gamma)$ and demanding that $\overline{U}(x_0) \in$ PSym. For a quadratic problem in the deformation gradient, elliptic regularity ensures that $\nabla\varphi(x_0)$ exists classically. The problem, however, is to choose x_0.

6 Conclusion and further direction of research

We have presented an exhaustive treatment of the simple glide problem for both linear and nonlinear Cosserat models.

The linear Cosserat model extremely over-simplifies the response. Insight gained for the linear Cosserat model is of not much help in the finite-strain setting, this can already be seen by the pitchfork bifurcation diagram in conjunction with our FEM-calculations. It is shown, that the solution of the boundary value problem depends sensitively on μ_c when μ_c passes μ_c^{crit}. This feature is not related to $\mu_c = 0$, but occurs already for small positive $\mu_c > 0$. The stability of solutions of the nonlinear problem as a function of $\frac{\mu_c}{\mu}$ is therefore highly intricate.

The exceptional role played by assuming a strictly positive Cosserat couple modulus $\mu_c > 0$ can already be appreciated for simple homogeneous situations: both consistent coupling and the first moment symmetry constraint have the power to enforce a unique homogeneous response in simple glide. This is automatically implied in the nonlinear case by taking $\mu_c \geq \mu$, which is often assumed when using the Cosserat model as a regularization device. In the linear case, already $\mu_c > 0$ suffices for this purposes. This may explain, why the necessity to define additional conditions on the microrotations has been systematically overlooked in the linear framework, since uniqueness is automatically ensured.

Our analytical and computational development for simple glide clearly shows that taking $\mu_c = 0$ is possible and has its merits: it is closer to classical elasticity, does not provide for unqualified uniqueness, excludes unphysical stiffening effects for small samples, allows to determine the internal length scale L_c independent of shear moduli and it has motivated the introduction of additional conditions on the microrotations. Moreover, a positive parameter $\mu_c > 0$ is rather a property of the boundary value problem (how boundary conditions are applied) but not a property of the material, as μ and λ are, see the discussion in sect. 5.4. In this sense, we provide an answer to the question of Cosserat parameters: the assumption of a positive Cosserat couple modulus $\mu_c > 0$ is not necessary, at best, it is a structural parameter. That this modulus must be zero viewed as a material parameter is also the result of investigations of the first author on linear Cosserat models in torsion and bending [36].

The nonlinear Cosserat model may have a microstructure response in the classical limit of very large samples $L_c \to 0$. This is exemplified by looking at the finite-strain reduced problem in section 3.2.2 and underlined by the numerical results in Figure 3.27. If the internal length is large enough, these highly oscillating solutions are effectively ruled out.

If the Cosserat model should do more than account for boundary layer effects, the need of specifying new boundary conditions is apparent. The different proposed additional conditions on the microrotations all have the power to provide for a unique classical aligned homogeneous response independent of material parameters. Moreover, they do not lead to boundary stiffening effects. The restricted setting of simple glide and planar shear, however, does not allow us to draw a unanimous conclusion as to which is the preferable one.

The consistent coupling condition has the advantage of being a (local) boundary condition, but the disadvantage of needing a numerical scheme which respects C^1-continuity in a neighbourhood of the Dirichlet-boundary. Moreover, the boundary value problem should guarantee C^1-continuity of the deformation. This may not always be the case but is true in our setting of simple glide.

The first moment symmetry constraint in the bulk does not need C^1-continuity but represents a nonlocal condition, which is difficult to implement.

It is also possible to impose the first moment symmetry constraint only in the interior of the Dirichlet-boundary at the surface. This is a weaker condition than consistent coupling but still needs C^1-continuity in a neighbourhood of the Dirichlet-boundary to make sense.

By requiring the first moment symmetry constraint, however, only in a boundary layer adjacent to the Dirichlet-boundary it seems to be possible to combine the advantages of the previous conditions without the disadvantages: the last condition is more or less local and does not need C^1-continuity, hence suited for standard FEM-implementation. This is our tentative answer as far as boundary conditions for microrotations are concerned: the microrotations must be coupled in some sense or other to the deformation gradient, but never locally, as would be implied by taking $\mu_c > 0$!

In the near future we will provide evidence for the convenient behaviour of finite-strain Cosserat models for large scale three-dimensional problems within the new boundary conditions.

Acknowledgements

The analytical part is an augmented and revised section of P.N.'s habilitation thesis on mathematical aspects of Cosserat elasticity. P.N. is grateful to all people who have made this thesis possible. I.M. is indebted to C. Sansour for introducing him to the numerics of Cosserat elastic bodies.

References

[1] E.L. Aero and E.V. Kuvshinskii. Fundamental equations of the theory of elastic media with rotationally interacting particles. *Soviet Physics-Solid State*, 2:1272–1281, 1961.

[2] A. Bertram, T. Böhlke, and M. Silhavy. On the rank 1 convexity of stored energy functions of physically linear stress-strain relations. *Tech. Report. Nr. 1, Fakultät f. Maschinenbau, Univ. Magdeburg*, 2005.

[3] G. Capriz. *Continua with Microstructure*. Springer, Heidelberg, 1989.

[4] G. Capriz and P. Podio Guidugli. Formal structure and classification of theories of oriented media. *Ann. Mat. Pura Appl., Ser. IV*, 115:17–39, 1977.

[5] G. Capriz and P. Podio-Guidugli. Structured continua from a Lagrangian point of view. *Ann. Mat. Pura Appl. Ser. IV*, 135:1–25, 1983.

[6] E. Cosserat and F. Cosserat. *Théorie des corps déformables*. Librairie Scientifique A. Hermann et Fils (Theory of deformable bodies, NASA TT F-11 561, 1968), Paris, 1909.

[7] R. de Borst. Simulation of strain localization: a reappraisal of the Cosserat continuum. *Engng. Comp.*, 8:317–332, 1991.

[8] R. de Borst. A generalization of J_2-flow theory for polar continua. *Comp. Meth. Appl. Mech. Engrg.*, 103:347–362, 1992.

[9] R. de Borst and L.J. Sluys. Localization in a Cosserat continuum under static and loading conditions. *Comp. Meth. Appl. Mech. Engrg.*, 90:805–827, 1991.

[10] S. Diebels and H. Steeb. The size effect in foams and its theoretical and numerical investigation. *Proc. R. Soc. London A*, 458:2869–2883, 2002.

[11] A. Dietsche, P. Steinmann, and K. William. Micropolar elastoplasticity and its role in localization. *Int. J. Plasticity*, 9:813–831, 1993.

[12] G. Duvaut. Elasticité linéaire avec couples de contraintes. Théorémes d'existence. *J. Mec. Paris*, 9:325–333, 1970.

[13] A. C. Eringen. *Microcontinuum Field Theories*. Springer, Heidelberg, 1999.

[14] A.C. Eringen. Theory of Micropolar Elasticity. In H. Liebowitz, editor, *Fracture. An advanced treatise.*, volume II, pages 621–729. Academic Press, New York, 1968.

[15] A.C. Eringen and C.B. Kafadar. Polar Field Theories. In A.C. Eringen, editor, *Continuum Physics*, volume IV: Polar and Nonlocal Field Theories, pages 1–73. Academic Press, New York, 1976.

[16] A.C. Eringen and E.S. Suhubi. Nonlinear theory of simple micro-elastic solids. *Int. J. Eng. Sci.*, 2:189–203, 1964.

[17] V. Gheorghita. On the existence and uniqueness of solutions in linear theory of Cosserat elasticity. I. *Arch. Mech.*, 26:933–938, 1974.

[18] V. Gheorghita. On the existence and uniqueness of solutions in linear theory of Cosserat elasticity. II. *Arch. Mech.*, 29:355–358, 1974.

[19] W. Günther. Zur Statik und Kinematik des Cosseratschen Kontinuums. *Abh. Braunschweigische Wiss. Gesell.*, 10:195–213, 1958.

[20] A.E. Green and R.S. Rivlin. Multipolar continuum mechanics. *Arch. Rat. Mech. Anal.*, 17:113–147, 1964.

[21] M.E. Gurtin and P. Podio-Guidugli. On the formulation of mechanical balance laws for structured continua. *Z. Angew. Math. Phys.*, 43:181–190, 1992.

[22] I. Hlavacek and M. Hlavacek. On the existence and uniqueness of solutions and some variational principles in linear theories of elasticity with couple-stresses. I: Cosserat continuum. II: Mindlin's elasticity with micro-structure and the first strain gradient. *J. Apl. Mat.*, 14:387–426, 1969.

[23] D. Iesan. Existence theorems in micropolar elastostatics. *Int. J. Eng. Sci.*, 9:59–78, 1971.

[24] D. Iesan and A. Pompei. On the equilibrium theory of microstretch elastic solids. *Int. J. Eng. Sci.*, 33:399–410, 1995.

[25] D. Iesan and R. Quintanilla. Existence and continuous dependence results in the theory of microstretch elastic bodies. *Int. J. Eng. Sci.*, 32:991–1001, 1994.

[26] D. Iesan and A. Scalia. On Saint-Venants principle for microstretch elastic bodies. *Int. J. Eng. Sci.*, 35:1277–1290, 1997.

[27] M.M. Iordache and K. William. Localized failure analysis in elastoplastic Cosserat continua. *Comp. Meth. Appl. Mech. Engrg.*, 151:559–586, 1998.

[28] W.T. Koiter. Couple stresses in the theory of elasticity I,II. *Proc. Kon. Ned. Akad. Wetenschap*, B 67:17–44, 1964.

[29] E. Kröner. *Mechanics of Generalized Continua.* Proceedings of the IUTAM-Symposium on the generalized Cosserat continuum and the continuum theory of dislocations with applications in Freudenstadt, 1967. Springer, Heidelberg, 1968.

[30] J.E. Marsden and J.R. Hughes. *Mathematical Foundations of Elasticity.* Prentice-Hall, Englewood Cliffs, New Jersey, 1983.

[31] G.A. Maugin. On the structure of the theory of polar elasticity. *Phil. Trans. Roy. Soc. London A*, 356:1367–1395, 1998.

[32] R.D. Mindlin and H.F. Tiersten. Effects of couple stresses in linear elasticity. *Arch. Rat. Mech. Anal.*, 11:415–447, 1962.

[33] P. Neff. A geometrically exact Cosserat-shell model including size effects, avoiding degeneracy in the thin shell limit. Part I: Formal dimensional reduction for elastic plates and existence of minimizers for positive Cosserat couple modulus. *Cont. Mech. Thermo.*, 16(6 (DOI 10.1007/s00161-004-0182-4)):577–628, 2004.

[34] P. Neff. On material constants for micromorphic continua. In Y. Wang and K. Hutter, editors, *Trends in Applications of Mathematics to Mechanics*, STAMM Proceedings, Seeheim 2004, pages 337–348. Shaker Verlag, Aachen, 2005.

[35] P. Neff. A geometrically exact microincompressible micromorphic elastic solid. Modelling and existence of minimizers. *Preprint 2318, http://wwwbib.mathematik.tu-darmstadt.de/Math-Net/Preprints/Listen/pp04.html, submitted to Proc. Roy. Soc. Edinb.*, 2/2005.

[36] P. Neff. The Cosserat couple modulus for continuous solids is zero viz the linearized Cauchy-stress tensor is symmetric. *Preprint 2409, http://wwwbib.mathematik.tu-darmstadt.de/Math-Net/Preprints/Listen/pp04.html, submitted to ZAMM*, 7/2005.

[37] P. Neff. Finite multiplicative elastic-viscoplastic Cosserat micropolar theory for polycrystals with grain rotations. Modelling and mathematical analysis. *Preprint 2297, http://wwwbib.mathematik.tu-darmstadt.de/Math-Net/Preprints/Listen/pp03.html, submitted*, 9/2003.

[38] P. Neff and K. Chelminski. Infinitesimal elastic-plastic Cosserat micropolar theory. Modelling and global existence in the rate independent case. *Preprint 2290, http://wwwbib.mathematik.tu-darmstadt.de/Math-Net/Preprints/Listen/pp03.html, to appear in Proc. Roy. Soc. Edinb. A*, 1/2005.

[39] P. Neff and S. Forest. A geometrically exact micromorphic model for elastic metallic foams accounting for affine microstructure. Modelling, existence of minimizers, identification of moduli and computational results. *Preprint 2373, http://wwwbib.mathematik.tu-darmstadt.de/Math-Net/Preprints/Listen/pp04.html, submitted to J. Elasticity*, 12/2004.

[40] W. Nowacki. *Theory of Asymmetric Elasticity.* Pergamon Press, Oxford, 1986.

[41] N. Oshima. Dynamics of granular media. In K. Kondo, editor, *Memoirs of the Unifying Study of the Basic Problems in Engineering Science by Means of Geometry*, volume 1, Division D-VI, pages 111–120 (563–572). Gakujutsu Bunken Fukyo-Kai, 1955.

[42] M. Ristinmaa and M. Vecchi. Use of couple-stress theory in elasto-plasticity. *Comp. Meth. Appl. Mech. Engrg.*, 136:205–224, 1996.

[43] C. Sansour. *Ein einheitliches Konzept verallgemeinerter Kontinua mit Mikrostruktur unter besonderer Berücksichtigung der finiten Viskoplastizität.* Habilitation-Thesis, Shaker-Verlag, Aachen, 1999.

[44] C. Sansour and W. Wagner. Multiplicative updating of the rotation tensor in the finite element analysis of rods and shells, a path independent approach. *Computational Mechanics*, 31:153–162, 2003.

[45] H. Schaefer. Das Cosserat-Kontinuum. *Z. Angew. Math. Mech.*, 47:485–498, 1967.

[46] R.A. Toupin. Elastic materials with couple stresses. *Arch. Rat. Mech. Anal.*, 11:385–413, 1962.

[47] R.A. Toupin. Theory of elasticity with couple stresses. *Arch. Rat. Mech. Anal.*, 17:85–112, 1964.

[48] C. Truesdell and W. Noll. The non-linear field theories of mechanics. In S. Fluegge, editor, *Handbuch der Physik*, volume III/3. Springer, Heidelberg, 1965.

[49] T. Valent. *Boundary Value Problems of Finite Elasticity.* Springer, Berlin, 1988.

Notation

Let $\Omega \subset \mathbb{R}^3$ be a bounded domain with Lipschitz boundary $\partial\Omega$ and let Γ be a smooth subset of $\partial\Omega$ with non-vanishing 2-dimensional Hausdorff measure. For $a, b \in \mathbb{R}^3$ we let $\langle a, b\rangle_{\mathbb{R}^3}$ denote the scalar product on $\mathbb{R}^3$ with associated vector norm $\|a\|^2_{\mathbb{R}^3} = \langle a, a\rangle_{\mathbb{R}^3}$. We denote by $\mathbb{M}^{3\times 3}$ the set of real 3×3 second order tensors, written with capital letters and by $\mathfrak{T}(3)$ the set of all third order tensors. The standard Euclidean scalar product on $\mathbb{M}^{3\times 3}$ is given by $\langle X, Y\rangle_{\mathbb{M}^{3\times 3}} = \operatorname{tr}\left[XY^T\right]$, and thus the Frobenius tensor norm is $\|X\|^2 = \langle X, X\rangle_{\mathbb{M}^{3\times 3}}$. In the following we omit the index $\mathbb{R}^3, \mathbb{M}^{3\times 3}$. The identity tensor on $\mathbb{M}^{3\times 3}$ will be denoted by $1\!\!1$, so that $\operatorname{tr}[X] = \langle X, 1\!\!1\rangle$. We let Sym and PSym denote the symmetric and positive definite symmetric tensors respectively. We adopt the usual abbreviations of Lie-group theory, i.e., $\mathrm{GL}(3, \mathbb{R}) := \{X \in \mathbb{M}^{3\times 3} \;|\det[X] \neq 0\}$ the general linear group, $\mathrm{SL}(3, \mathbb{R}) := \{X \in \mathrm{GL}(3, \mathbb{R}) \;|\det[X] = 1\}$, $\mathrm{O}(3) := \{X \in \mathrm{GL}(3, \mathbb{R}) \mid X^TX = 1\!\!1\}$, $\mathrm{SO}(3, \mathbb{R}) := \{X \in \mathrm{GL}(3, \mathbb{R}) \;|X^TX = 1\!\!1,\ \det[X] = 1\}$ with corresponding Lie-algebras $\mathfrak{so}(3) := \{X \in \mathbb{M}^{3\times 3} \;|X^T = -X\}$ of skew symmetric tensors and $\mathfrak{sl}(3) := \{X \in \mathbb{M}^{3\times 3} \;|\operatorname{tr}[X] = 0\}$ of traceless tensors. We set $\operatorname{sym}(X) = \frac{1}{2}(X^T + X)$ and $\operatorname{skew}(X) = \frac{1}{2}(X - X^T)$ such that $X = \operatorname{sym}(X) + \operatorname{skew}(X)$. The set PSym denotes positive definite symmetric matrices. For $X \in \mathbb{M}^{3\times 3}$ we set for the deviatoric part $\operatorname{dev} X = X - \frac{1}{3}\operatorname{tr}[X]\,1\!\!1 \in \mathfrak{sl}(3)$ and for vectors $\xi, \eta \in \mathbb{R}^n$ we have the tensor product $(\xi \otimes \eta)_{ij} = \xi_i\,\eta_j$. The operator $\operatorname{axl} : \mathfrak{so}(3, \mathbb{R}) \mapsto \mathbb{R}^3$ is the canonical identification. We write the polar decomposition in the form $F = RU = \operatorname{polar}(F)\,U$ with $R = \operatorname{polar}(F)$ the orthogonal part of F. For a second order tensor X we define the third order tensor $\mathfrak{h} = \mathrm{D_x}X(x) = (\nabla(X(x).e_1), \nabla(X(x).e_2), \nabla(X(x).e_3)) = (\mathfrak{h}^1, \mathfrak{h}^2, \mathfrak{h}^3) \in \mathbb{M}^{3\times 3} \times \mathbb{M}^{3\times 3} \times \mathbb{M}^{3\times 3}$. For third order tensors $\mathfrak{h} \in \mathfrak{T}(3)$ we set $\|\mathfrak{h}\|^2 = \sum_{i=1}^3 \|\mathfrak{h}^i\|^2$ together with $\operatorname{sym}(\mathfrak{h}) := (\operatorname{sym}\mathfrak{h}^1, \operatorname{sym}\mathfrak{h}^2, \operatorname{sym}\mathfrak{h}^3)$ and $\operatorname{tr}[\mathfrak{h}] := (\operatorname{tr}\left[\mathfrak{h}^1\right], \operatorname{tr}\left[\mathfrak{h}^2\right], \operatorname{tr}\left[\mathfrak{h}^3\right]) \in \mathbb{R}^3$. Moreover, for any second order tensor X we define $X \cdot \mathfrak{h} := (X\mathfrak{h}^1, X\mathfrak{h}^2, X\mathfrak{h}^3)$ and $\mathfrak{h} \cdot X$ correspondingly. Quantities with a bar, e.g. the micropolar rotation $\overline{R}_p$, represent the micropolar replacement of the corresponding classical continuum rotation R. In general we work in the context of nonlinear, finite elasticity. For the total deformation $\varphi \in C^1(\overline{\Omega}, \mathbb{R}^3)$ we have the deformation gradient $F = \nabla\varphi \in C(\overline{\Omega}, \mathbb{M}^{3\times 3})$ and we use ∇ in general only for column-vectors in $\mathbb{R}^3$. Furthermore, $S_1(F)$ and $S_2(F)$ denote the first and second Piola Kirchhoff stress tensors, respectively. The first and second differential of a scalar valued function $W(F)$ are written $D_FW(F).H$ and $D_F^2W(F).(H, H)$, respectively. Sometimes we use also $\partial_XW(X)$ to denote the first derivative of W with respect to X. We employ the standard notation of Sobolev spaces, i.e. $L^2(\Omega), H^{1,2}(\Omega), H^{1,2}_\circ(\Omega)$, which we use indifferently for scalar-valued functions as well as for vector-valued and tensor-valued functions. Moreover, we set $\|X\|_\infty = \sup_{x\in\Omega}\|X(x)\|$. For $X \in C^1(\overline{\Omega}, \mathbb{M}^{3\times 3})$ we define $\operatorname{Curl} X(x)$ and $\operatorname{Div} X(x)$ as the operation curl and Div applied row wise, respectively. For $\mathfrak{h} \in \mathfrak{T}(3)$ we define $\operatorname{Div}\mathfrak{h} = \left(\operatorname{Div}\mathfrak{h}^1 | \operatorname{Div}\mathfrak{h}^2 | \operatorname{Div}\mathfrak{h}^3\right)^T \in \mathbb{M}^{3\times 3}$. We define $H^{1,2}_\circ(\Omega, \Gamma) := \{\phi \in H^{1,2}(\Omega) \mid \phi_{|_\Gamma} = 0\}$, where $\phi_{|_\Gamma} = 0$ is to be understood in the sense of traces and by $C_0^\infty(\Omega)$ we denote infinitely differentiable functions with compact support in Ω. We use capital letters to denote possibly large positive constants, e.g. C^+, K and lower case letters to denote possibly small positive constants, e.g. c^+, d^+. The smallest eigenvalue of a positive definite symmetric tensor $P \in \mathrm{PSym}$ is abbreviated by $\lambda_{\min}(P)$. Finally, w.r.t. abbreviates with respect to.